

**Probing Single-Molecule Polymer-Solid Interactions in Water by Single
Molecule Force Spectroscopy and Its Preliminary Applications**

by

Yuechao Tang

A thesis submitted in partial fulfillment of the requirements for the degree of

Doctor of Philosophy

in

Materials Engineering

Department of Chemical and Materials Engineering
University of Alberta

© Yuechao Tang, 2018

Abstract

The interactions between polymers and solid-water interfaces involve various interesting physical processes, which are fundamental questions for both scientific research and a variety of practical applications, such as underwater adhesives, anti-fouling and stabilization of interested materials/particles. This study focuses on investigating the fundamental single-molecule interactions between polymers and solid surfaces in an aqueous environment using Single Molecule Force Spectroscopy (SMFS).

With the help of stimuli-responsive oligo ethylene glycol copolymer, the influence of polymer hydrophobicity on single-molecule adhesion force was studied using one polymer-substrate pair. By changing the NaCl concentration, the polymer underwent a transition from a hydrophilic to a hydrophobic state due to the suppressed hydration of side chains. It was found that the single-molecule adhesion force on a MoS₂ basal surface in the presence of 1 mM NaCl was around 53 pN. The force almost remained constant in low NaCl concentration up to 0.5 M, followed by a significant increase with increasing NaCl concentration before approaching a plateau at NaCl concentration as high as 1 M, which indicated that the single-molecule adhesion force was sensitive to polymer hydrophobicity.

To further understand the probed dependence of single-molecule force on polymer hydrophobicity, the anisotropic property of MoS₂ was utilized to separate the contributions of electric double layer interaction (EDL), van der Waals interaction (vdW) and hydrophobic attraction from total single-molecule interactions. The observed pH-independent force excludes the contribution of EDL to the total single-molecule interaction. Compared with the hydrophobic basal surface of MoS₂, the single-molecule adhesion force between the hydrophilic edge surface of MoS₂ and the studied

copolymer was found to be smaller than the lower detection limit of SMFS (9 pN). Thus, the vdW interaction was demonstrated to play a minor role in single-molecule interaction between the studied polymer and MoS₂ surface. The overall investigations ruled out the dominant role of EDL and vdW interactions on single-molecule interactions and illustrated that the hydrophobic attraction might be the main driving force of single-molecule interaction between hydrophobic polymers and surfaces.

To capture the underlying physics, a simple thermodynamic model was derived in the third part of this study. Based on the law of energy conservation, the energy inputted into the system by peeling the polymer chain from a solid-water interface under external force was related to the change of entropic free energy and adhesion free energy of the polymer chain. As the driving force holding the polymer on the MoS₂-water interface was demonstrated to be mainly hydrophobic attraction, in common with other investigations, the adhesion free energy was quantified using hydrophobic hydration free energy. The single-molecule forces of polymers on MoS₂ and highly oriented pyrolytic graphite (HOPG) surfaces were used to test the validity of the derived model. The good agreement between the experimental data and theoretical model further confirmed the dominant role of hydrophobic attraction in single-molecular interactions between polymers and hydrophobic surfaces.

In the fourth part of this thesis, the in-depth understanding of SMFS investigation between different polymers and MoS₂ surfaces was used to navigate the structure design of polymers for MoS₂ exfoliation. The performance of MoS₂ for various applications can be significantly improved when exfoliated into a single-layer. The key for the efficient aqueous exfoliation relies on the proper selection of polymer that is able to functionalize and stabilize the exfoliated MoS₂ nanosheets in water. Therefore, the understanding and quantification of polymer-solid interaction

in water is highly desired for the selection of suitable organic functionalization agents. Among the polymers studied, cationic poly (vinylbenzyl trimethyl ammonium chloride) (PVBTA) was indicated to be promising for efficient exfoliation of MoS₂ due to its good water compatibility and strong interaction with both the basal and edge surfaces of MoS₂. Compared with previously reported values, scaled production of single-layer MoS₂ nanosheet exfoliated by the selected polymer was achieved to be one magnitude higher concentration using magnitude less treatment time. These results demonstrated that the insights from SMFS investigation is highly effective to optimize the functionalization and stabilization of interested materials in practical applications. To be noted, this study provided an efficient approach to discover appropriate surface active polymer for effective functionalization of MoS₂ and could be applied in a variety of practical applications demanding optimization of materials, including underwater adhesion, dispersion or functionalization.

Preface

This thesis is composed of a series of papers. Chapters 3-6 are research papers that has been published, submitted or still in preparation. The following is a statement of contributions made to the jointly authored papers contained in this thesis:

- Chapter 1 Introduction. Original work by Yuechao Tang.
- Chapter 2 Literature review. Original work by Yuechao Tang.
- Chapter 3 A version of this chapter has been published as: Tang, Y. C., Zhang, X. R., Choi, P., Liu, Q. X., Xu, Z. H., Probing Single-Molecule Adhesion of a Stimuli Responsive Oligo (ethylene glycol) Methacrylate Copolymer on a Molecularly-Smooth Hydrophobic MoS₂ Basal Plane Surface, *Langmuir* 2017, 33 (40), 10429-10438. Tang was responsible for the SMFS experiment, data processing, theoretical analysis and model development and manuscript preparation. Xu and Liu supervised the project. Xu, Liu, Choi, Zhang and Manica provided proofread of the manuscript prior to submission.
- Chapter 4 A manuscript based on this chapter is in preparation: Tang, Y. C.; Zhang, X. R.; Choi, P.; Liu, Q. X.; Xu, Z. H. How Much does Hydrophobic Effect/Attraction Contribute to Single-Molecule Adhesion on Hydrophobic Surface in Solution?, In preparation. Tang was responsible for the SMFS experiment, following data processing and manuscript preparation. Xu and Liu supervised the project. Xu, Liu, Choi and Zhang provided proofread of the manuscript prior to submission.
- Chapter 5 A version of this chapter has been submitted: Tang, Y. C.; Zhang, X. R.; Choi, P.; Liu, Q. X.; Xu, Z. H. Underwater Adhesion of a Stimuli-Responsive Polymer on Highly Oriented Pyrolytic Graphite (HOPG): A Single-Molecule Force Study, submitted. Tang was responsible for the SMFS experiment, data processing, theoretical analysis and model development and manuscript preparation. Xu and Liu supervised the project. Xu, Liu, Choi and Zhang provided proofread of the manuscript prior to submission.
- Chapter 6 A manuscript based on this chapter has been submitted: Tang, Y. C.; Zhang, X. R.; Choi, P.; Manica, R.; Liu, Q. X.; Xu, Z. H. Noncovalent Functionalization of MoS₂: Single-molecule MoS₂-Polymer Interaction and Efficient Aqueous Exfoliation of MoS₂ into Single-

layer, submitted. Tang was responsible for the SMFS experiment, exfoliation experiment, following data processing and manuscript preparation. Xu and Liu supervised the project. Xu, Liu, Choi, Zhang and Manica provided proofread of the manuscript prior to submission.

- Chapter 7 Conclusions. Original work by Yuechao Tang.

The Appendices at the end of the thesis provide addition calculations, figures and tables for each chapter.

Acknowledgements

I would like to express my gratitude and appreciation to:

- My supervisors, Prof. Qingxia Liu and Prof. Zhenghe Xu for their patience, encouragement, support and supervision in my research and throughout each stage of my graduate studies.
- Prof. Phillip Choi for his kind help, instruction and guidance on my research.
- Mr. James Skwarok, Ms. Jie Ru and Mr. Carl Corbett for their help in locating supplies and instrument training.
- Ms. Lisa Carreiro, Ms. Patricia Siferd and Ms. Lily Laser for administrative assistance.
- All the fellow members and friends in the group, in particular, Dr. Rogerio Manica, Dr. Zhenzhen Lu and Dr. Natalie Kuznicki for the help and enjoyable research experience.
- NSERC Industrial Chair Program in Oil Sands Engineering and The Canadian Centre for Clean Coal/Carbon and Mineral Processing Technologies (C5MPT) for financial support.

Finally, I would like to express my deepest gratitude to my parents, wife and daughter. I am who I am now because of the everlasting love and support from them. It is them that helped me pass the highly stressful time, figure out solutions and being persistent on the academic research. In the meantime, encouraged and inspired me to be better and better. It is to them that I dedicate this work.

Table of contents

Chapter 1 Introduction.....	1
1.1 Background and motivations.....	2
1.2 Objectives and scope of the thesis.....	3
1.3 Structure of the thesis.....	5
Chapter 2 Literature Review-Experimental Techniques and Theories Related with Single-Molecule Investigations of Polymer-Substrate Interactions	7
2.1 Introduction	8
2.2 Single-molecule force study using Atomic Force Microscopy (AFM).....	9
2.2.1 Principle of Atomic Force Microscopy (AFM).....	9
2.2.2 Single Molecule Force Spectroscopy (SMFS)	12
2.2.3 Cantilever calibration	14
2.2.4 Force curves and data analysis	15
2.3 Experimental studies of single chain mechanics using single molecule force spectroscopy (SMFS).....	16
2.3.1 Single-molecule study of entropic-elastic behavior of synthetic polymers.....	17
2.3.2 Single-molecule study of intermolecular interactions	18
2.3.3 Single-molecule study of macromolecule-small molecule interactions	19
2.3.4 Single-molecule study of macromolecules unfolding	20
2.3.5 Single-molecule study of polymer-substrate interactions	20
2.4 Theoretical study of single-molecule polymer-substrate interaction	24
2.4.1 Theory of single polymer chain peeling mechanics	24
2.4.2 Single polymer chain mechanics	34
2.4.3 Hydrophobic hydration.....	37
2.5 The interaction between stimuli-responsive polymer and hydrophobic-water interfaces...	40
Chapter 3 Probing Single-Molecule Adhesion of a Stimuli Responsive Oligo (ethylene glycol) Methacrylate Copolymer on a Molecularly-Smooth Hydrophobic MoS₂ Basal Plane Surface	42
3.1 Introduction	43
3.2 Materials, characterization and methods	44

3.2.1 Materials	44
3.2.2 Synthesis of oligo (ethylene glycol) methacrylate copolymer (P(MEO ₂ MA _x -co-PEGMA _y), x:y=10:1) and polymer brush.	45
3.2.3 Polymer analysis.....	46
3.2.4 Transmittance measurement.	46
3.2.4 Cantilever modification.	46
3.2.5 Single Molecular Force Spectroscopy (SMFS).....	47
3.2.6 Contact angle measurement.....	47
3.3 SMFS results of oligo (ethylene glycol) methacrylate copolymer in solution with various NaCl concentration.....	47
3.4 Discussions.....	55
3.5 Adhesion energy per monomer	57
3.6 Origin of the increased polymer-substrate interaction	59
3.7 Conclusions	61
Chapter 4 The Contribution of Hydrophobic Attraction to Molecular Adhesions on Hydrophobic Surface in Water.....	62
4.1 Introduction	63
4.2 Materials, characterization and methods	65
4.2.1 Materials	65
4.2.2 Synthesis of oligo (ethylene glycol) methacrylate based copolymer	65
4.2.3 Polymer Analysis.....	65
4.2.4 Cantilever Modification.....	66
4.2.5 Single Molecular Force Spectroscopy (SMFS).....	66
4.3 SMFS results of oligo (ethylene glycol) methacrylate copolymer with surfaces of MoS ₂	66
4.3.1 Contribution of electric double layer interaction.....	68
4.3.2 Contribution of van der Waals interaction	69
4.3.3 Contribution of hydrophobic attraction	70
4.4 Discussions.....	74
4.5 Conclusions	76
Chapter 5 Underwater Adhesion of a Stimuli-Responsive Polymer on Highly Oriented Pyrolytic Graphite (HOPG): A Single-Molecule Force Study.....	77
5.1 Introduction	78

5.2 Materials, characterization and methods	80
5.2.1 Materials	80
5.2.2 Synthesis of oligo (ethylene glycol) copolymer	80
5.2.3 Polymer Analysis.....	80
5.2.4 Cantilever Modification.....	81
5.2.5 Single Molecule Force Spectroscopy (SMFS).	81
5.2.6 Contact angle measurement.....	81
5.3 SMFS Investigation of oligo (ethylene glycol) copolymer on HOPG surface	82
5.4 Theory of polymer desorption in SMFS experiment	85
5.5 Discussions.....	89
5.6 Conclusions	91
Chapter 6 Noncovalent Functionalization of MoS₂: Single-Molecule MoS₂-Polymer Interactions and Efficient Aqueous Exfoliation of MoS₂ into Single-Layer	92
6.1 Introduction	93
6.2 Materials, characterization and methods	94
6.2.1 Materials	94
6.2.2 MoS ₂ preparation for SMFS	95
6.2.3 Synthesis of oligo (ethylene glycol) polymer/copolymer and Poly (vinylbenzyl trimethyl ammonium chloride).....	95
6.2.4 Polymer analysis.....	95
6.2.5 Transmission Electron Microscopy (TEM) Characterization	96
6.2.6 Cantilever modification	96
6.2.7 Single Molecular Force Spectroscopy (SMFS).....	96
6.2.8 Aqueous solution exfoliation of MoS ₂ in the presence of polymer.....	96
6.2.9 UV-Vis characterization of produced exfoliated MoS ₂ sheets	97
6.3 Study of MoS ₂ -polymer interaction by single molecule force spectroscopy	97
6.4 Polymer assisted exfoliation of MoS ₂ in aqueous solution	101
6.5 Conclusions	106
Chapter 7 Conclusions and Recommendations for Future Work.....	107
7.1 Conclusions	108
7.2 Recommendations for future work.....	109
Bibliography	111

Appendix A	138
Appendix B	143
Appendix C	148
Appendix D	154

List of Tables

Table 5-1 List of parameters used in the Model.....	88
Table A-1 The measured interfacial energy of MoS ₂ /NaCl aqueous solution and polymer/NaCl aqueous solution.....	142
Table B-1 Chemical structures and molecular weights of the studied polymers	144
Table C-1 The measured HOPG-solution and polymer-solution interfacial tension.....	152
Table D-1 The chemical structures and molecular weights of studied polymers	161
Table D-2 The Zeta potential measurement of the obtained exfoliated MoS ₂ sheets after 2 h combined treatment of grinding and 2 h tip sonication	161

List of Figures

Figure 2-1 Zooming of a AFM chip with 6 cantilevers (MCST, Bruker). A: the AFM cantilevers mounted on both sides of a silicon chip; B: the zooming of the cantilevers which illustrates the two designs of cantilever: triangle and rectangle; C: the zooming into the tip of the cantilever. (figures B and C are adopted from the Bruker website for MSCT AFM probe ³⁸).....	10
Figure 2-2 Schematic representation of the mechanism of AFM ¹⁶ (A) and the Quad Photodetector Arrangement ⁴⁰ (B).	11
Figure 2-3 Schematic illustration of the principles of SMFS. (A) extension of polymer chain ⁴⁴ . and (B) desorption of polymer chain from solid surface ⁴⁵	13
Figure 2-4 Single Molecule Force Spectroscopy (SMFS). (A) Cartoon of the setup of the single molecule force experiment, which consists of an AFM probe, a protein and a piezoelectric scanner. The force on the molecule is quantified by the deflection of cantilever ⁴⁶ ; (B) the typical force representative of the un-folding of a protein ⁴⁶ ; (C) the typical force curve when a polymer is peeled from the substrate shows plateau feature ³⁴	13
Figure 2-5 The typical force curve with plateau feature obtained when a polymer chain is peeled from interested substrate (A) and the corresponding single polymer peeling statics (B) ³⁴	16
Figure 2-6 SMFS experiment of peeling a bio-polymer from hydrophobic diamond surface. (A) A typical SMFS force curve of peeling a spider silk peptide (C16) from substrate in 20 mM NaCl background solution. (B) The schematic representation of the setup of the SMFS experiment. (C) Plateau height. (D) The statistical distribution of the SMFS results, giving a mean single-molecule adhesion force of 58 ± 8 pN ⁶⁶	21
Figure 2-7 A freely-jointed-chain.	25
Figure 2-8 A worm-like-chain.	32

Figure 2-9 (A) Illustration of pulling a polymer chain out of its collapsed globule; (B) superposition of ~ 300 force-extension curves, which indicates the pulling of several single chains simultaneously; (C) Histograms showing the force distribution of baseline and the first step ¹⁰⁰ .	35
Figure 2-10 (A) Typical force curve obtained in SMFS experiment representing single-molecule peeling event. The inset shows the experimental setup; (B) The peeling of the polymer chain from substrate and the dependence of free energy on the pulling distance H ⁹⁵ .	36
Figure 2-11 Configurations of water molecules near hydrophobic cavities obtained with molecular-dynamics simulations ¹⁰³ .	39
Figure 2-12 (A) Solvation free energy for a spherical cavity in water as a function of the cavity size ¹⁰³ .	40
Figure 3-1 (A) Atomic Force Microscope (AFM) image of a MoS ₂ basal plane surface in air. (B) Schematic representation of detaching an oligo (ethylene glycol) methacrylate copolymer chain from a MoS ₂ substrate in an aqueous solution. (C) The chemical modification process to link the polymer to the AFM tip.	48
Figure 3-2 Single molecular adhesion (detachment) force measurement: (A) A typical force curve of an AFM cantilever with attached oligo (ethylene glycol) methacrylate copolymers was retracted from MoS ₂ basal plane surface at 500 nm/s in the presence of 0.14 M NaCl background solution. (B) Schematics showing multiple polymer chains probed during the experiment. Histogram of adhesion forces in 0.14 M NaCl (C) and 2 M NaCl (D). The last three detachment events in the force-extension curve were selected and analyzed although more plateaus were observed for some of the force curves.	50
Figure 3-3 The force required to peel a single oligo (ethylene glycol) methacrylate copolymer chain in 2 M NaCl background solution from (A) MoS ₂ and (B) PTFE surface and plateau length	

distribution for last polymer detachment event on MoS₂ (C) and PTFE (D). The plateau length distribution for last polymer detachment event on MoS₂ in presence of 1mM NaCl..... 52

Figure 3-4 Force required to detach a single oligo (ethylene glycol) methacrylate copolymer chain from MoS₂ surface in aqueous solutions of different NaCl concentrations (the red line was drawn to guide the eyes). 54

Figure 3-5 (A) Illustration of the force balance when the polymer chain is peeling from the MoS₂ substrate. (B) Geometric parameters of the monomer and (C) Dependence of adhesion force and adhesion energy on NaCl concentration. Red dots represent the adhesion force originating from the entropic free energy of the chain, the blue triangles denote the contribution of monomer-substrate interaction on the total measured adhesion force. The empty circles show the adhesion energy per monomer on the substrate. Trend lines were drawn to guide the eyes (using black trend lines for adhesion force and red color for adhesion energy). (D) relationship between the adhesion force contributed by adhesion energy per monomer and the polymer-solution interfacial tension. 58

Figure 4-1 AFM images of basal surface (A) and edge surface (B). Typical force curves obtained in experiment for oligo ethylene glycol copolymer on MoS₂ basal surface in presence of 1 mM NaCl with pH around 3.3 (C). Schematics showing multiple polymer chains being probed during experiment (D). 67

Figure 4-2 Single-molecule adhesion force of a single oligo (ethylene glycol) copolymer chain on basal surface of MoS₂ as a function of pH in presence of 1 mM NaCl background solution (A).69

Figure 4-3 Typical force curves obtained in a SMFS experiment between polymer and hydrophilic edge surface of MoS₂ in the presence of 1 mM NaCl with pH around 5.5: (A) oligo (ethylene glycol) copolymer and (B) poly (vinylbenzyl trimethyl ammonium chloride) (PVBTA). The insets

shows the histogram of adhesion forces corresponding to double and single chain peeling events in a single force curve. 70

Figure 4-4 The adhesion force of a single polymer chain on the basal surface of MoS₂ as a function of ethanol addition: adhesion forces of polymer A (a) and polymer B (b). The transmittance of aqueous solution of polymer B (4 mg/ml in 1 mM NaCl) as a function of ethanol addition (B).72

Figure 4-5 The adhesion force of a single oligo (ethylene glycol) methacrylate based polymer on the basal surface of MoS₂ in the presence of 1 mM NaCl background solution: (A): polymer A; (B): polymer C; (C): polymer D. The single-molecule adhesion forces as a function of polymer composition (D). 73

Figure 5-1 (A) An Atomic Force Microscope (AFM) image of HOPG surface in air. (B) Schematic representation of peeling a polymer chain from substrate in aqueous solution. (C) Typical approaching (red) and retracting force (black) curves obtained in the experiment representing a polymer chain peeling event. 82

Figure 5-2 Analysis of SMFS results: (A) Retracting force curve after baseline correction and inversion. (B) Histogram shows the distribution of data points in force curves. The bottom peak represents the baseline. The second and the third peaks indicate the forces required to peel single or double polymer chains from the HOPG surface..... 84

Figure 5-3 Single molecule adhesion forces of oligo (ethylene glycol) copolymer on the HOPG surface in electrolyte solutions with different NaCl concentrations: (A) 0.14 M; (B) 0.5 M; (C) 1.0 M and (D) 2.0 M. 85

Figure 5-4 (A) Illustration of the force balance when the polymer chain is peeling off from the substrate and (B) Single-molecule adhesion force plotted against the total interfacial energy. The dots are experimental results and the solid line is the adhesion force calculated by the model. The

squares and triangles represent the single-molecule adhesion forces of HOPG-polymer and MoS₂-polymer, respectively. The data on HOPG-polymer were obtained in this study and the data of MoS₂-polymer interaction were taken from our previous work¹⁶⁷. 88

Figure 6-1 AFM image of MoS₂ basal surface (A), schematic representation showing the SMFS experiment on basal surface of MoS₂ (B) and typical force curves obtained in a SMFS experiment when a chain of Polymer C1 was peeled from basal surface of MoS₂ in 1 mM NaCl aqueous solutions of pH around 5.5 (C). 98

Figure 6-2 Representative force curve obtained in the SMFS experiment when a chain of Polymer N2 was peeled from basal surface of MoS₂ (A). The statistical SMFS results obtained between MoS₂ basal surface and polymer N2 (B) or polymer N1 (C). The experiments were carried out in the presence of 1 mM NaCl (pH 5.5) background solution. 99

Figure 6-3 Influence of the solution pH on the strength of the single-molecule adhesion force on MoS₂ basal surface for Polymer C1. (A) pH = 3.3, (B) pH = 5.5 and (C) pH = 9.9. 100

Figure 6-4 (A) Schematic representation showing the SMFS experiment probing single-molecule adhesion force on hydrophilic edge surface of MoS₂, (B) typical force curve showing no single-molecule interaction of polymer N2 on hydrophilic edge surface and (C) histogram of single-molecule adhesion forces of positively charged polymer C1 on negatively charged hydrophilic edge surface of MoS₂ in the presence of 1 mM NaCl with a pH around 5.5..... 101

Figure 6-5 (A) Temporal evolution of the absorption intensity at 666 nm with the increase of treatment time (The raw dispersion was diluted for 4 times). The inset is UV-vis spectra of the obtained exfoliated MoS₂ nanosheets in water after treatment for different time. (B) Optical images of the obtained exfoliated MoS₂ nanosheets dispersion using polymer C1 as exfoliation agent. (C) TEM image of the MoS₂ nanosheets exfoliated by using polymer C1 as functionalization agent.

The insets are the high-resolution TEM images showing the lattices structure of single-layer MoS₂ nanosheet (1), the edge of nanosheet (2) and the Fast Fourier Transform (FFT) pattern (3). (D) AFM image of single-layer MoS₂, (E) statistical analysis of layer thickness of the obtained exfoliated MoS₂ nanosheets showing the thickness of a single-layer is around 0.7 nm and (F) AFM image of raw mica..... 104

Figure 6-6 Schematics for the exfoliation of bulk MoS₂ nanosheets into single-layer using Polymer C1 as a functionalization/exfoliation agent..... 106

Figure A-1 Chemical structure of oligo (ethylene glycol) methacrylate copolymer (A), UV-Vis transmittance curves (cooling) measured using 400 nm in aqueous solution with various amount of NaCl (B). The transmittance as a function of NaCl concentration in isothermal condition (C) 138

Figure A-2 GPC (A) and ¹H-NMR (10 mg/L, CDCl₃, 200 MHz) (B) characterization of synthesized oligo ethylene copolymer. The design molecule weigh of the copolymer is 330 kDa. The obtained molecular weight (M_w) is 200 kDa and PDI is 1.7. As gel was formed during synthesis, broad distribution of the molecular weight was obtained due to gel acceleration. 139

Figure A-3 The typical force curves obtained in the SMFS experiment in presence NaCl solution with different concentration..... 140

Figure A-4 Contact angle of NaCl aqueous solution on oligo (ethylene glycol) methacrylate copolymer brush in heptane 141

Figure B-1 GPC characterization of synthesized polymers. The designed molecule weight of all the synthesized polymer was 330 kDa. The obtained molecular weight (M_n) for Polymer A is 118 kDa with PDI close to 1.9. The M_n of polymer B is 200 kDa (PDI = 1.7). For Polymer C, the

molecular weight (M_n) is 94 kDa (PDI around 1.8). The molecular weight (M_n) of polymer D is 61 kDa (PDI = 2.8).	143
Figure B-2 Single-molecule adhesion force of studied polymer on basal surface of MoS_2 as a function of pH in presence of 1 mM NaCl solution.....	145
Figure B-3 NMR characterization of the studied oligo ethylene glycol copolymer. (A) Polymer A; (B) Polymer B; (C) Polymer C and (D) Polymer D.....	146
Figure B-4 Optical and AFM images of fresh peeled MoS_2 basal surface (A,C,E) and exposed smooth edge surface (B,D,F). The root-mean-square roughness of basal and edge surfaces were 0.3 nm and 2.1 nm, respectively.	147
Figure C-1 The force required to peel a single oligo (ethylene glycol) copolymer chain from HOPG surface (A) in NaCl solution. The comparison of the single-molecule adhesion force quantified on different surfaces (B): copolymer- MoS_2 (a) and copolymer-HOPG (b) (the lines are drawn to guide the eyes). The data of single-molecule force on MoS_2 were taken from previous work ¹⁶⁷	148
Figure C-2 Geometric parameters of the monomer.	149
Figure C-3 Illustration of the force balance when the polymer chain is peeling from substrate.	150
Figure C-4 Contact angle of NaCl solution on the HOPG surface (A) and the calculated HOPG-solution interfacial tension.	152
Figure C-5 Single-molecule adhesion force plotted against the total interfacial energy of polymer-solution and substrate-solution. The dots are experimental results and the curves are the adhesion force calculated with the model. The squares and triangles represent the single-molecule adhesion forces of HOPG-polymer and MoS_2 -polymer respectively. The data on HOPG-polymer was	

obtained in this study and the data of MoS ₂ -polymer interaction were taken from ref.1. The interfacial tension of polymer-HOPG and polymer-MoS ₂ in this study is fitting parameter.	153
Figure C-6 1H-NMR (10 mg/L, CDCl ₃ , 400 MHz) characterization of synthesized oligo ethylene copolymer.	153
Figure D-1 1H-NMR analysis of the studied polymers: (A) polymer C1 and (B) polymer N1.	154
Figure D-2 Dependence of the single-molecule adhesion force on the retracting velocity of AFM cantilever for polymer N2 (A) and polymer C1 (B).	155
Figure D-3 Optical and AFM images of fresh peeled MoS ₂ basal surface (A,C,E) and exposed smooth edge surface (B,D,F). The root-mean-square roughness of basal and edge surfaces were 0.1 nm and 2.1 nm, respectively.	155
Figure D-4 Comparison of the exfoliation performance of the synthesized polymers.	156
Figure D-5 TEM characterization of exfoliated MoS ₂ (G: grinding; S: tip sonication). (A) Exfoliated MoS ₂ sheets without addition of polymer exfoliation agent. As no exfoliated MoS ₂ sheets were found in the supernatant after 8000 rpm centrifugation for 30 min, the precipitants were characterized. Exfoliated MoS ₂ sheets obtained using polymer N2 (B) and polymer C1 (C) as exfoliation agent (centrifuge@8000 rpm for 30 min). (D) MoS ₂ nanosheets produced after 2 h grinding and 2 h tip sonication (centrifuge @11500 for 30 min).	157
Figure D-6 The XRD pattern of the original bulk MoS ₂ and the exfoliated MoS ₂ nanosheets.	158
Figure D-7 Raman spectrum of single-layer MoS ₂ nanosheets exfoliated by combined grinding and tip sonicating MoS ₂ powder using polymer C1 as exfoliation agent.	158
Figure D-8 Thermal gravimetric analysis (TGA) of the original bulk MoS ₂ and exfoliated sample prepared using polymer C1 as exfoliation agent.	159

Figure D-9 GPC characterization of synthesized polymers. The polymers were synthesized using RAFT polymerization technique. The obtained molecular weight (M_n) for poly (vinylbenzyl trimethyl ammonium chloride) is 10.5 kDa with PDI close to 2. The molecular weight (M_n) for PMEO₂MA is 118 kDa with PDI close to 1.9. The M_n of oligo ethylene glycol copolymer is 200 kDa (PDI = 1.7). 160

List of symbols

ΔZ_c	Displacement of the cantilever, nm
ΔZ_p	Displacement of the Z-Piezo, nm
k_c	Spring constant of AFM cantilever
ΔV	Photo diode signal, mV
k_B	Boltzmann constant, 1.23×10^{-23} J/K
T	Absolute temperature, K
P	Area of the resonant peak in power spectrum,
\vec{r}_i	Bond vector of each monomer in polymer chain,
\vec{R}_n	Bond vector of each monomer relative to the origin,
$\langle R^2 \rangle$	Mean-square end-to-end distance, nm ²
b_0	Length of each monomer, nm
L	Contour length of polymer chain
n	Number of monomers in polymer chain
n_f	Number of forward steps in one dimensional walk
n_b	Number of backward steps in one dimensional random walk
$P(d)$	The probability of a random walk of the total n step stops at the position d
$P(\vec{R})$	The possibility of finding the other end of the polymer chain at \vec{R} in 1 D random
\vec{R}_g	The radius of gyration polymer, nm
Ω	Number of conformations
S	Entropy, J/K
A	Helmholtz free energy, J
U_0	Internal energy, J
l_p	Persistence length, nm
B	Bending modulus
θ	Bending angle of an elastic rod, rad
G_{ad}	The adsorption free energy, J
λ	The adsorption free energy per unit length, J/nm
s	Contour length of the polymer chain portion that is stretched, nm

G_{en}	Entropic free energy of polymer chain upon stretched, J
H	End-to-end distance of polymer chain under external force, nm
G_{el}	Elastic free energy of the cantilever, J
ε	Adhesion energy per monomer, J
F_{WLC}	The external force need to stretch a polymer chain calculated by WLC model, pN
F_p	The plateau force needed to peel a single polymer chain from the substrate, pN
a	Length of each monomer along the backbone of the polymer chain, nm
γ_{ps}	Polymer-solution interfacial tension, mJ/m ²
γ_{ss}	Substrate-solution interfacial tension, mJ/m ²
$\gamma_{sub.p}$	Substrate-polymer interfacial tension, mJ/m ²
b	Width of each monomer perpendicular to the backbone of the polymer chain, nm

Chapter 1

Introduction

1.1 Background and motivations

Polymers are very large molecules composed of many repeating units. Due to their broad range of physical and chemical properties, they play essential and ubiquitous roles in our daily life. Some of their applications rely on their bulk mechanical properties. However, for other applications, interfacial adhesion properties are very important. For example, the performance of polymer brush surfaces that offer controllable attachment and detachment properties relies on the stimuli-responsive interfacial adhesion between a polymer and foreign objects/surfaces. In the field of underwater adhesion, the overall adhesion strength is strongly dependent on the interfacial adhesion of polymers and studied surface. In flocculation systems, the capability of designed flocculants in removing suspended solid particles from suspension is significantly influenced by the interaction between polymers and solid particles. Among these practical applications, one can easily extract a fundamental scientific problem: how do polymers interact with solid surfaces in water?

To answer these fundamental questions, having appropriate equipment is indispensable. Up until now, a variety of techniques have been utilized to probe the interaction between interested polymers and solid surfaces in water. These techniques are surface force apparatus (SFA), quartz crystal microbalance with dissipation monitoring (QCM-D) and atomic force microscopy (AFM) with a colloidal probe. SFA works by sensing the interaction between two smooth macroscopic cylindrically curved raw or polymer coated Mica surfaces positioned at 90 ° to each other. QCM-D technique probes the interaction between polymers and solid substrates in liquid by monitoring the resonance frequency and dissipation. These information can be linked to the adsorption amount and the layer's viscoelastic property using appropriate theoretical models. By using a colloidal probe, AFM can also reliably reveal the interaction between polymers and substrates by monitoring the deflection of the AFM cantilever. However, the aforementioned techniques probe the integral behavior of numerous interacting polymer chains and can only provide macroscopic averaged results. To decipher the underlying mechanisms, it is highly desirable to unravel the fundamental single-molecule interactions. However, investigations of interactions between polymers and solid surfaces at a single-molecule level remains limited.

In the past several decades, tremendous attention has been devoted to investigating existing natural systems. As in nature, how living things adapt themselves to the environment is inspiring for the

optimization of current synthetic systems. For example, in order to increase the strength of underwater adhesives, efforts were devoted to understanding the adhesion mechanisms of mussels. Rigorous research on the adhesive proteins in mussels revealed the essential role of 3,4-dihydroxyphenethylamine (Dopa) in interfacial adhesion through its capability of forming bidentate coordination and/or hydrogen bonding. Recently, it was found that Dopa is not the only important parameter that determines underwater adhesion. Hydrophobic domains in mussel adhesive proteins were demonstrated to provide extra attractive interaction when interacting with hydrophobic surfaces. These findings open a new direction in understanding the naturally occurring adhesion systems and offer a new strategy in improving the performance of synthetic underwater adhesive systems. However, up to now, the quantitative influence of polymer hydrophobicity on interfacial adhesion and insights at the single-molecule level remained elusive.

1.2 Objectives and scope of the thesis

The main objective of this work is to fill the knowledge gap of current investigations on single-molecule interactions between stimuli-responsive polymers and solid surfaces in aqueous environment. To provide insights into the partitioning of electric double layer interaction, van der Waals interaction and hydrophobic attraction on the total interaction between a single polymer chain and solid-liquid interface. Moreover, efforts were also devoted to link the fundamental SMFS study to practical applications.

The first part of the thesis focuses on how a single stimuli-responsive polymer chain interacts with hydrophobic surfaces, as well as the dependence of the single-molecule force as a function of environmental stimuli. In this part, Single Molecule Force Spectroscopy (SMFS) was applied to study the single-molecule interaction between stimuli-responsive oligo ethylene glycol copolymer and the hydrophobic basal surface of MoS₂. The objective is to understand the interfacial behavior of oligo ethylene glycol copolymer on solid-water interface in response to the change of environmental stimuli.

In the second part, the focus of the study is partitioning the contributions of van der Waals interactions and hydrophobic interactions to the total single-molecule adhesion force. Therefore, single-molecule adhesion forces probed on the hydrophobic basal surface and hydrophilic edge surface were compared to claim that the van der Waals interaction plays a minor role in our studied system. The validity of the proposed method is supported by the fact that the hydrophobic

interaction cease to play a role on hydrophilic surfaces and the van der Waals interaction in polymer-edge and polymer basal scenarios are exactly the same or in same magnitude. The partitioning is highly relevant to a series of fundamental investigations in a variety of disciplines.

The third part of the thesis focuses on deriving a thermodynamic model to relate the single-molecule force with entropic free energy and hydrophobic hydration free energy. It confirmed the dominant role of hydrophobic attraction in governing the single-molecule interaction between stimuli-responsive polymer and hydrophobic. It is desirable to link the experimental and theoretical investigations. Meanwhile, it is beneficial to a variety of applications because guidelines for molecular optimization of polymers are provided.

The last part of the thesis extended the scope of SMFS from fundamental investigations to practical applications. MoS₂ was used as an example with an objective to show that the insights from single-molecule force spectroscopy can be very beneficial for materials preparation.

The major contributions of this thesis to science is revealing the fundamental single-molecule interaction between stimuli-responsive polymer and MoS₂, which allows the determination of the magnitude of the force and its dependence on environmental stimuli. By varying the water chemistry, substrates and polymer composition, partitioning of the individual fundamental interactions was realized and the hydrophobic attraction was demonstrated to be the dominant contribution between neutral polymer and hydrophobic surfaces. Meanwhile, the knowledge gap on the van der Waals interaction between an organic molecule and extended surface in solution was filled. The van der Waals interaction in this scenario was found accounted for less than 10% of the total single-molecule adhesion force. Theoretical model relating the single-molecule force with entropic free energy and hydration free energy was derived and confirmed the important role of hydrophobic attraction in single-molecule adhesion force. Meanwhile, an efficient approach of finding suitable polymers for functionalization and stabilization of desired materials was proposed that was beneficial for determining solutions to problems encountered in materials science.

1.3 Structure of the thesis

This thesis has been structured as a compilation of papers. Chapters 3-5 are research papers that have been published in, submitted to scientific journals or still in preparation. The key content of each chapter is shown as follows:

- Chapter 1 presents the overall introduction of the thesis which includes the background, motivations, objectives and scope of the thesis.
- Chapter 2 provides a comprehensive literature review on the experimental and theoretical researches related with the single-molecule investigation of polymer-solid interaction in liquid.
- Chapter 3 introduces the investigation of the single-molecule interaction between a neutral oligo ethylene glycol copolymer with hydrophobic basal surface of MoS₂ and the influence of water chemistry. A version of this chapter has been published as: Tang, Y. C., Zhang, X. R., Choi, P., Liu, Q. X., Xu, Z. H., Probing Single-Molecule Adhesion of a Stimuli Responsive Oligo (ethylene glycol) Methacrylate Copolymer on a Molecularly-Smooth Hydrophobic MoS₂ Basal Plane Surface. *Langmuir* 2017, 33 (40), 10429-10438.
- Chapter 4 illustrates the interactions between the neutral copolymers with hydrophobic basal and hydrophilic edge surfaces of MoS₂ and their dependence on solution pH and polymer compositions. The experimental results excluded the presence of electric double layer interaction and demonstrated that van der Waals interaction is negligible in the total single-molecule adhesion force, indicating the essential role of hydrophobic attraction in governing the polymer-MoS₂ interaction. A manuscript based on this chapter is still in preparation: Tang, Y. C.; Zhang, X. R.; Choi, P.; Liu, Q. X.; Xu, Z. H. The Contribution of Hydrophobic Attraction to Molecular Adhesions on Hydrophobic Surface in Water, In preparation.
- Chapter 5 A theoretical model which quantitatively relates the single-molecule adhesion force with entropic free energy and hydrophobic hydration was derived. The good agreement between the experiments and model confirmed the dominant role of hydrophobic attraction between the neutral oligo ethylene copolymer and hydrophobic surfaces. A version of this chapter has been submitted: Tang, Y. C.; Zhang, X. R.; Choi, P.; Liu, Q. X.; Xu, Z. H. Underwater Adhesion of a Stimuli-Responsive Polymer on Highly Oriented Pyrolytic Graphite (HOPG): A Single-Molecule Force Study, submitted.

- Chapter 6 SMFS technique was utilized to find appropriate functionalization agent for the efficient exfoliation of MoS₂ into single-layer. Compared with reported values, an order of magnitude higher concentration of single-layer MoS₂ nanosheets in water was produced in magnitude less time. A manuscript based on this chapter has been submitted: Tang, Y. C.; Zhang, X. R.; Choi, P.; Manica, R.; Liu, Q. X.; Xu, Z. H. Noncovalent Functionalization of MoS₂: Single-molecule MoS₂-Polymer Interaction and Efficient Aqueous Exfoliation of MoS₂ into Single-layer, submitted.
- Chapter 7 presents the conclusions of this thesis and recommendations for future research.

Chapter 2

Literature Review-Experimental Techniques and Theories Related with Single-Molecule Investigations of Polymer-Substrate Interactions

2.1 Introduction

Interactions between macromolecule/polymer and solid-liquid interfaces is one of the most fundamental questions for various scientific research and practical applications. Up to now, tremendous efforts have been devoted to this area and various technical methods have been utilized to fill the knowledge gap. Though techniques such as QCM-D and SFA have been widely utilized to investigate the interplay between polymers and solid substrates, the available information are quite limited. In QCM-D, the shift of resonance frequency and dissipation observed in the experiment can only be linked to the adsorption amount and the layer's viscoelastic property¹. In the case of surface force apparatus (SFA), only macroscopic averaged results are obtained²⁻³. Though combined SFA and AFM investigation has confirmed the scaling law between the macroscopic SFA results and single-molecule AFM interactions⁴⁻⁵, the direct quantification of single molecule interactions by SFA is challenging because it is very difficult to quantify the number of interacting polymer chains. When microscopic investigation is desired to reveal the force relevant to a single-molecule adhesion and the underlying thermodynamics, new approaches are highly desired.

The pursuit on this has led to the development of several experimental tools to realize the investigations at molecular scale. Nowadays, optical tweezer⁶⁻¹⁰, magnetic tweezers¹¹⁻¹⁵ and single molecule force spectroscopy (SMFS)¹⁶⁻²¹ have been demonstrated to be applicable for investigations in molecular scale. Among them, the single molecule force spectroscopy (SMFS) technique has relatively low requirements on the instrument because it is based on traditional atomic force microscopy (AFM) technique. The other two require special sophisticated instruments and procedures. In general, the SMFS technique allows the quantification of the force corresponding to peel a single polymer chain from solid-liquid interface with force sensitivity at pN level. As it is the primary equipment we use for the single-molecule study, this chapter begins with the description of the principles of AFM and how it was accommodated to study the behavior of a single molecule at solid-water interface. Certain key technical aspects for SMFS study will be introduced, as well as data analysis methods and fundamental theoretical theories in polymer physics.

2.2 Single-molecule force study using Atomic Force Microscopy (AFM)

The Atomic Force Microscopy (AFM) was invented in 1986 as a scanning tool by Binnig, Quate and Gerber for investigation in nanoscale²². Besides serving as a powerful tool for surface topography characterization, the improvements made to AFM have expanded its application scope from surface characterization to direct measurements of intermolecular/surface forces with high resolution and sensitivity²³. Nowadays, the broad spectrum of its applications covers electronics, semi-conductors, materials, manufacturing, polymers, biology and biomaterials.

The Single Molecule Force Spectroscopy (SMFS) technique is based on the AFM platform. It probes the force mediating by a single polymer chain between the AFM tip and the substrate during experiment. The early work in this field involves the investigation of the changes of polymer conformation upon external mechanical perturbation²⁴. In such experiments, the conformation of the single polymer chain can be manipulated to test the validity of the fundamental theories in polymer physics, which couldn't be achieved using macroscopic experimental techniques, such as SFA. Meanwhile, the key parameters describing the elasticity of a polymer chain (Kuhn length, persistence length) can be obtained by fitting the experimental collected force curves²⁵⁻²⁶. When this technique is applied to study the polymer-solid interactions²⁷⁻²⁸, the dynamics and statistical distributions of the single-molecule force is obtained rather than the ensemble average from the microscopic bulk experiments. The emergence of this technique offers new approach that is promising to extract more fundamental information for bio macromolecules and synthetic polymers in solution or at solid-liquid interface.

In general, the high sensitivity of the technique allows its application into various fields, including DNA unfolding¹², DNA-molecule interactions²⁹⁻³⁰, protein unfolding¹³, the single polymer stretching³¹⁻³³, the polymer-substrate interactions³⁴ and antibody-antigen interactions³⁵. These investigations provide single macromolecule insights on conformation, chain elasticity, ligand-receptor interactions and energies associated with the change of water chemistry or detachment from the solid-water interface.

2.2.1 Principle of Atomic Force Microscopy (AFM)

The atomic force microscope was initially developed to overcome the limitations of the scanning tunneling microscope (STM), which can only be utilized to image conductive samples³⁶⁻³⁷. Instead

of based on the concept of quantum tunneling, the AFM works by sensing the force interacting between the sharp tip and the studied surface^{19, 22}.

The typical setup of AFM involves a very sharp tip (mounted on cantilever), a piezoelectric (PZT) actuator and a position sensitive photo detector. The cantilever acts as force sensor in AFM, which deflects under loads. Usually, the cantilever can be regarded as spring and the relationship between the force and deflection follows the Hooke's law. The spring constant of a cantilever depends on the mechanical property of the material used and its geometric design. In general, longer, narrower and thinner cantilevers have smaller spring constants. Due to the high force sensitivity, these cantilevers are good for force measurements. The cantilevers with high spring constants are ideal for surface topography characterization in tapping mode.

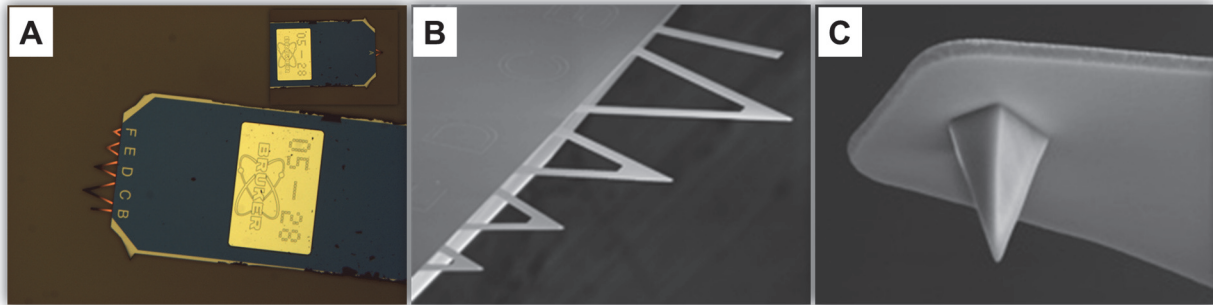


Figure 2-1 Zooming of a AFM chip with 6 cantilevers (MCST, Bruker). A: the AFM cantilevers mounted on both sides of a silicon chip; B: the zooming of the cantilevers which illustrates the two designs of cantilever: triangle and rectangle; C: the zooming into the tip of the cantilever. (figures B and C are adopted from the Bruker website for MSCT AFM probe³⁸).

The working mechanism of AFM relies on sensing the interactions between the tip and sample when scanning a very sharp tip over the sample surface with very small separation distance³⁹. Usually, the specimen is mounted on a piezoelectric scanner which can position the sample three-dimensionally with high accuracy. However, in other cases, the relative movement of the sample and AFM tip is realized by moving the AFM tip as the AFM tip is mounted on the scanner. A schematic representation of the setup of the AFM is briefly shown in Figure 2-2 which describes the scenario that the sample is mounted on the scanner. When the tip (or sample) is being scanned in the (x,y) directions in imaging mode, the force interacting between the tip and the sample induces deflection on the soft cantilever (the common spring constant is between 0.01 N/m to

several N/m). At the same time, a laser beam is focused on the free end of the cantilever and reflected into the photodiode sensor. The position of the laser spot in the photodiode changes when the cantilever bends, which is used to monitor the status of the cantilever. Usually, the force interacting between the sample and the tip is very small (in Nano newton scale). Thus, a design called “laser lever” is incorporated into the design of AFM to amplify the tiny bending/deflection signal of cantilever. Typically, there are 4 elements in the photodiode⁴⁰. The differential signal between the two top elements (A) and the two bottom elements (B) provides signal on the vertical deflection of the cantilever. It is used to generate vertical information. Similarly, the differential signal between C and D provides a measurement of the torsional deflection of the cantilever and is used to obtain lateral information.

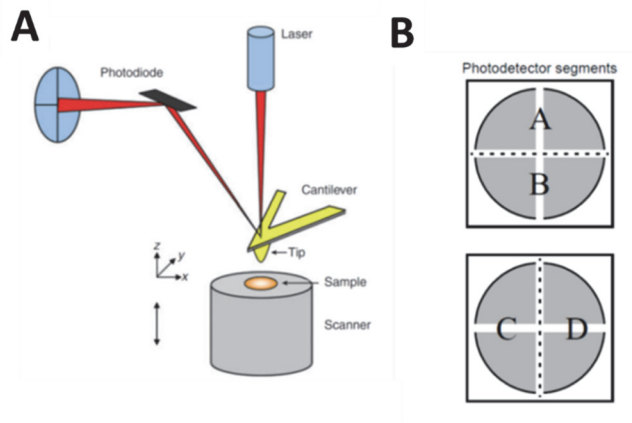


Figure 2-2 Schematic representation of the mechanism of AFM ¹⁶ (A) and the Quad Photodetector Arrangement⁴⁰ (B).

The two most common modes available for surface topography characterization in the AFM technique are contact mode and tapping mode. The contact mode relies on the feedback of the Z-position of the tip so that a constant cantilever deflection is maintained. In this mode, the tip is usually in contact with the surface and is not suggested for soft or unstable samples. The tapping mode imaging is performed when the cantilever is mechanically excited at its resonance frequency. Now, it is widely accepted that the amplitude of the oscillation is dependent on the proximity of the tip to the sample surface. Meanwhile, its phase is linked with the visco-elastic response of the sample. Thus, the topography and the visco-elastic information of the sample can be obtained simultaneously when the amplitude is maintained as a constant during tapping mode imaging.

2.2.2 Single Molecule Force Spectroscopy (SMFS)

Besides imaging across a certain area of the sample, the AFM can also be utilized to stretch a single molecule or peel it from solid surface, a method known as single molecule force spectroscopy (SMFS)²⁴. The general idea is to approach and retract the tip from the substrate continuously at interested locations aiming to probe the interactions mediated by one or several polymer chains. The polymer-substrate interactions, inter/intra molecular interactions can be quantified statistically by analyzing the collected force curves.

When the tip has been engaged, the piezo is subjected to a voltage ramp generated by computer that is fed to the piezo power supply. First, the piezo extends to establish the tip-sample contact and then move back to its original position. This completes a measurement cycle. When the piezo retracts, it pulls the cantilever with it, as well as the attached molecules. Pulling the molecule from surface generates tension and bends the cantilever by ΔZ_c (Figure 2-3). The cantilever deflection, ΔZ_c is measured by the photodiode. The weak point in the system (inter/intra molecular interactions, interactions between polymer and substrate, interactions between polymer and tip) tends to break when the force is increased to a certain extent. When it breaks, the cantilever would fully or partially restore its relaxed state. In the case when a polymer chain is peeling from the substrate, the cantilever would back to its undisturbed state when the whole polymer chain detached from the surface. ΔZ_c , ΔZ_p is recorded by the computer and utilized to plot the force curve. The force is proportional to ΔZ_c and their relationship follows the well-known Hook's law. Therefore, the force can be calculated using the following equation: $F = K\Delta Z_c$. In the equation, K is the spring constant of the cantilever which should be calibrated before each experiment using the available calibration methods⁴¹. The K value determined by different methods may differ by as much as 10-20%. Normally, the method based on thermal noise developed by Hutter and Bechhoefer⁴² and later modified by Butter and Jaschke⁴³ is favored due to its simplicity and acceptable accuracy.

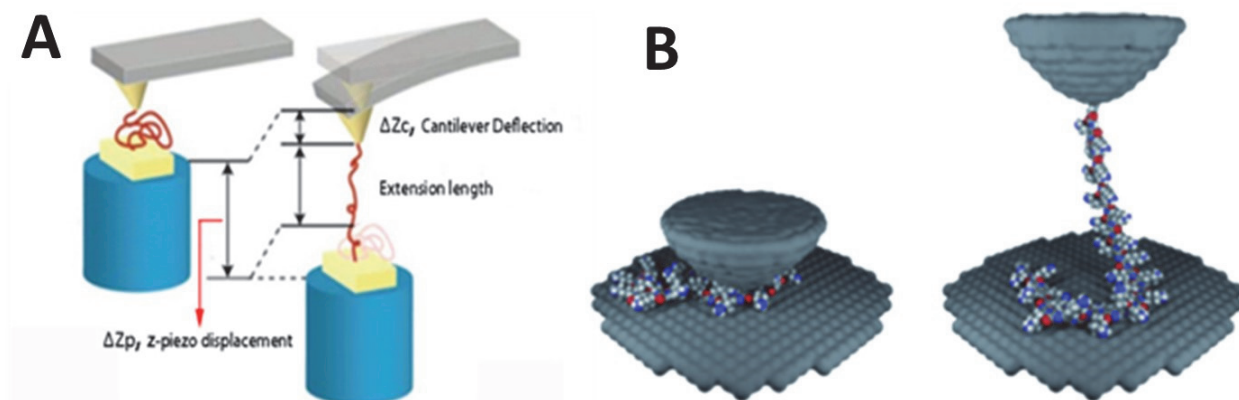


Figure 2-3 Schematic illustration of the principles of SMFS. (A) extension of polymer chain⁴⁴. and (B) desorption of polymer chain from solid surface⁴⁵.

The difference of the probed single-molecule events usually lead to different features of the collected force curves. The occurrence of thaw-teeth pattern in the collected force curves²⁵⁻²⁶ usually can be attributed to the stretching of polymer chain/chains. By fitting the force curve with appropriate models, the elasticity of the studied polymer chain can be estimated. When unfolding a protein molecule under external force, thaw-teeth pattern in the collected force curves is frequently observed. Figure 2-4 (A) shows the experiment setup and Figure 2-4 (B) shows the representative force curves in the experiment. Multiple thaw-teeth patterns in the force curve indicate that several domains in the protein are probed and unfolded sequentially⁴⁶. However, when a polymer chain is peeled from the substrate, plateau of constant force is usually observed in the collected force curves (Figure 2-4 (C)).

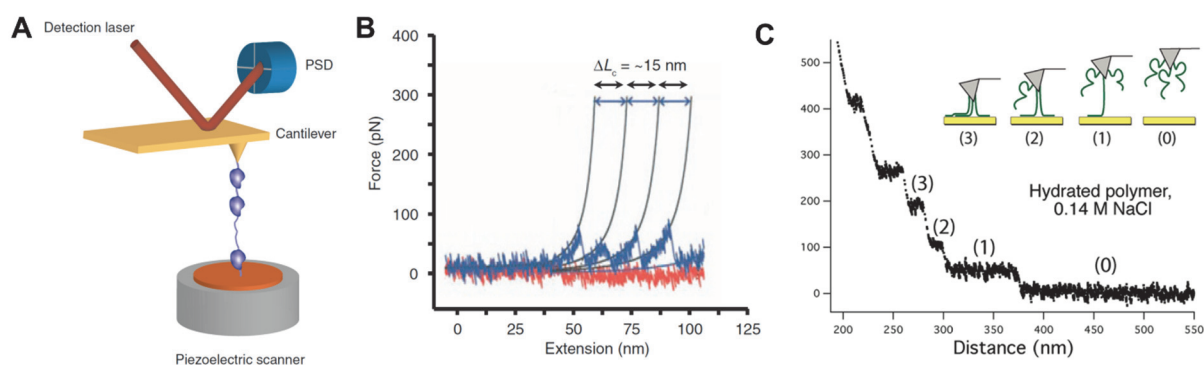


Figure 2-4 Single Molecule Force Spectroscopy (SMFS). (A) Cartoon of the setup of the single molecule force experiment, which consists of an AFM probe, a protein and a piezoelectric scanner.

The force on the molecule is quantified by the deflection of cantilever⁴⁶; (B) the typical force representative of the un-folding of a protein⁴⁶; (C) the typical force curve when a polymer is peeled from the substrate shows plateau feature³⁴.

Generally, the force measured by SMFS is loading rate dependent⁴⁷. In the fast loading regime, the pull-off force increases logarithmically with the loading rate⁴⁸. As is widely accepted, the stretching of a polymer chain at interface should be analyzed in this regime. When in low loading regime, the SMFS is performed in near-equilibrium state. As a result, the measured force is solely determined by the thermal equilibrium between bound and unbound states and shows no dependence on the velocity of the cantilever³⁴. This is the case when a polymer chain is peeled from solid-water interface.

2.2.3 Cantilever calibration

The calibration of the cantilever is important in the SMFS measurement. This step basically determines the accuracy and the reproducibility of the experimental results. Generally, the quantification of the cantilever spring constant can be divided into two steps: the determination of the deflection sensitivity and thermal tune. The deflection sensitivity of the cantilever relates the relationship between the signals obtained in photodiode (with unit in mV) with the deflection of the cantilever (with unit in nm). The thermal tune provides the spring constant of the cantilever. Usually, the spring constant provided by the supplier for commercial AFM probes is not used in the data analysis because it only represents the average values and may deviate significantly from the real value of a specific cantilever. In this study, the calibration of the cantilever was done before and after each experiment.

The deflection sensitivity (*Defl. Sens.*) was defined as the measure of the cantilever deflection (ΔZ_c) over the photodiode signal (ΔV), the unit is nm/V:

$$Defl. Sens. = \frac{\Delta Z_c}{\Delta V} \quad 2.1$$

In the experiment, approaching and retracting force curves were collected to determine the deflection sensitivity. For a typical force curve obtained in the experiment, the inverse slope is by definition, the deflection sensitivity of the used AFM cantilever. Usually, 20-30 force curves were

collected to obtain a statistical average value of deflection sensitivity. The correct value of the deflection sensitivity converts the raw force curves to analyzable force curves.

The determination of the spring constant of the cantilever is performed using the method developed by Hutter and Bechhoefer⁴². The thermal fluctuation of an AFM cantilever is in the order of 3 Å at room temperature. Therefore, the AFM cantilever can be approximated as one dimensional harmonic oscillator. According to the equipartition theory, the energy associate with it is $k_B T/2$:

$$K \langle \Delta Z_c^2 \rangle = k_B T \quad 2.2$$

Where K is the spring constant of the cantilever, ΔZ_c is the displacement of the cantilever, k_B is the Boltzmann's constant and T is the absolute temperature. As a result, the spring constant of the cantilever can be quantified using the following equation:

$$K = \frac{k_B T}{\langle \Delta Z_c^2 \rangle} \quad 2.3$$

However, due to the presence of noise from the environment (acoustic noise or the noise from the building) and the electronic noise from the equipment, the direct calculation of the K with equ. 2.3 using root-mean-square (RMS) fluctuations of a freely moving cantilever is not accurate. This problem is solved by using power spectral density of the fluctuation, which follows a Lorentzian shape in absence of noise sources. Even when the noise sources is present, it only adds a background to it and can be easy subtracted. The area below the resonance peak is a measure of the cantilever fluctuations and its integral relates the spring constant by:

$$K = \frac{k_B T}{P} \quad 2.4$$

Where P is the area under the characteristic peak of the power spectrum of representing the bending mode of the cantilever⁴⁹.

2.2.4 Force curves and data analysis

A force curve representing one or few polymer chains peeled from substrate is shown in Figure 1-5A. The way that how the force curve should be analyzed to extract insights is one of the fundamental questions for the SMFS study. Up to now, theories have been developed to show the physical picture that how a single polymer chain is peeled from the substrate. It is wildly accepted

that the plateau event represents the polymer chain moves freely as it is peeling from the substrate³⁴. This is usually called as frictionless assumption⁵⁰⁻⁵¹. It means that the macromolecule on the surface cannot support a net horizontal friction force⁵¹. When the polymer chain is continually peeled from substrate, the portion of the polymer that is still in contact with the surface is sliding over the surface⁵² to maintain a constant angle between the peeled portion of polymer chain and the substrate (90° for plateau force case).

As force curves with characteristic equilibrium desorption feature are obtained, the heights of the plateaus can be used to determine the strength of polymer-substrate interactions at single-molecule scale. However, significant fluctuation of probed forces is observed due to the instability of the system and noise from environment or equipment. Thus, reasonable analysis of the SMFS data always includes a statistical study. In general, the heights of the force plateaus are analyzed, and the Gaussian equation is applied to get statistical average adhesion force for a single polymer chain (Figure 2-5).

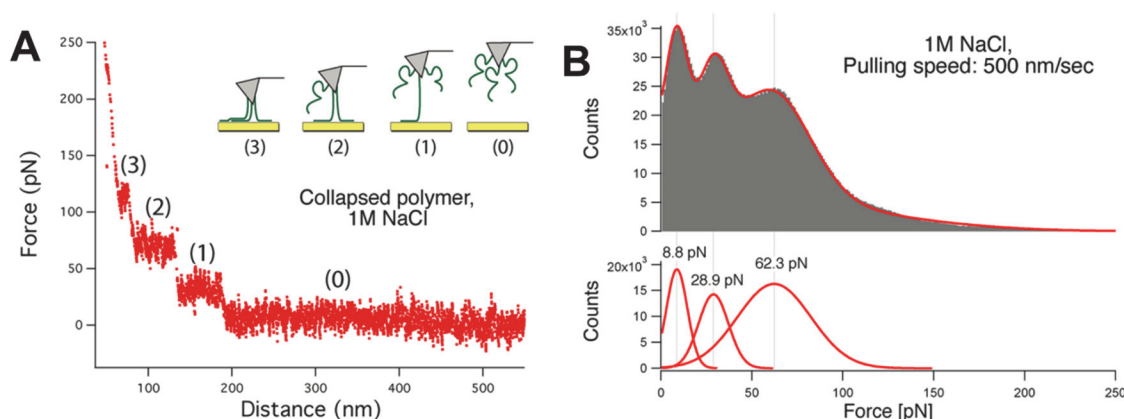


Figure 2-5 The typical force curve with plateau feature obtained when a polymer chain is peeled from interested substrate (A) and the corresponding single polymer peeling statics (B)³⁴.

2.3 Experimental studies of single chain mechanics using single molecule force spectroscopy (SMFS)

A variety of scientific research and practical applications calls for the deep understanding of single polymer chain mechanics. The understanding level may help to bridge the relationship between the first order chemical structures, the behavior of the polymer under the perturbation of external forces or adsorption of small molecules and the final macroscopic properties. In addition, the single

chain mechanics may also help to test the existing theories in the field of polymer physics and drive necessary optimization or development. The ability to study fundamental interactions at the molecular scale has been revolutionized in the past several decades and several examples were shown to give a brief introduction on the applications of SMFS.

2.3.1 Entropic-elastic behavior of synthetic polymers at the molecular scale

The entropic-elastic behavior of a single polymer chain is one of the several fundamental questions in polymer physics. Up until now, theoretical treatments have been proposed to understand the statistical behavior of a single polymer chain and explain the macroscopic properties of bulk polymers, such as the elasticity of rubber. However, the lack of appropriate technique that is able to probe the entropic-elasticity of a single polymer chain plagues the society. With the emergence of the SMFS, the experiments at the molecule scale began to be accessible.

These updates were of great importance for understanding of the influence of side chain on the entropic-elastic properties of polymer. For example, the Zhang and his coworkers²⁶ studied the behavior of poly(dimethylacrylamide) (PDMA) and poly(diethylacrylamide) (PDEA) in response to external forces. The results elucidated that the force-extension curve of these two polymers are almost identical in low force regime. However, deviate significantly in the high force regime. As these two polymers share the same backbone, the difference was attributed to the difference on the side chain. After a series of SMFS experiments, the different behavior of the polymer under external force was demonstrated to be due to the bulkiness of the side chain, the hydrophobic interactions and hydrogen bonding. Meanwhile, the steric effects were also revealed to be important⁵³.

Furthermore, based on the collected force-extension curves, the validity of the existing theories were tested. The nice agreement of the theories and the experiment results in low force regime demonstrated that the underlying physics of the entropic-elastic properties of polymers are indeed captured by the theories. However, the results also suggested that enthalpy should not be neglected⁵⁴.

2.3.2 Single-molecule study of intermolecular interactions

Beyond the scope of the entropic-elastic properties of polymers, the SMFS is also demonstrated to be powerful to reveal the intermolecular interactions. One typical example of such investigation was performed on self-complementary recognition quadruple hydrogen-bonded 2-ureido-4[1*H*]-pyrimidinone (UPy)⁵⁵⁻⁵⁶. In the measurement, both substrate and the cantilever were modified with short chain UPy disulphide. The molecular scale interactions confirmed that the unbonding behavior of the supermolecular complexes is loading rate dependent. The force corresponding to the cross-over regime between loading rate dependent and pseudo loading rate independent is around 145 pN.

Probing the single molecule adhesion force of amino acid 3,4-dihydroxy-L-phenylalanine (Dopa) on solid-water interface is another typical example⁵⁷. In the measurement, a clean metal oxide substrate and a Dopa modified cantilever were utilized. The results demonstrated that the bonding of catechol on metal oxide surface is surprisingly strong and reversible. In detail, the force corresponding to detaching a single catechol from the substrate can be as high as 700 pN. Furthermore, the force is shown to be sensitive to oxidation. Higher irreversible forces were probed when Dopa is oxidized. This is attributed to the formation of covalent bond between the catechol and amine modified surface.

The van der Waals interaction was demonstrated to act ubiquitously among bodies and molecules⁵⁸. However, it is very difficult to isolate and measure pure vdW forces at the molecular scale. Recently, breakthrough was made and the direct measurement of the van der Waals interaction between an organic molecule and solid surface in vacuum was reported⁵⁹. The choice of the studied molecules and the large molecule-surface separation during force measurement ensures that the probed interaction can be interpreted as purely vdW interaction. The interaction between the conjugated organic molecules and substrate were found highly dependent on the size of the molecule. The linear growth of the vdW attraction with molecular size was then attributed to the increased deconfinement of electrons in the molecules. The author advocated that such interactions should be taken into account in new proposed theoretical treatments.

2.3.3 Single-molecule study of macromolecule-small molecule interactions

Usually, the SMFS experiments are performed in liquid environment. It allows the direct study of the interactions between polymer and interested small molecules. Such kind of study relies on the analysis of the single chain elasticity before and after the addition of the small molecules.

Hydrogen binding/interaction is one of the most important interactions between solute and water molecules in aqueous environment. Thus, the bonding of water molecules to a series of polymers were studied⁶⁰⁻⁶¹. As it demonstrated, poly(ethylene glycol) (PEG) behaves like an ideal entropic string in organic solvent (hexadecane). However, in aqueous solution, due to the hydrogen bonding with water molecules, an evident deviation with FJC model was observed. The data analysis indicates that the bonding energy between a water molecule and each repeating unit of PEG is around 3.0 ± 0.3 kBT.

Besides the hydrogen bonding, the interactions between polymer and iodine was also investigated⁶². The experiments were carried out in aqueous solution (aqueous solution of KI, KI₃) using poly(N-vinyl-2-pyrrolidone) (PVPr) as a molecular probe. By integrating the deviated area between the collected force and the ideal FJC fitting curve, the interaction energy was estimated to be 3.6 kBT per unit repeating unit.

Furthermore, the SMFS attracted also great academic interests in the past several decades in the field of biology. This is because the provided insights at the molecular scale is indispensable to understand a variety of phenomenon. For example, the bonding of small molecule to the DNA⁶³. In such systems, the probing of the interaction is realized by quantifying the rapture interactions between DNA and small molecules. Thus, the DNA need to be immobilized onto gold surface and the small molecule attached to the AFM tip to facilitate the experiment. As was shown in Zhang and his coworker's work⁶³, the interaction between acridine and DNA is around 36 pN. Two energy barrier with distinctively different interaction length were observed⁶⁴ when the data is analyzed with appropriated models. Hydrophobic interaction and π - π interactions were believed to responsible to the energy barrier with long and short interactive.

2.3.4 Single-molecule study of macromolecules unfolding

In biology systems, all the biological motions, is believed driven by forces at the molecular scale. On the other side, the reduction of motion by binding of ligands to its corresponding receptors or folding of a polypeptide to three-dimensional structure involves the formation of interactions that overcome the thermal and other opposing forces. Thus, it is desirable to understand the behavior of a biological macromolecule (protein) in response to external forces.

Fernandez and his coworker studied the response of Ubiquitin under the perturbation of external forces¹⁸. Trajectories were found continuous and marked by several distinct stages in the collated force curves. Meanwhile, the time needed for folding is found dependent on the contour length of the unfolded protein and the force applied during folding. In a following paper, the ubiquitin polyprotein extends in discrete steps of 20.3 ± 0.9 nm marking each unfolding event upon a step increase in the stretching force⁶⁵. Furthermore, the unfolding rate was demonstrated to be exponentially dependent on the applied force and can be described by a two-state Markovian process that obeys the Arrhenius equation.

Besides protein, RNA was also studied with SMFS. In the experiment, mechanical force was manipulated to induce the unfolding and refolding of single RNA molecules¹⁰. It is found in the experiment that the RNA is bi-stable when kept at constant force within a critical force range and hop between folded and unfolded states. Furthermore, the force-dependent equilibrium constants for folding/unfolding was also determined.

2.3.5 Single-molecule study of polymer-substrate interactions

The adhesion of polymer at solid substrates is of critical importance for a broad range of applications ranging from medical treatment, coating industry, mining industry, adhesive industry, *etc.* However, various traditional techniques such as QCM-D and surface force apparatus (SFA) can only provide macroscopic averaged information and has no access to study the interaction in single molecular level. With the emergence and development of SMFS, the study of polymer–interface interaction in single-molecule level becomes readily accessible.

The SMFS is powerful as it can be used to study the adhesion of bio-macromolecules on solid–water interface. It is one of the several fundamental questions for life science and bio processes in living organisms. Usually, the possibility of observing macromolecule peeling event can be

increased by covalently linking the studied polymer/macromolecule to AFM tip. The revised experimental approach gives rise to readily collection of force curves with plateau feature. By using this method, the single-molecule adhesion force of spider silk peptide (C16) on diamond surface was determined to be 58 ± 8 pN. It is close to the value predicted by Molecular dynamics (54 ± 15 pN)⁶⁶. Based on the combined experimental and theoretical investigations, Hugel and his coworker claimed that the standard force fields used in classical simulations are applicable in modeling the hydrophobic attraction of peptides on hydrophobic surface⁶⁶. Meanwhile, they also advocated that the contribution of the hydrophobic effect and the van der Waals interactions are comparable and largely cancelled out.

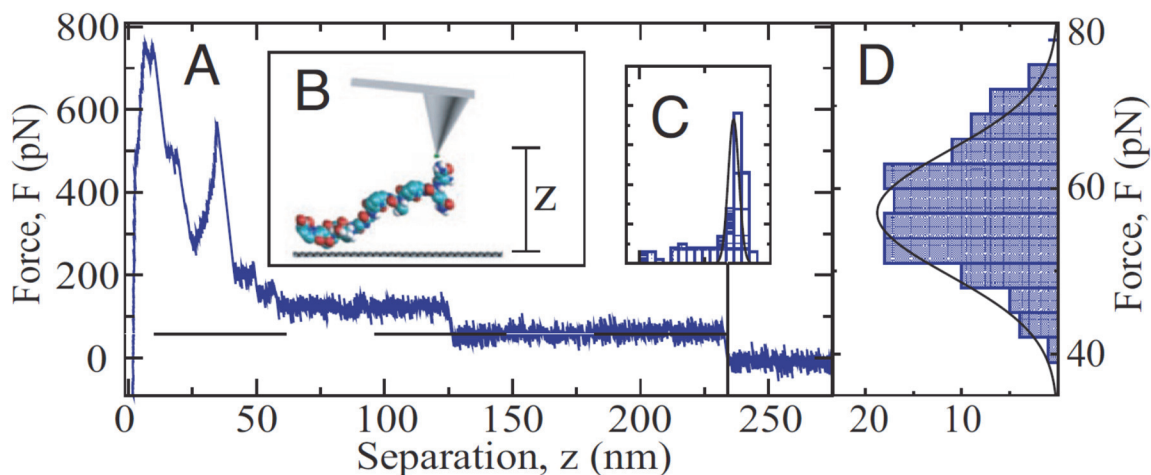


Figure 2-6 SMFS experiment of peeling a bio-polymer from hydrophobic diamond surface. (A) A typical SMFS force curve of peeling a spider silk peptide (C16) from substrate in 20 mM NaCl background solution. (B) The schematic representation of the setup of the SMFS experiment. (C) Plateau height. (D) The statistical distribution of the SMFS results, giving a mean single-molecule adhesion force of 58 ± 8 pN⁶⁶.

Furthermore, with the help of SMFS, the influence of surface potential, pH, surface property and salt concentrations on the interaction between polymer and interested surfaces could also be revealed. The desorption force obtained was found dependent on the surface hydrophobicity⁶⁷. The single-molecule desorption force increases monotonically with increasing hydrophobicity of the substrate. However, the influence of electrical properties of the substrate was found to be within 15%⁶⁸ and the influence of surface roughness is negligible⁶⁹. Although the desorption force obtained by SMFS decreases with increasing salt concentration (NaCl, NaI and NaH₂PO₄) and

follows the Hofmeister series, the effect is found to be very weak and only obvious at high salt concentrations^{67, 70}.

Besides biopolymers, the SMFS technique was also widely applied to investigate the interactions between synthetic polymers and solid substrates. Seitz and coworkers studied the interaction of partial hydrolyzed poly-N-vinylformamide (PVA) with silica surface²⁷. The peeling force was found increases with increasing degree of hydrolysis. This is attributed to hydrolysis, which generate more positive charges along the PVA chain. Furthermore, the interactions between PVA and silica surface is found to be sensitive to ionic strength. Smaller desorption force is probed in solution with high salt concentration. The force reaches its lower limit at 45 pN when the electrolyte concentration is high enough (100 mM). Based on a simple linear model derived from Debye-Hückel approximation, the interaction of PVA with silica surface was divided into two contributions: electrostatic interactions and non-electrostatic interactions. The electrostatic contribution is screened in high salt concentration while the non-electrostatic interaction keeps constant.

By utilizing the SMFS technique, non-electrostatic interaction is also found important in determine the interactions between a single polymer chain and studied solid surface in water. Zhang and his coworkers probed the interactions between an home-synthesized polyelectrolyte (poly(2-acryamido-2-methylpropanesulfonic acid), PAMPS) and amine functionalized silica surface via SMFS⁷¹. Since the force curve shows a long plateau, the polyelectrolyte is believed to adopt a train like conformation at the solid-water interface. The desorption force between polyelectrolyte and positively charged solid surface is found around 120 pN and insensitive to ionic strength. The authors believed these results can be attributed to the major contribution of non-electrostatic interactions between PAMPS and solid surface.

Besides that, the SMFS also provides insights on influence of the molecular architecture on the single-molecule adhesion force²⁸. In the experiment, brush polymer and dendronized polymer were used as model polymers. Their single-molecule interactions were probed on hydrogenated diamond in water. Surprisingly, the side chains of polymer brush showed no significant effect on the magnitude of the probed desorption force. For highly branched dendronized polymer, it was found still mobile on the surface. Similarly, the results demonstrated that the single-molecule

adhesion force corresponding to the polymer chain peeling event is not affected by the presence of long side chain.

Stimuli-responsive polymer is a hot topic in polymer science⁷²⁻⁷⁷. The unique properties of them entitle them to be able to sense the change of environmental stimuli and respond to in its characteristic way. Based on these properties, smart surfaces offering interesting controlled attachment/detachment⁷⁸⁻⁸⁰ and self-cleaning properties⁸¹ have been developed. For these systems, one fundamental question arises: how does a single polymer chain interact with solid surface in aqueous solution. Recently, SMFS technique was applied to study the single-molecule adhesion of a stimuli-responsive polymer on model gold surface. In the experiment, a statistical copolymer composed of di(ethylene glycol) methyl ether methacrylate (MEO₂MA, Mw188.22) and poly(ethylene glycol) methyl ether methacrylate (PEGMA, average Mw 500) was synthesized. The UV-vis illustrates that the copolymer underwent a transition from hydrophilic state to hydrophobic state when the NaCl concentration in background solution is increased. The detailed SMFS experimental results demonstrate that the copolymer adopts different conformation on Au surface in high NaCl concentration buffer because the bridging length was dramatically reduced³⁴. Meanwhile, the single-molecule adhesion force on gold was found lower when the copolymer is in collapsed state. Meanwhile, the cooperativity effects is profound in collapsed state compared to that in hydrated state.

Furthermore, SMFS was also employed to understand certain systems that directly linked with industrial processes. HPAM was reported to be capable of improving bitumen recovery when added during extraction process⁸². With the help of SMFS, the desorption force between HPAM and various substrates were measured at single molecular resolution⁸³. Silica, mica and bitumen coated silica were utilized to represent the sand grain, clay and bitumen droplets. Highest desorption force around 100 pN was measured from mica surface while bitumen surface shows the lowest single-molecule adhesion force (around 40 pN). Based on the obtained data, a mechanism was proposed which explain the previous reported data very well.

The interactions of polymer with clay surfaces is of vital in governing the flocculation performance. Deep understanding is needed to propose reasonable working mechanisms and update the guidelines for designing new flocculants. The interaction of Al(OH)₃-polyacrylamine hybrids flocculants (Al-PAM) and silica surface was then quantified via SMFS. Ionic bonds

between $\text{Al}(\text{OH})_3$ particles and silica substrate with strength around 1253 pN was monitored. The interaction of PAM and silica surface was believed to be based on hydrogen bonding which generate moderate desorption force around 250 pN. Based on the SMFS results, the author believed that the enhanced flocculation performance of Al-PAM can be attributed to the reduced electrostatic repulsion between clay particles after $\text{Al}(\text{OH})_3$ particles adsorption and easily accessible PAM chains by clay surfaces for polymer bridging.

2.4 Theoretical study of single-molecule polymer-substrate interaction

The rapid development of the experimental SMFS study promotes the development of the theories that are capable of capturing the underlying physics of the polymer chain peeling event. Up to now, the physical picture of the polymer chain peeling is clear, and the theoretical analysis agrees well with experiment results.

2.4.1 Theory of single polymer chain peeling mechanics

The SMFS experiments resolve the detaching of a single polymer chain from substrate under mechanical perturbation. The experiment involves a sharp AFM probe, a desorbed portion of the polymer chain, the polymer chain portion on the substrate and the substrate. From the view point of force balance, the elastic force associated with the deflection of the cantilever is balanced by the force holding the polymer on substrate. The desorbed portion of the polymer chain between the cantilever and the substrate served as a spring, which transfer the force from the AFM probe to the polymer chain on substrate. Thus, the analysis of the polymer chain peeling process calls for a clear understanding of the behavior of single polymer chain upon stretching, in other words, the force-extension relationship of a single polymer chain.

Freely-jointed-chain (FJC) and worm-like-chain (WLC) models are two commonly used theoretical models in polymer physics, which describe the relationship between the mechanical force and the end-to-end distance. In this thesis, these two models are introduced.

2.4.1.1 Freely-jointed-chain model

The freely-jointed-chain (FJC) model is the simplest model that describes the statistics of a polymer chain. It assumes that the monomers of a polymer chain are connected with no restriction⁸⁴. Thus, the polymer is treated as a chain of rigid bonds linked together by flexible

connections. In general, the steric interactions between the monomers are neglected, which means that the polymer has no volume. Though it is too ideal to describe the real polymer chain in this way, the FJC model still provides important insights to the behavior of a single polymer chain and its statistics.

The polymer chain can be considered as a string of N monomers with length of b_0 each. As is shown in Figure 2-7, each monomer is described as a bond vector $(\vec{r}_1, \vec{r}_2, \dots, \vec{r}_N)$, and the length of the each vector equals to b_0 ($|\vec{r}_i| = b_0$). When one end of the chain is fixed as the origin, the position of the monomers can be specified though position vectors:

$$\vec{R}_n - \vec{R}_{n-1} = \vec{r}_n \quad \text{For } n=1, 2, 3, \dots, N \quad 2.5$$

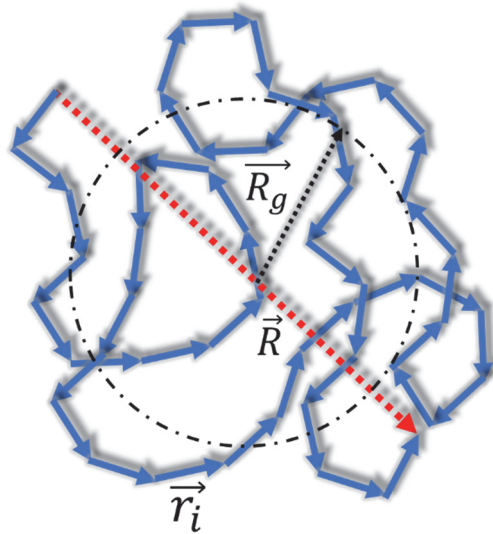


Figure 2-7 A freely-jointed-chain.

Thus, the end-to-end vector connecting two ends of the polymer chain can be calculated as the sum of the all bond vectors.

$$\vec{R} = \sum_{i=1}^N \vec{r}_i \quad 2.6$$

However, due to the random conformation of the polymer, the vector \vec{R} does not offer much insight into the statics of the polymer chain as its value and direction is not known (it can point to any

direction and the value of \vec{R} can varies from 0 to Nb_0). From the view point of statics, the ensemble average end-to-end vector is zero ($\langle \vec{R} \rangle = 0$) as the monomers are randomly oriented with respect to each other and their orientation are independent with each other. This problem can be solved by estimating the mean-square end-to-end distance $\langle R^2 \rangle$.

$$\begin{aligned} \langle R^2 \rangle = \langle \vec{R}^2 \rangle &= \sum_{i=1}^N \sum_{j=1}^N \langle \vec{r}_i \cdot \vec{r}_j \rangle = \sum_{i=1}^N \langle \vec{r}_i^2 \rangle + 2 \sum_{i=1}^N \sum_{j=i+1}^N \langle \vec{r}_i \cdot \vec{r}_j \rangle \\ &= Nb_0^2 + 2b_0^2 \sum_{i=1}^N \sum_{j=i+1}^N \langle \cos \theta_{ij} \rangle = Nb_0^2 \end{aligned} \quad 2.7$$

where θ_{ij} is defined as the angle between two bond vectors. As no correlation is found between bond vectors, the ensemble average value of $\sum_{i=1}^N \sum_{j=i+1}^N \langle \cos \theta_{ij} \rangle$ is 0. Then, the equation 2.8 gives a typical mean-square end-to-end distance estimation based on the monomer number and monomer length.

$$\sqrt{\langle R^2 \rangle} = \sqrt{N}b_0 \quad 2.8$$

However, describing a real polymer by this model is too crude. During the derivation of the aforementioned mathematical relationship, assumption was made that the monomers are linked together freely. It is definitely not true for real polymers. Restrictions do exist between adjacent or remote monomers due to the presence of preferred angle for chemical bond ($109^\circ 23'$ for C-C chemical bond) and steric interactions. Thus, real polymer chain is not as flexible as an ideal freely-jointed-chain. This problem was addressed by the introduction of Kuhn segment and Kuhn length (l). The concept of Kuhn length is defined as the length of a segment that contains multiple monomers and such segments can be treated as freely jointed units in the chain⁸⁴. Therefore, the Kuhn length is always larger than the monomer length. The length of the Kuhn segment indicates the stiffness of polymer chain and is influenced by the above-mentioned restrictions. The statistical behavior of a real polymer chain can be described using Kuhn segment (l) (longer than the monomer length) and its number (n) (smaller than the monomer number N).

$$\begin{aligned} nl &= L \\ nl^2 &= \langle R^2 \rangle \end{aligned} \quad 2.9$$

Up until now, the statistical description of mean-square end-to-end distance using Kuhn length has been introduced. In order to obtain the mathematical relationship between the single polymer chain restoration force and mean-square end-to-end distance, probability distribution function of the end-to-end distance is required. In detail, if the long polymer chain can be regarded as a freely-jointed-chain and one end of the polymer chain is assumed to be at the origin, a mathematical expression that estimates the possibility of finding the other end of the chain in a unit volume $dx dy dz$ can be obtained. In order to simplify the derivation, the introduction starts from one dimensional case.

Assume that a random walk of the total n step stops at the position d , the number of forward and backward steps would have to satisfy the following relationship:

$$\begin{aligned} n_f + n_b &= n \\ n_f - n_b &= d \end{aligned} \quad 2.10$$

Thus, the total possibility of this case can be described as:

$$P(d) = C_n^{n_f} * p^{n_f} * p^{n-n_f} = \frac{n!}{n_f! n_b!} * 2^{-n} = \frac{n!}{\left(\frac{1}{2}(n+d)\right)! \left(\frac{1}{2}(n-d)\right)!} * 2^{-n} \quad 2.11$$

Where p is assumed to be the possibility of moving a step forward and $1-p$ for backward. As the random walk has no bias, the possibilities of the forward and backward steps are identical (0.5).

The Equation (2.11) is then simplified by taking natural log on both side of the equation:

$$\ln P(d) = \ln n! - \ln \left(\frac{1}{2}(n+d)\right)! - \ln \left(\frac{1}{2}(n-d)\right)! - n \ln 2 \quad 2.12$$

As the number of n is very large, Stirling's approximation is applied:

$$\begin{aligned} \ln P(d) &= \left(n + \frac{1}{2}\right) \ln n - \left(\frac{1}{2}(n+d) + \frac{1}{2}\right) \ln \frac{1}{2}(n+d) \\ &\quad - \left(\frac{1}{2}(n-d) + \frac{1}{2}\right) \ln \frac{1}{2}(n-d) - \frac{1}{2} \ln 2\pi - n \ln 2 \end{aligned} \quad 2.13$$

The Equation (2.13) is again simplified with Taylor's expansion to approximate $\ln(n-d)$:

$$\ln P(d) = -\frac{1}{2} \ln n - \frac{d^2}{n} + \frac{1}{2} \left(\frac{d}{n}\right)^2 (n+1) + (n+1) \ln 2 - \frac{1}{2} \ln 2\pi - n \ln 2 \quad 2.14$$

As n is much larger than 1 ($n \gg 1$), the equation is finally simplified to:

$$P(d) = \left(\frac{1}{2\pi n}\right)^{\frac{1}{2}} \exp\left(-\frac{d^2}{2n}\right) \quad 2.15$$

Thus, the possibility of finding the other end of the polymer chain at \vec{R} in 1 D random walk can be obtained as:

$$P(\vec{R}) = C * \exp\left(-\frac{\vec{R}^2}{2nl^2}\right) \quad 2.16$$

where C is a normalization factor and can be determined by summing the probabilities over all possible states of a chain, which should be 1. Thus the value of C was determined:

$$\int_{-\infty}^{+\infty} P(\vec{R}) d\vec{R} = C \int_{-\infty}^{+\infty} \exp\left(-\frac{\vec{R}^2}{2nl^2}\right) d\vec{R} = C * \sqrt{2\pi nl^2} = 1 \quad 2.17$$

$$C = \frac{1}{\sqrt{2\pi nl^2}}$$

Now, the possibility of finding one end of the polymer chain in one dimensional random walk is obtained, which can be extended to 3 dimensional random walk easily. Since the random walk has no preference on x , y , z direction, the steps on x , y , z direction is one thirds of the total number of walks ($\frac{1}{3}n$, assumes that the total number of three dimensional walk is n). In three dimensional random walk, the \vec{R} can be divided into three non-correlated components: $\vec{R}_x, \vec{R}_y, \vec{R}_z$ ($\vec{R}_x^2 + \vec{R}_y^2 + \vec{R}_z^2 = \vec{R}^2$). Thus, 3D random walk is simplified into three 1D random walks. The probabilities for all of them can be expressed as:

$$P(\vec{R}_x) = \frac{\sqrt{3}}{\sqrt{2\pi nl^2}} * \exp\left(-\frac{3\vec{R}_x^2}{2nl^2}\right) \quad 2.18$$

$$P(\vec{R}_y) = \frac{\sqrt{3}}{\sqrt{2\pi n l^2}} * \exp\left(-\frac{3\vec{R}_y^2}{2n l^2}\right)$$

$$P(\vec{R}_z) = \frac{\sqrt{3}}{\sqrt{2\pi n l^2}} * \exp\left(-\frac{3\vec{R}_z^2}{2n l^2}\right)$$

Thus, the total probability of a 3D randomly picked chain has the end-to-end vector \vec{R} is:

$$\begin{aligned} P(\vec{R}) &= P(\vec{R}_x) * P(\vec{R}_y) * P(\vec{R}_z) \\ &= \left(\frac{\sqrt{3}}{\sqrt{2\pi n l^2}}\right)^3 * \exp\left(-\frac{3\vec{R}_x^2}{2n l^2}\right) * \exp\left(-\frac{3\vec{R}_y^2}{2n l^2}\right) * \exp\left(-\frac{3\vec{R}_z^2}{2n l^2}\right) \\ &= \left(\frac{3}{2\pi n l^2}\right)^{\frac{3}{2}} * \exp\left(-\frac{3(\vec{R}_x^2 + \vec{R}_y^2 + \vec{R}_z^2)}{2n l^2}\right) \\ &= \left(\frac{3}{2\pi n l^2}\right)^{\frac{3}{2}} * \exp\left(-\frac{3\vec{R}^2}{2n l^2}\right) \end{aligned} \tag{2.19}$$

Obviously, the probability distribution function of end-to-end distance in 3D space is Gaussian. This the reason why this model is also referred as Gaussian chain model. With this probability distribution function in hand, the radius of gyration (\vec{R}_g), which is another important parameter for polymer can be easily calculated:

$$\vec{R}_g^2 = \frac{1}{n} \left\langle \sum_{j=1}^n (\vec{r}_j - \vec{r})^2 \right\rangle = \frac{n l^2}{6} = \frac{1}{6} \langle R^2 \rangle \tag{2.20}$$

By knowing the probability distribution function ($P(\vec{R})$), the thermodynamic properties of the system, such as entropy and entropic free energy of the polymer chain can be estimated. Furthermore, mathematical expression which describes the relationship between applied force and end-to-end distance can be derived. This relationship is important since it is indispensable for SMFS experimental data analysis. The number of conformations (Ω) available for a polymer chain with end-to-end distance is \vec{R} can be related to $P(\vec{R})$ by:

$$\Omega(\vec{R}) = P(\vec{R}) * \Omega_{total} \quad 2.21$$

where Ω_{total} is the total number of the available conformation for a polymer chain with n segments. The exact value of the Ω_{total} does not influence the calculation of the entropy of the polymer chain, S .

$$S(\vec{R}) = k_B \ln \Omega(\vec{R}) = S_0 - \frac{3k_B \vec{R}^2}{2nl^2} \quad 2.22$$

Here, S_0 is a constant and k_B is Boltzmann's constant. As is evident in the equation, the entropy of the polymer chain decreases as the polymer chain is stretched/extended. As the polymer is extended, or in other word, the end-to-end distance is increased, the segments of the polymer has to realign to accommodate themselves with the specific separation. When the polymer chain is fully stretched to its contour length, the segments has to be perfectly aligned. In the derivation of the FJC model, the interactions between monomers/segments are neglected. Thus, the internal energy of the polymer chain does not change upon stretching/extending. The Helmholtz free energy is then obtained:

$$A = U - TS = U_0 + \frac{3k_B T \vec{R}^2}{2nl^2} - TS_0 \quad 2.23$$

The equation 2.23 correlate the extension/stretching of single polymer chain with the free energy of the system. The Helmholtz free energy A reaches its minimum value when the end-to-end distance is zero ($\vec{R} = 0$). Meanwhile, by differentiate the Helmholtz free energy with the end-to-end vector, the relationship of the restoring force with end-to-end distance can be obtained, as the energy inputted into the system only stored as Helmholtz free energy.

$$\vec{F} = \frac{\partial A}{\partial \vec{R}} = \frac{3k_B T \vec{R}}{nl^2} = \frac{3k_B T}{nl^2} \vec{R} \quad 2.24$$

It is easy to notice that the polymer chain that can be treated as FJC behaves as a traditional spring and the stiffness is dependent on the environmental temperature T . The stiffness of the polymer chain is linearly proportional to the environmental temperature.

However, the previous derivation is only valid for very weak force so that the distributions of the segments still follows the Gaussian distribution. In the real cases, the mathematical function

describes the probability of segment distribution changes when the polymer is subjected to an external force. The partition function can be calculated as:

$$Z = \int d\vec{r}_1 \int d\vec{r}_2 \dots \int d\vec{r}_n \exp\left(\frac{-\vec{F}\vec{R}}{k_B T}\right) \quad 2.25$$

As the energy is separable,

$$\vec{F}\vec{R} = \vec{F} \sum_{i=1}^n \vec{r}_i = F \sum_{i=1}^n \vec{r}_i \cdot \vec{f} = F \sum_{i=1}^n l * 1 * \cos \theta_i = Fl \sum_{i=1}^n \cos \theta_i \quad 2.26$$

where \vec{f} is the unit vector of the applied force, $|\vec{r}_i| = l$ and θ_i is the angle between unit vector of applied force (\vec{f}) and bond vector of segment i . We have $Z = Z_1^n$ because each segment is independent with each other.

$$Z_1 = \int_0^{2\pi} d\varphi_1 \int_0^\pi \sin \theta_1 \exp\left(\frac{-Fl \cos \theta_1}{k_B T}\right) d\theta_1 = 4\pi \frac{k_B T}{Fl} \sinh\left(\frac{Fl}{k_B T}\right) \quad 2.27$$

Thus, the end-to-end distance of the polymer under external force can be obtained:

$$\begin{aligned} \langle R \rangle &= -\frac{\partial A}{\partial \vec{F}} = k_B T \frac{\partial \ln Z}{\partial F} = nk_B T \frac{\partial}{\partial F} \left(\ln \left(\sinh \left(\frac{Fl}{k_B T} \right) \right) - \ln F \right) \\ &= nl \left(\coth \left(\frac{Fl}{k_B T} \right) - \frac{k_B T}{Fl} \right) \end{aligned} \quad 2.28$$

This is the well-known FJC model which relates the external force with the end-to-end distance. It has been widely applied to study the single molecule stretching mechanics and provide updated insights.

In general, it fits the experimental data well in low force range, when the entropic effects govern the relationship between force and end to end distance⁸⁵⁻⁸⁷. However, when the external force is high, the FJC model is not suitable as the enthalpic effects could not be neglected⁸⁸. A revised version of FJC model was then proposed by Smith and his coworkers by adding a new parameter- the segment elasticity K_{segment} . The new model is referred as extended FJC model⁸⁹.

$$\langle R \rangle = x = \left(\coth \left(\frac{Fl}{k_B T} \right) - \frac{k_B T}{Fl} \right) \left(L_{\text{contour}} + \frac{nF}{K_{\text{segment}}} \right) \quad 2.29$$

where x is the end-to-end distance of the polymer chain under mechanical force. Different with the FJC, the extended FJC model treat the segment as a unit spring which is able to deform under external force. With this optimized model, elastic properties of various polymers were obtained by fitting the collected force curves^{26, 60, 90-93}.

2.4.1.2 Worm-like-chain model

Instead of representing the polymer as a string of segments with flexible connection in FJC model, the WLC model treat the polymer as a continuous flexible rod that has a characteristic term of bending modulus or persistence length l_p . Thus, the worm-like-chain (WLC) model provides better description for stiff polymers.

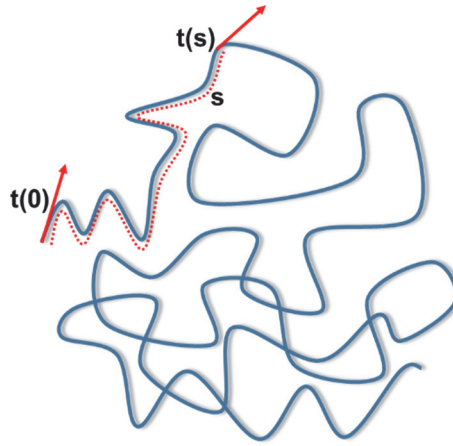


Figure 2-8 A worm-like-chain.

l_p is defined as the characteristic length over which the correlation of the direction of the tangent vector is lost. Thus, it is a parameter that represents the stiffness of the polymer chain.

$$\langle t(0) \cdot t(s) \rangle = \exp\left(-\frac{s}{l_p}\right) \quad 2.30$$

Meanwhile, the persistence length is also linked with the bending modulus (B) of a polymer chain⁹⁴:

$$B = k_B T l_p \quad 2.31$$

Based on these, the energy associated with bending an elastic rod by angle of θ can be described as:

$$E_{bending} = k_B T \frac{B}{2L} \theta^2 = \frac{k_B T l_p}{2} \int_0^L \left| \frac{d\overrightarrow{t}(s)}{ds} \right|^2 ds \quad 2.32$$

This question mathematically relates the persistence length with the thermal energy of the chain. Then, the mean square end-to-end distance can be obtained⁹⁴:

$$\begin{aligned} \langle R^2 \rangle &= \langle R \cdot R \rangle = \left\langle \int_0^L t(s) ds \cdot \int_0^L t(s') ds' \right\rangle = \int_0^L ds \cdot \int_0^L \langle t(s) \cdot t(s') \rangle ds' \\ &= \int_0^L ds \cdot \int_0^L \exp\left(-\frac{|s-s'|}{l_p}\right) ds' = 2l_p L \left(1 + \frac{l_p}{L} \left(e^{-\frac{L}{l_p}} - 1\right)\right) \end{aligned} \quad 2.33$$

When the contour length of the polymer is much larger than the persistence length ($L \gg l_p$), the term $e^{-\frac{L}{l_p}} = 0$. Thus, parameter of persistence length can be linked with the Kuhn length in FJC model, where $l_{Kuhn} = 2l_p$. The relationship of the restoring force and end-to-end distance can be described:

$$F = \frac{k_B T}{l_p} \left[\frac{1}{4 \left(1 - \frac{x}{L}\right)^2} - \frac{1}{4} + \frac{x}{L} \right] \quad 2.34$$

This is the basic form of the mathematical expression that relates the force with end-to-end distance using WLC model. It was widely applied to analyze the experimental SMFS results. However, deviation of this model with the experimental data is found when force is large. Odijk added an enthalpic bond stretching modulus K_0 to this model and gave the following mathematical relationship:

$$x = L_0 \left[1 - \frac{1}{2} \left(\frac{k_B T}{F l_p} \right)^{\frac{1}{2}} + \frac{F}{K_0} \right] \quad 2.35$$

Later on, the model was further modified by Want et.al.

$$F = \frac{k_B T}{l_p} \left[\frac{1}{4 \left(1 - \frac{x}{L}\right)^2} - \frac{1}{4} + \frac{x}{L} - \frac{F}{K_0} \right] \quad 2.36$$

The modified model shows good agreement with the experimental data both in low or relatively high force range.

2.4.2 Single polymer chain mechanics

The emergence of the SMFS technique allows the experimental determination of the response of single molecules under external mechanical force. The results provide insights into its elasticity and the behavior of a single polymer chain at solid-liquid interface. Such experiments are not resolvable by traditional macroscopic techniques⁹⁵. Typical setup of SMFS experiment that focuses on the investigation of single-polymer chain at the solid-liquid interface includes a polymer modified AFM probe and an interested substrate. The attractive interaction between the polymer and substrate in liquid promotes the adhesion of polymer on solid-liquid interface. The response of the polymer chain adsorbed on the interface upon external mechanical perturbation is probed and recorded when the polymer modified AFM tip approaches and retracts continuously.

Up to now, two distinctively different situations has been encountered: Polymer stretching or polymer chain peeling. The polymer chain stretching is typical when the studied polymer anchors on the substrate or the interaction is very strong. Much longer relaxation time compared to the time scale of the experiment leads to the occurrence of saw-teeth feature in the collected force curves. Important information such as the elasticity of the polymer chain or the binding of cosolutes on macromolecule can be obtained by analyzing the results with suitable theoretical models. On the other hand, when the relaxation time for polymer-substrate interaction is smaller than that of the SFMS experiment, the obtained force curves represent the breaking of the polymer-substrate interaction can be used to quantify the equilibrium interactions between a single polymer chain and substrate in solution.

In this thesis, the study is focusing on the second scenario as only the polymer-peeling event provides opportunities to determine the equilibrium single-molecule adhesion force. The characteristic plateau feature in the collected force curves indicates the polymer chain moves freely when peeling from substrate³⁴. This is usually called as frictionless assumption⁵⁰⁻⁵¹. It means that the macromolecule on the surface cannot support a net horizontal friction force and be peeled from substrate at an average angle of 90 ° with respect to the substrate⁵¹. Such scenarios have been found on flat homogenous substrates, such as diamond surfaces⁶⁶, self-assembled monolayers⁹⁶,

silica surfaces⁹⁷ and gold surfaces³⁴. Thus, the influence of charge effect^{67, 98-99}, the hydrophobic effect⁶⁶ and surface roughness⁶⁹ on single-molecule interaction were able to be studied.

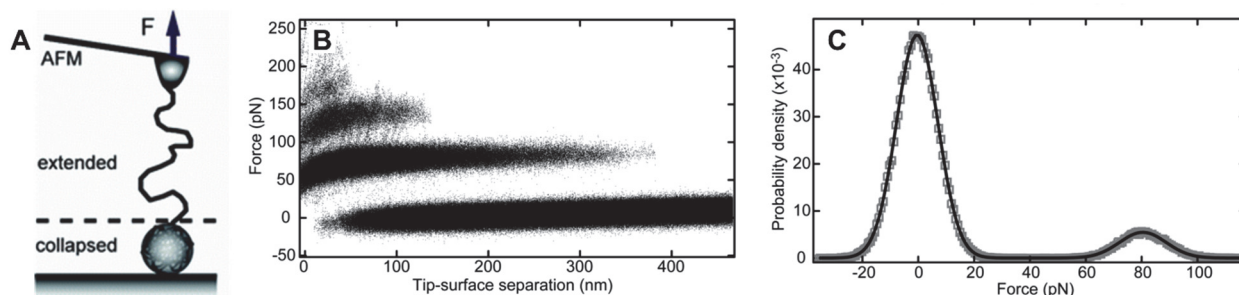


Figure 2-9 (A) Illustration of pulling a polymer chain out of its collapsed globule; (B) superposition of ~ 300 force-extension curves, which indicates the pulling of several single chains simultaneously; (C) Histograms showing the force distribution of baseline and the first step¹⁰⁰.

It is worth pointing out that polymer chain peeling event is not the only case that plateau feature can be observed in the collected force curves. Walker and his coworker reported that plateau event is also typical when polymer chain is pulling out of its collapsed globule in poor solvent¹⁰⁰ (Figure 2-9). Thus, when a plateau force is obtained in the experiment, it is important to find out the real physical process during the SMFS experiment. In polymer chain peeling cases, the polymer-substrate bond is broken when the polymer is peeling from the substrate. Therefore, the plateau height is dependent on substrate, which leads to a substrate dependent single-molecule adhesion force. On the other hand, when polymer chain is pulled out of its collapsed globule, the single-molecule force is substrate independent as the force only relies on the solvent-solvent, solvent-monomer and monomer-monomer interactions¹⁰⁰. Thus, in SMFS experiment, the dependence of the single-molecule force on the substrate can be used as a criterion to judge which scenario should be used to describe the underlying physical process.

To be noted, when polymer adsorbs on the solid-water interface, only part of the chain lay flat on the interface. The rest part of the polymer chain is either in loops conformation or in tails conformation¹⁰¹. Theories have been developed to understand the size statistical distribution of train, loop and tail¹⁰². However, only the polymer in train conformation can be probed during peeling process. Since the loop is already in the solution, no force can be selected.

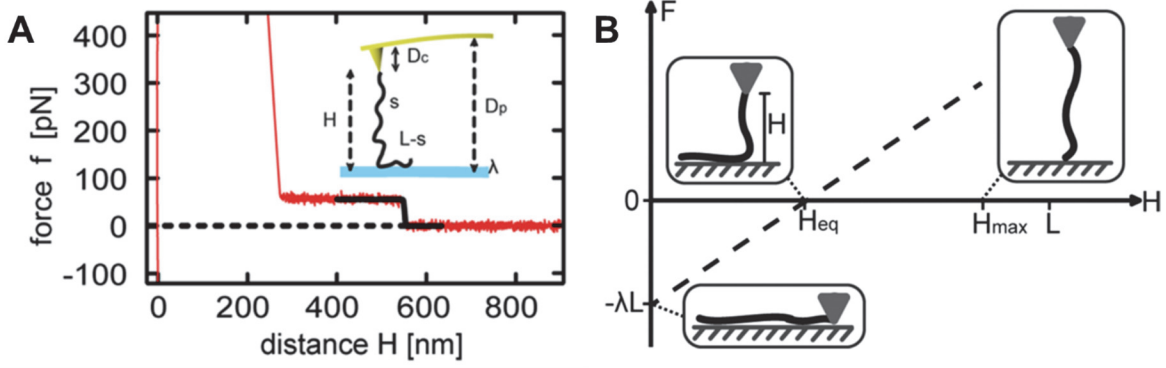


Figure 2-10 (A) Typical force curve obtained in SMFS experiment representing single-molecule peeling event. The inset shows the experimental setup; (B) The peeling of the polymer chain from substrate and the dependence of free energy on the pulling distance H ⁹⁵.

During the SMFS experiment, the free energy of the system is composed of three terms: the adhesion free energy of the adsorbed portion of the polymer chain, the entropic free energy of the stretched portion of the chain and the elastic free energy of the deflected AFM cantilever⁹⁵. The adsorption free energy can be obtained as the product of the adsorption free energy per unit length, λ , and the contour length of the polymer chain portion that adsorbs on the substrate, $L-s$.

$$G_{ad} = \lambda(L - s) \quad 2.37$$

where L is the contour length of the whole polymer chain and s is the contour length of the polymer chain portion that is stretched. The entropic free energy is obtained by integrating the entropic force f of the stretched polymer chain portion from the initial state with almost no extension to the final extension H .

$$G_{en} = \int_0^H f(H'/s) dH' \quad 2.38$$

The function of $f(H'/s)$ is the mathematical relationship between the entropic stretching force and the end-to-end distance. It is dependent on the model utilized in the analysis. Usually, the WLC model is believed appropriate to describe the polymers with certain stiffness. The relationship is given by:

$$\frac{Fl_p}{k_B T} = \frac{1}{4 \left(1 - \frac{H}{s}\right)^2} - \frac{1}{4} + \frac{H}{s} \quad 2.39$$

The last portion for the total free energy of the system is the elastic free energy of the cantilever. This form of free energy can be determined using the spring constant of the cantilever (K) and the deflection of the cantilever:

$$G_{el} = \frac{1}{2} K x^2 = \frac{1}{2} K (D_p - D_c - H)^2 \quad 2.40$$

The relationship between the adhesion free energy per unit length λ and the peeling force can be obtained by minimization of the free energy G with respect to the contour length of the desorbed portion of the polymer chain⁹⁵.

$$\frac{dG}{ds} \big|_{s_{min}} = \frac{d(G_{ad} + G_{en} + G_{el})}{ds} = \lambda + \int_0^{\frac{H'}{s_{min}}} f\left(\frac{H'}{s}\right) d(H'/s) - \frac{H}{s_{min}} f\left(\frac{H}{s_{min}}\right) = 0 \quad 2.41$$

Thus, when the equation is rearranged and WLC model is used, we have:

$$f\left(\frac{H}{s_{min}}\right) = \frac{s_{min}}{H} \lambda + \frac{s_{min}}{H} \int_0^{\frac{H'}{s_{min}}} f\left(\frac{H'}{s}\right) d(H'/s) \quad 2.42$$

It is evident from the equation that the peeling force is always larger than the adhesion free energy per unit length as part of the energy is stored as entropic free energy in the stretched polymer chain. In general, the value of $\frac{H}{s_{min}}$ is smaller than 1. However, it may approach and close to 1 when the force is large, which effectively stretches the polymer chain to its contour length.

2.4.3 Hydrophobic hydration

The process of peeling a polymer chain from substrate leads to the transfer of the polymer from solid-water interface to water. At this time, the hydration of the polymer chain occurs. In general, the hydration of a molecule can be defined as the process to insert a molecule into water phase.

Usually, the hydration process can be divided into two steps: 1) the creation of cavity to accommodate the foreign molecule and 2) placing the molecule into the cavity. The first step is energetically unfavorable as the breaking of water-water interactions and reduction of

conformational freedom of the water molecules are encountered. On the other hand, the second step is usually energetically favorable as attractive interactions such as hydrogen bonding, electrostatic, polar and dispersive interactions are established.

In this thesis, the term of hydrophobic hydration needs to be introduced. As the name implies, it is defined as the process that insert a hydrophobic solute into water. It is a special case for hydration. In this case, the cavitation free energy dominates the overall hydration free energy because the attractive interactions between the hydrophobic solute and polar water is weak. The determination of the free energy associated with the hydrophobic hydration is found to be complicate. A size dependent hydration phenomena is predicted¹⁰³ and observed¹⁰⁴. The small solute case is shown in Figure 2-11A. In the graph, methane is used as a model small hydrophobic molecule. Due to the presence of methane, the water molecules are excluded from the space where methane occupies. As the volume is small, the water molecules does not have to loss the hydrogen bonding to stay at the interface. The water molecule only need to reorient to cover the surface of solute, which allows the maintaining of the hydrogen-bonding. However, distinctly different situation is encountered in large solute case. The presence of large surface does not allow the survival of all hydrogen bonding. As a result, a fraction of the hydrogen bonding is lost. Usually, for the water molecules near the extended hydrophobic surface, approximately one hydrogen bonding is lost per water molecule.

The idea, which advocates that the hydrogen bonding of water molecules near a small hydrophobic particles is maintained and partially lost when close to a large hydrophobic surface was first proposed by Frank Stillinger many years ago³⁰. It provide physical basis for the understanding of hydrophobic effects.

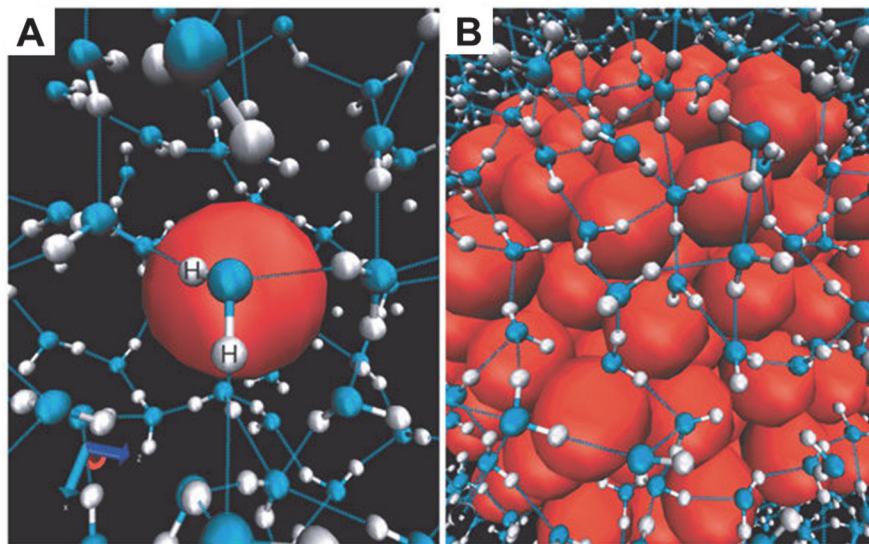


Figure 2-11 Configurations of water molecules near hydrophobic cavities obtained with molecular-dynamics simulations¹⁰³.

The term of free energy change ΔG can be utilized to predict if one process is likely to happen or not. In the case of solvating a molecule, the free energy change ΔG is the reversible work for the solvent to solvate the solute. At room temperature and 1 atm pressure, the free energy difference between water in its vapor and liquid phase is relatively small compared to its thermal energy. This ensures that the cavities in water has an interface similar to that between liquid and vapor³⁰, which was confirmed recently by theoretical analysis^{30, 32} and simulation^{19, 31, 38, 46}. Then the free energy cost to hydrate the spherical cavity of radius R can be estimate as $\Delta G = 4\pi R^2\gamma + (\frac{4}{3})\pi R^3p \approx 4\pi R^2\gamma$, where p refers to the pressure and γ is the water-vapor surface tension. For macroscopic cavities, the contribution of pressure-volume term is significant. However, it is negligible when the size of the cavity (R) is small and less than several nanometers at room temperature.

In the case of large solute size, the hydrophobic solute induces the presence of extended hydrophobic-water interface. As a result, the solvation free energy includes a component which scales with the surface area. However, the hydration of a small solute is completely different. Its hydration only leads to the re-ordering of hydrogen bonding. The re-ordering only influence the surrounding water within about one correlation length, which gives a solvation free energy scales

more likely to the volume rather than the surface area of the solute. Thus, the hydration free energy ΔG is proportional more accurately to R^3 than to R^2 .

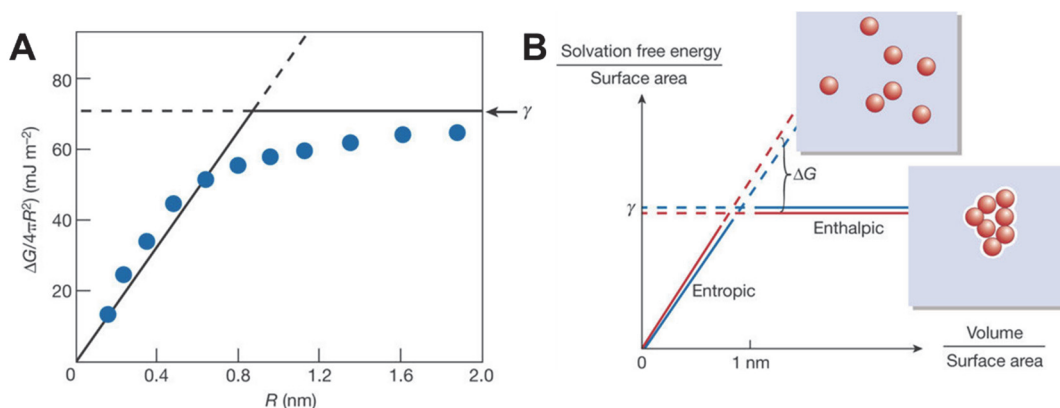


Figure 2-12 (A) Solvation free energy for a spherical cavity in water as a function of the cavity size¹⁰³.

The Figure 2-12 clearly shows how the normalized solvation free energy changes with the solute size. The solvation free energy grows linearly with the solute volume when its size is small. In the case that a large solute is used, the hydration free energy is proportional to the exposed surface area. The crossover region is about 1 nm. However, one has to be clear that the transition is collective rather than a sharp and sudden phase transition.

2.5 The interaction between stimuli-responsive polymer and hydrophobic-water interfaces

The concept of stimuli-responsive polymer has been proposed for years. It is a special type of polymer which is able to sense the environmental stimulus and respond to it in its own way. Up to now, various kinds of switching polymer were developed and synthesized⁷⁵. The effective stimuli can be light¹⁰⁵, salt²⁻³, temperature¹⁰⁶⁻¹⁰⁷, pH¹, CO₂¹⁰⁸ and so on. Various polymeric materials for practical applications have been developed based on these stimuli-responsive polymers, which couple the stimuli-responsive behavior with the control of molecular activities, such as the adhesion of polymer to solid-water interface⁶. Such behavior of polymers is of paramount importance in many applications, including treatment of medical device surfaces, controlled attachment/detachment⁷⁸⁻⁸⁰ and self-cleaning⁸¹. Thus, understanding the interaction between a single stimuli-responsive polymer chains with interested solid-water interface is important to reveal the fundamental interactions and provide updated insights.

Meanwhile, the main driving force that promotes the interaction between polymer and substrate is highly desired to be understood and their individual contribution be quantified. Besides the common van der Waals interactions and electric double layer interactions, hydrophobic attraction is also important. Though it has been investigated for decades, its role in molecular scale and more importantly, the underlying physical mechanism remains to be explored. The above two points consist the backbone of this thesis, which strives to provide updated single-molecule interaction of stimuli-responsive polymer with model hydrophobic surfaces. Furthermore, quantify the role of hydrophobic attraction at molecular scale.

Besides that, the SMFS was also utilized to find an appropriate functionalization polymer for the effective exfoliation of MoS₂ into single-layer for its practical applications. The results confirmed that this approach is efficient and effective. Meanwhile, the results demonstrate that the proposed approach can be extended to other applications where interaction between polymer and solid surface in liquid is important.

Chapter 3

Probing Single-Molecule Adhesion of a Stimuli Responsive Oligo (ethylene glycol) Methacrylate Copolymer on a Molecularly-Smooth Hydrophobic MoS₂ Basal Plane Surface

3.1 Introduction

The chalcogenide derivatives of Molybdenum (Mo) have been shown to be versatile building blocks of high performance functional materials for various applications, including nanotribology¹⁰⁹, photocatalysis¹¹⁰⁻¹¹¹, drug delivery¹¹²⁻¹¹³, catalysis of hydrogen evolution reactions (HER)¹¹⁴⁻¹¹⁵ and power generator¹¹⁶, *etc.* Nano-size MoS₂ with one- or two- dimensional structures on the other hand were found to be necessary for practical use since interesting properties such as optical¹¹⁷⁻¹¹⁸, mechanical¹¹⁹, electronic and chemical properties¹²⁰ of nano-MoS₂ disappeared in the corresponding large 3D bulk materials. Furthermore, MoS₂ flakes in nano- or micron-size with one or few molecular layer thickness favor applications concerning size limitations and/or pursuing high efficiency.

Such unique characteristics of MoS₂ has led to the development of several exfoliation methods to prepare single- or few layered MoS₂ flakes. Lithium intercalation is a typical chemical exfoliation method¹²¹. The lithium inserted into the MoS₂ layers reacts with water to generate the hydrogen gas at the interface that promotes the exfoliation process. Ultrasonication has also been used to exfoliate MoS₂ in the presence of appropriate organic solvent¹²²⁻¹²³. This protocol is able to produce mono- or multilayered MoS₂ sheets of small lateral sizes¹²⁴. Recently, milling combined with ultrasonication has been shown to produce high concentration monolayer MoS₂ flakes¹²⁵.

Although the exfoliated MoS₂ flakes provide an excellent platform for applications, further proper surface modification by organics has been shown to be critical. A MoS₂-graphene composite sheet of high lithium storage capacity was developed for lithium-ion batteries. MoS₂-graphene hybrid material in the robust paper form was produced with addition of poly(ethylene oxide) (PEO) while loose powder which is not suitable for further application was encountered without any polymer additives¹²⁶. Drug carrier for effective cancer therapy is another application field that nano-size MoS₂ has been employed¹²⁷. In particular, Doxorubicin was loaded on Chitosan-modified nano-MoS₂ flakes and applied as chemotherapeutic drug nanocarriers. It provided combined chemotherapy and photothermal therapy, showing promising results on cancer treatment¹¹². In the experiment, the results indicated that the biocompatibility and stability of the MoS₂ nanosheets, which were critical for drug carrier applications, were improved by modification of Chitosan.

Due to the importance of polymer modification in tailoring the properties of nano-size MoS₂ for specific applications, a clear understanding of the polymer-MoS₂ interaction especially down to

single-molecule level would be highly desired to optimize the current systems and promote future development. Recently, it was reported that the nonpolar segments of protein can firmly bind to MoS₂ surface¹²⁸. Thus, it is interesting to know how does the hydrophobicity of the polymer influences the final polymer-MoS₂ interaction.

To address these problems, in this study, the polymer-MoS₂ interaction down to single-molecule level was studied. The oligo (ethylene glycol) methacrylate copolymer which has been proven to be promising polymer for biomedical applications¹²⁹ was used as a model polymer. This well-known stimuli-responsive polymer is composed of a hydrophobic backbone of methacrylate and oligo ethylene glycol (OEG) side chains with varying lengths. The OEG side chains form H-bonds with surrounding water molecules, which are regarded as the main factor that is responsible for the hydrophilicity of the polymer¹³⁰⁻¹³¹. The overall behavior of the copolymer, especially at high polymer concentration in water, depends on the competition of polymer-polymer interaction and polymer-water interaction. Thus, the oligo (ethylene glycol) methacrylate copolymer would undergo a hydrophilic to hydrophobic transition¹³²⁻¹³⁴ in response to environmental stimuli (*e.g.* temperature, salt) due to the suppressed hydration of side chains^{129, 135-138}.

By using this copolymer, we aim to quantify its single-molecule interaction on MoS₂ basal plane surface, as well as exploring the influence of the hydrophobicity of the polymer on the single-molecule adhesion force with MoS₂ basal plane surfaces. The emergence of the Single Molecule Force Spectroscopy (SMFS) provides an excellent platform to probe the single-molecule adhesion force of a polymer chain on various substrates^{25, 27, 34, 67, 83}. In this study, it was used to characterize the single-molecule adhesion force of oligo (ethylene glycol) methacrylate copolymer on a MoS₂ basal plane surface. Force curves with characteristic equilibrium desorption features were obtained for the first time between a copolymer and hydrophobic MoS₂ basal plane surface. The heights of the plateaus were used to determine the strength of the single polymer chain-MoS₂ interaction.

3.2 Materials, characterization and methods

3.2.1 Materials

The water used in the experiment was particle free and purified with Milli-Q system. (3-Aminopropyl) triethoxysilane (APTES), N-Hydroxysuccinimide (NHS), N-(3-Dimethylaminopropyl)-N'-ethylcarbodiimide hydrochloride (EDC), triethylamine (Et₃N), copper

(I) bromide (Cu(I)Br), dioxane, N,N-Dimethylformamide (DMF), α -Bromoisobutyryl bromide (BIB), 2,2'-bipyridyl (bpy), di(ethylene glycol) methyl ether methacrylate (MEO₂MA, 95%, MW 188.22), poly(ethylene glycol) methyl ether methacrylate (PEGMA, average Mn 500), 4,4'-Azobis(4-cyanovaleric acid) (ACVA) and the RAFT agent 2-(Dodecylthiocarbonothioylthio)-2-methylpropionic acid were purchased from Aldrich. The silica wafer was purchased from nanoFAB in University of Alberta. The bulk crystalline MoS₂ used in the study is a pure mineral purchased from WARD's science.

3.2.2 Synthesis of oligo (ethylene glycol) methacrylate copolymer (P(MEO₂MA_x-co-PEGMA_y), x:y=10:1) and polymer brush.

The copolymer was synthesized *via* RAFT polymerization and the detailed procedure can be found elsewhere³⁴. The monomers were purified by passing through a neutral aluminum oxide column to remove the inhibitors. In a typical experiment, 3.2 g di(ethylene glycol) methyl ether methacrylate (MEO₂MA) and 0.8 g poly(ethylene glycol) methyl ether methacrylate (average Mn 500) (PEGMA or MEO₈MA) were mixed with 8 mL dioxane (solvent). After that, 3 mg 2-(Dodecylthiocarbonothioylthio)-2-methylpropionic acid (RAFT agent) and 1.1 mg ACVA (initiator) were added into the flask. The function of the RAFT agent used in the synthesis is critical for the polymerization to be performed in pseudo living polymerization manner rather than traditional radical polymerization with high possibility of chain termination. The flask was then sealed and purged with nitrogen for 1 h to remove the oxygen inside. After polymerized for 24 h in 75 °C, the system was exposed to air. Milli-Q water was added to dissolve the gel-like polymer solution. The polymer was further purified by dialysis against Milli-Q water and dried by lyophilization.

The stimuli-responsive oligo (ethylene glycol) methacrylate copolymer brush with same composition was grown on silica surface using SI-ATRP according to the method described by Brown et al¹³⁹. In general, the silica wafer was cleaned and oxidized with plasma for 15 min. The resultant wafer was placed in a glass vial containing 50 μ L APTES and 20 μ L Et₃N. The vial was then sealed and left at room temperature for 2 h. After that, the wafer was placed in an oven for 1 h to crosslink the APTES. The APTES modified silica wafer was further modified in solution containing BIB (0.37 cm³, 3 mmol, 0.05M), Et₃N (0.41 cm³, 3 mmol, 0.05M) and CH₂Cl₂ (60 cm³) to form an initiator monolayer. MEO₂MA (MW 188.22) (3.2g, 17 mmol) and PEGMA (average

Mn 500) (0.8g, 1.6 mmol) was dissolved in DMF/Water (V/V=1:1) at room temperature and degassed by continuous purging with dry argon. Then, bipy (234 mg, 1.5 mmol), Cu(I)Br (107 mg, 0.75 mmol) was added to this solution. The mixture was further stirred and degassed. The initiator coated silica surface was sealed in flask and degassed (3 high-vacuum pump/Ar refill cycles). The solution was syringed into the flask to submerge the sample completely. After 20 h, the sample was removed and washed with DI water and dried under a stream of N₂. The sample was stored under N₂ until needed.

3.2.3 Polymer analysis.

THF phase size-exclusion chromatography was performed in GPC system equipped with Styragel HR1 GPC column and light scattering detector (ELSD 2000). A series of polystyrene standards were used for GPC calibration. The polymer was dissolved in 5 mg/L and 10 μ L was injected at a flow rate of 0.5 mL min⁻¹. The design molecular weight of the polymer is 330 kDa while the measured M_w= 200 kDa with PDI=1.7. ¹H NMR was performed in 10 mg/mL in CDCl₃ on a 200 MHz NMR spectrometer (Bruker).

3.2.4 Transmittance measurement.

The cloud point representing the lower critical solution temperature (LCST) property of the copolymer was characterized using a UV-Vis spectrometer (Varian Carey 50). In general, the polymer was dissolved at 4 mg/ml in phosphate buffer solution (PBS, pH 7.4) containing different concentration of NaCl. The solution was quickly heated up to 52.5 °C in 30 s and the transmittance was then monitored using the wavelength of 400 nm during the cooling process.

3.2.4 Cantilever modification.

Rectangular silicon nitride cantilevers purchased from Bruker (MLST) were used in the experiments. The cantilevers were functionalized with (3-Aminopropyl) triethoxysilane (APTES) according to the well-developed procedure³⁴. The amine-silanized cantilevers were deprotonated by immersing in sodium borate buffer solution (150 mM, pH 8.5) for 30 min. Then, 0.5 mL 4 mg/mL poly(oilgo(ethylene glycol)) copolymer solution was mixed with 0.5 mL sodium phosphate buffer solution(10 mM phosphate, 137 mM NaCl, pH 7.4) (transparent solution). After that, 50 mg EDC and 50 mg NHS were added. The coupling reaction of the polymer and cantilever proceeded for 1 h in room temperature. To be noted, the chemical linkage (amide group) that links

the polymer chain to APTES modified AFM cantilever tend to hydrolyze when is exposed to water. Thus, the polymer linked cantilever was used immediately after the modification process. The shelf life can be extended to 2 days if stored in chloroform.

3.2.5 Single Molecular Force Spectroscopy (SMFS).

The SMFS measurement was performed on Multimode 8 AFM using picoforce scanner with a fluid cell. The spring constant of the cantilever was calibrated before or after each experiment using equipartition theorem⁴⁹. The cantilevers used in the experiment were bought from Bruker (MLCT) and the typical spring constant was around 0.03 nN/nm with a mean resonance frequency of 10 kHz. The MoS₂ was peeled with Scotch tape to expose the clean surface before each experiment. The sampling rate was 6 kHz and various pulling velocity and surface delay time were used. Data were then baseline corrected and analyzed. Each experiment was repeated at least 3 times with different cantilevers in different days.

3.2.6 Contact angle measurement.

The samples were placed on top of glass slides immersed in a quartz cuvette. The cuvette was then filled with heptane. Typically, a water droplet with various concentration of NaCl (approx. 5 μ L) was generated at the tip of metal needle and brought in contact with the sample surface. The needle was then retracted and the contact angle measured. Contact angle equilibrium typically took 10 to 1000 s depending on the solution concentration. The plateau regions of the curves were taken as equilibrium contact angles. The reported values are average ones with standard error obtained from at least three different experimental results.

3.3 SMFS results of oligo (ethylene glycol) methacrylate copolymer in solution with various NaCl concentration

The layered structure of crystalline MoS₂ with molecularly-smooth basal planes¹⁴⁰ was characterized by Atomic Force Microscopy (AFM) technique and a typical AFM image obtained in air is shown in Figure 3-1A. The root mean squared (RMS) roughness of MoS₂ within the same layer is less than 0.1 nm, as calculated from a typical 1000 x 1000 nm scan size AFM image. The basal plane surface of MoS₂ is naturally hydrophobic with a water contact angle in the range of 80 - 90°¹⁴¹. A fresh molecularly smooth MoS₂ surface was prepared by peeling off the top layer of the surface with Scotch tape immediately prior to the experiment. To increase the possibility of

observing polymer detachment event, the Si_3N_4 AFM cantilevers were chemically modified and linked with oligo (ethylene glycol) methacrylate copolymer chains (Figure 3-1B) before the SMFS experiment (detailed information can be found in experimental section). Typically, an oligo (ethylene glycol) methacrylate copolymer functionalized AFM tip was first lowered onto a MoS_2 surface in the liquid at constant rate of 500 nm/s with a maximum load of 2 - 4 nN and then retracted at the same rate. Both approaching and retracting force curves were recorded in each force measurement cycle. In the data analysis, the retracting force curves were baseline corrected.

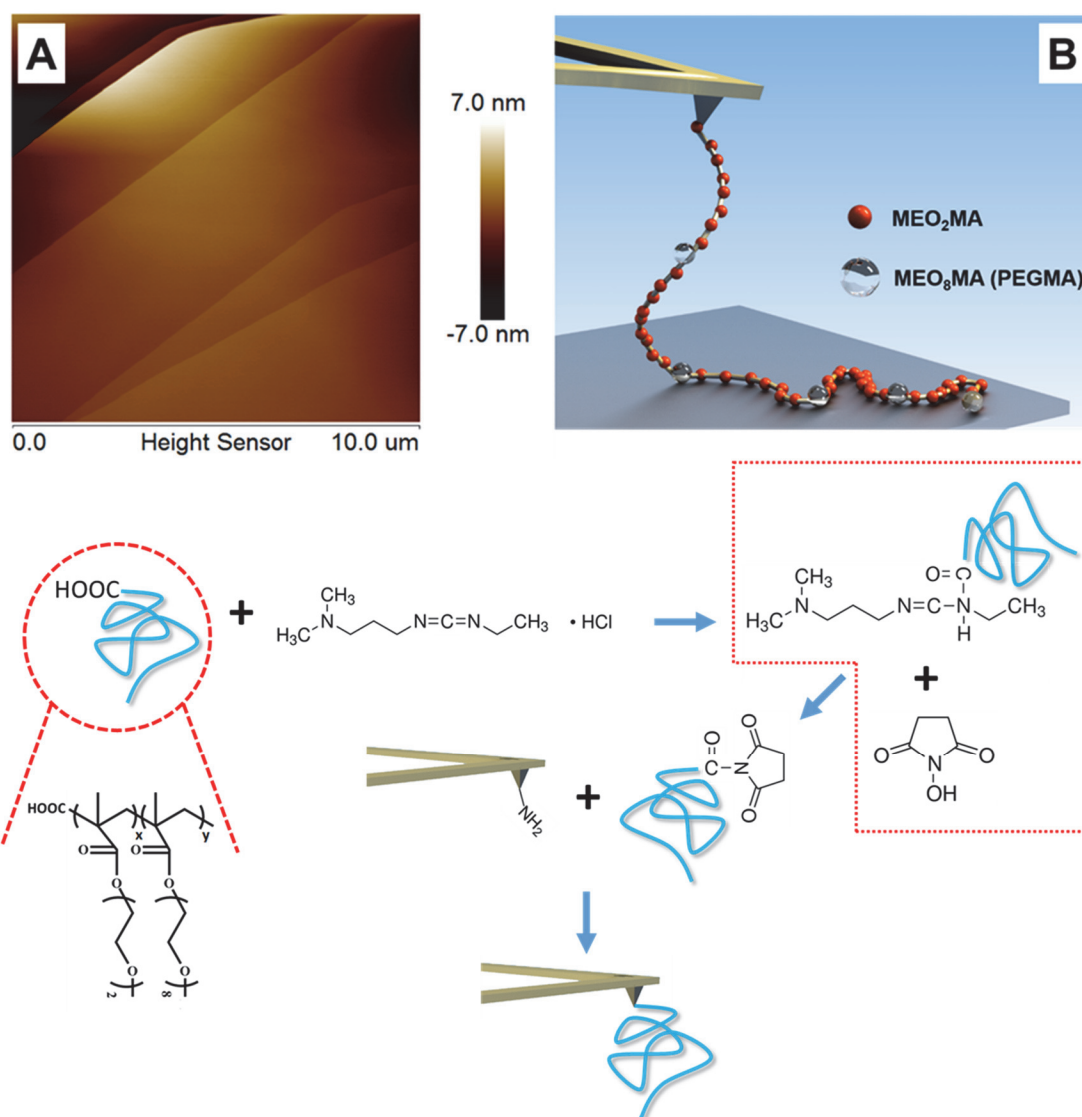


Figure 3-1 (A) Atomic Force Microscope (AFM) image of a MoS_2 basal plane surface in air. (B) Schematic representation of detaching an oligo (ethylene glycol) methacrylate copolymer chain from a MoS_2 substrate in an aqueous solution. (C) The chemical modification process to link the

polymer to the ATM tip.

As is widely accepted, the attractive interaction between the polymer and the substrate promotes a part of the polymer chain to lay flat on the substrate in aqueous solutions^{70, 142}. When the cantilever is retracted during the SMFS experiment, the polymer chains previously adhered to the substrate are forced into the solution, initiating the peeling process of the polymer from pre-adhered substrate (Figure 3-1B). Usually, a plateau of a constant force is observed when the polymer chain detaches from the substrate. Since the binding or rebinding of the polymer segments on surface occurs much faster than the experimental sampling rate¹⁴³, the plateaus in the staircase-like force curves are characteristics of equilibrium desorption process. The height of the plateaus can be interpreted as the adhesion force between a single polymer chain and the substrate³⁴. It is noted that when a macromolecule adsorbs on a solid substrate, there is a distribution of the loops and trains¹⁰². The trains contain the monomers that are in direct contact with the solid substrate while the loops are the segments that are out into the solution. In the experiment, the interaction of the polymer-substrate is quantified by peeling a single polymer chain from the interface. Thus, the presence of trains on the interface is a prerequisite for our measurement. For loops, since they are already in the solution, no valuable information on single-molecule polymer-substrate interaction can be obtained. However, we did obtain force curves that were representative of the presence of loops (two ends of the loop are in direct contact with the substrate). The presence of the loops would lead to the U shape like features on the collected force curves. In particular, the force would drop when one end of the loop (previously on the substrate) was forced into solution. Meanwhile, the force increased and then formed a plateau when the other end of the loop, which previously laid flat on the substrate, was pulled and peeled from the substrate. However, the possibility of such an event is relatively too low to obtain reliable statistics.

The interaction force curve of the stimuli-responsive polymer with MoS₂ basal plane surface in the presence of 0.14 M NaCl aqueous solution as shown in Figure 3-2 was used as an example to illustrate how we obtained the typical adhesion force between a single polymer and substrate from raw data. A typical force curve obtained in the SMFS experiment after baseline correction is shown in Figure 3-2A. The multiple steps on the staircase-like force curve indicate that multiple polymer chains were probed during the experiment. The detailed peeling process of three polymer chains that is associated with the force curve is shown schematically in Figure 3-2B. In the initial stage,

three polymer chains are in contact with the substrate as shown in Case 1 and the probed force corresponding to peeling three polymer chains is represented by the first plateau (step) in Figure 3-2A. The force curve jumps to the second plateau at approximately 2/3 force magnitude of the first plateau (Figure 3-2A Case 2) at the point when one of the three polymer chains completely detaches from the substrate. As the cantilever is further retracted from the substrate, the measured force plateau represents peeling off the two remaining polymer chains from the substrate until detaching the second polymer chain shown as a sharp decrease in the adhesion force to the third plateau (Case 3) where the force between a single polymer chain and MoS₂ is measured (Figure 3-2A). Finally, baseline was obtained after a third sharp decrease in the adhesion force, marked as the detachment of the last polymer chain from the surface (Case 4).

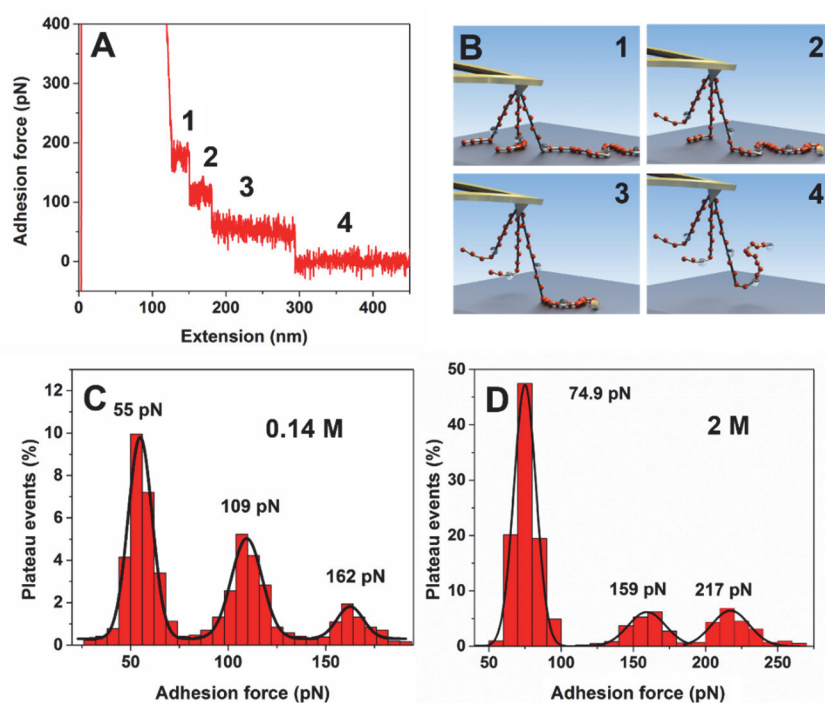


Figure 3-2 Single molecular adhesion (detachment) force measurement: (A) A typical force curve of an AFM cantilever with attached oligo (ethylene glycol) methacrylate copolymers was retracted from MoS₂ basal plane surface at 500 nm/s in the presence of 0.14 M NaCl background solution. (B) Schematics showing multiple polymer chains probed during the experiment. Histogram of adhesion forces in 0.14 M NaCl (C) and 2 M NaCl (D). The last three detachment events in the force-extension curve were selected and analyzed although more plateaus were observed for some of the force curves.

As shown in Figure 3-2C, the trimodal distributions represent multiple polymer chains being involved in the detachment process. In the experiment, a considerable amount (more than 2000) of force curves akin to the one shown in Figure 3-2A were collected using different cantilevers to obtain statistically representative adhesion force distributions. The fitting of the histogram using Gaussian equation provides the mean typical adhesion force for the peeling events of single, double and triple chains. The detachment force of a single, double and triple polymer chains from MoS₂ surface measured from a Gaussian distribution fitting is 55 ± 6 pN, 109 ± 8 pN and 162 ± 7 pN, respectively. The near integral multiple of the adhesion force demonstrates that the multiple chains were indeed probed in the measurement.

One may argue that the measured plateau does not necessarily represent the detachment force of a polymer chain from the substrate since similar force plateau was reported when stretching (forcing out) a hydrophobic polymer chain from its collapsed globule in an aqueous solution^{100, 144}. To confirm the measured force plateau is indeed representative of adhesion force between the polymer chains and substrate surface, the SMFS measurement was performed on various surfaces in 2 M NaCl aqueous solutions, in which the force to stretch a polymer chain from its globule should be the same. At this NaCl concentration, the polymer tends to form a collapsed globule, which offers the highest probability to measure the force of pulling out a single polymer chain by stretching it in the given solution^{100, 144}. As shown in Figure 3-3, for oligo (ethylene glycol) methacrylate copolymer in 2 M NaCl solution, the adhesion force is around 116 ± 11 pN on PTFE surface, in comparison to 75 ± 8 pN on MoS₂ surface. Meanwhile, no adhesion force was detected on hydrophilic silica surface. However, it is important to check the conformation of the polymer are similar in both conditions to reach the conclusion that the we are observing polymer chain peeling event rather than polymer chain pulling out of its collapsed globule. The distributions of the plateau length for last polymer detachment event on MoS₂ and PTFE surfaces were shown in Figure 3-3C and 3D. Meanwhile, the distribution of the pull length in the 1 mM solution is shown below as well (Figure 3-3E). In solution containing 1mM NaCl, the distribution of the pull length was bimodal with one population centered on 50 nm and the other at 120 nm. When 2 M NaCl solution was used, the bimodal distribution was also observed. However, the plateau length distribution shifted to higher values. The bimodal peaks were found centered at 100 and 250 nm. These results illustrate that the polymer does not adopt collapsed conformation on the MoS₂-liquid interface in high salt (2 M) background solutions. As the plateau length distribution for the same polymer on

PTFE surface in 2 M solution was found higher than that of MoS₂, the result indicates that the conformation states of the polymer are similar on these two studied surfaces. Thus, it is safe to conclude that the plateau force observed in this study originates from the polymer chain peeling from MoS₂-water interface.

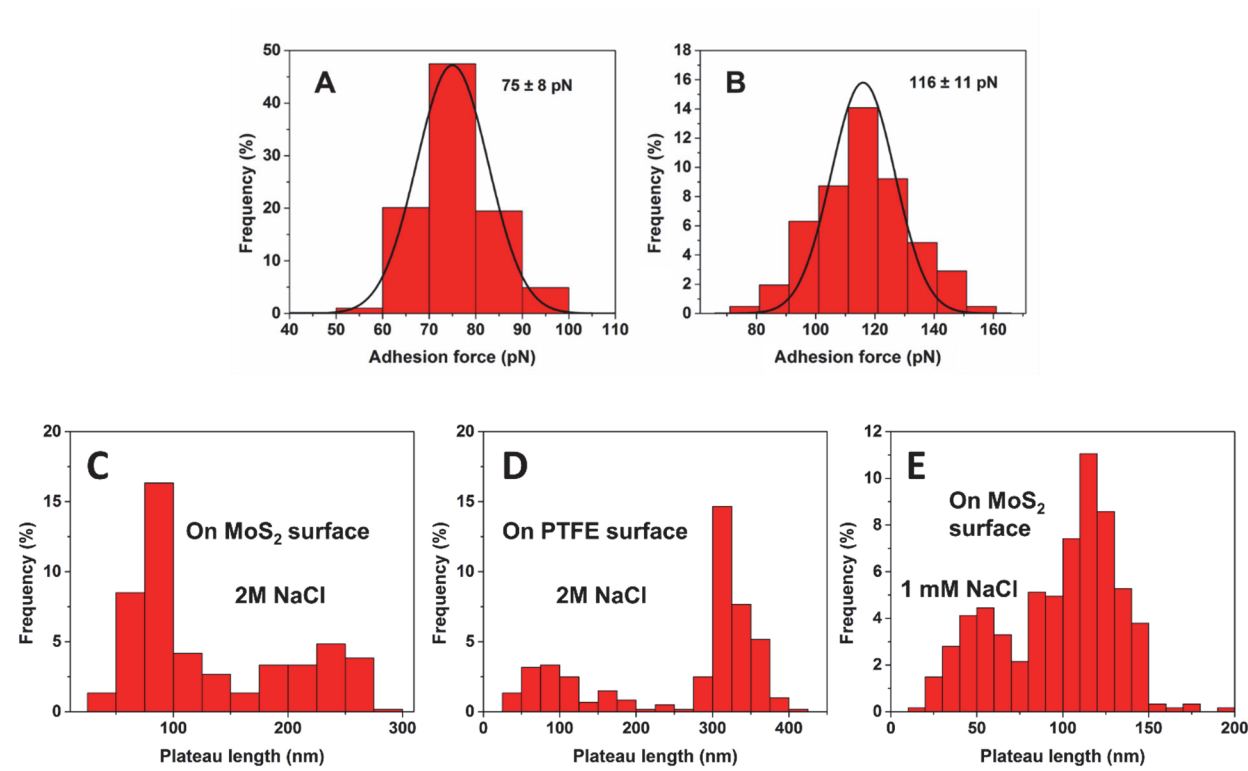


Figure 3-3 The force required to peel a single oligo (ethylene glycol) methacrylate copolymer chain in 2 M NaCl background solution from (A) MoS₂ and (B) PTFE surface and plateau length distribution for last polymer detachment event on MoS₂ (C) and PTFE (D). The plateau length distribution for last polymer detachment event on MoS₂ in presence of 1mM NaCl.

In our study, the hydrophilic-to-hydrophobic transition of the polymer was modulated under isothermal conditions around 23°C by changing the concentration of NaCl aqueous solutions. As an effective stimulus for hydrophilic-to-hydrophobic transition of the oligo (ethylene glycol) methacrylate copolymer (see Appendix A for details), the NaCl concentration was varied from 1 mM to 2 M. The average adhesion force for a single polymer chain as a function of NaCl concentration is shown in Figure 3-4. The force remained almost constant in low NaCl concentration up to 0.5 M, followed by a significant increase with further increasing NaCl concentrations until a plateau at very high NaCl concentrations. Similar stimuli responsive

behavior of the oligo (ethylene glycol) methacrylate copolymer from hydrophilic-to-hydrophobic transition in the same range of NaCl concentrations was observed using cloud-point characterization under the isothermal condition around 23°C (Appendix A). The contact angle of NaCl solution with different concentrations on polymer surface confirms that the transition did happen for the polymer we used in the experiment (Appendix A). The critical NaCl concentration for transition at 23°C is around 0.5 M which is consistent with the results of SMFS study that the single-molecule adhesion force begins to change noticeably at NaCl concentration around 0.5 M. Since the hydrophobicity of the MoS₂ was not sensitive to the electrolyte concentration (Appendix A), these results demonstrate that the observed increase in the adhesion force between the oligo (ethylene glycol) methacrylate copolymer and MoS₂ with increasing NaCl concentration indeed reflect the dependence of molecular interaction (adhesion) between the two on the change of the hydrophobicity of polymer.

Previous investigation has shown that polymer adopts the shape of a collapsed hydrophobic globule in high salt aqueous solutions³⁴. The loss or partially loss of the polymer-solvent interaction had shown its impact not only on the conformation of the polymer, but also on the adhesion of polymer with the Gold substrate³⁴. As Nash and his coworkers reported, the monomer-monomer (inter- or intra molecule) attractive interaction result in a 33% increase in the adhesion force per molecule for two-molecule peeling case on gold³⁴. Furthermore, the adhesion force per single-molecule was found to decrease by 45 % when the salt concentration was increased from 0.14 to 1 M. Unlike these previous results, we did not observe the inter- or intra-monomer interaction. Only polymer-substrate interaction was probed since the adhesion force per single-molecule adhesion for one-molecule, two-molecules and three molecules pulling cases were almost identical. Furthermore, in our experiments, the single-molecule adhesion force was found to increase by 36% when the salt concentration increased from 1 mM to 2 M. This significant increase in the adhesion force is much larger than any deviation due to the uncertainty of the AFM force measurement ($\pm 10\%$). One possible explanation of the different results observed using the same polymer lies in the fact that different substrates were used. We believe the influence of the substrate is important as there is no adhesion between the oligo (ethylene glycol) methacrylate copolymer and hydrophilic silica surface in NaCl aqueous solutions of all concentrations studied. The adhesion force between the polymer and gold substrate might be mainly van der Waals interaction which was significantly screened in high salt concentration and resulted in a decreased

adhesion force at high salt concentration solutions. Previous theoretical work has shown that the driving force for hydrophobically driven assembly near hydrophobic surfaces is weaker than that in bulk which suggests that the hydrophobic surface will bind to and catalyze the unfolding of macromolecule¹⁴⁵. Detailed results showed that the hydrophobic polymer chain folded (adopt collapsed globule) in bulk solution while unfolded/conformation rearranged at the hydrophobic substrate-water interface (quasi-2-dimensional conformation)¹⁴⁶. As a result, monomers of the polymer are in direct contact with the substrate. To confirm this, experimental data was analyzed to determine the distribution of the plateaus length for the last polymer detachment event (Figure 3-3). Instead of observing a reduced plateau length, the distribution of the plateau length was found shifted to higher values when the NaCl concentration was increased from 1 mM to 2 M. Thus, in our study, the catalytic effect of hydrophobic surface on macromolecule unfolding¹⁴⁵ was believed to exist when the collapsed polymer globule was forced to contact with the hydrophobic basal surface of MoS₂ which makes the peeling process possible. In the following part of the paper, the data were analyzed with current single polymer chain stretching and desorption theories to understand the underlying mechanism.

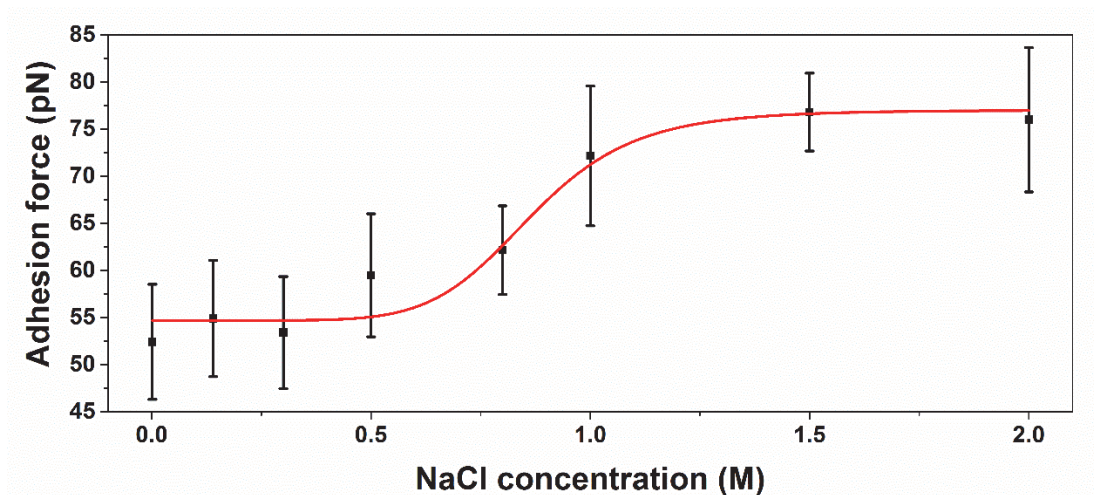


Figure 3-4 Force required to detach a single oligo (ethylene glycol) methacrylate copolymer chain from MoS₂ surface in aqueous solutions of different NaCl concentrations (the red line was drawn to guide the eyes).

3.4 Discussions

During the SMFS measurement, when the AFM tip is retracted, there is an intricate force balance at the interface of the AFM tip and detached segments of the polymer chain (Figure 3-5A). At the interface, the force of the detached and stretched polymer chain originates from its entropic elasticity (F_{WLC}) balances the elastic force of the cantilever which is quantified in the experiment using AFM as F_p ($F_p = F_{WLC}$)¹⁰⁰. As the cantilever moves upward, the polymer chain segments previously on the substrate are forced detached from substrate, as well as stretched⁹⁵. Thus, the energy input into the system not only overcomes the adhesion energy between the polymer and the substrate, but is also stored as entropic free energy in the desorbed polymer segments due to the stretching⁹⁵. The worm-like-chain model^{95, 147-148} has been widely used to depict the entropic force (F_{WLC}) of the polymer chain upon stretching. Thus, the entropic free energy of the detached polymer segment can be obtained by integrating the F_{WLC} over the stretching/detaching distance. The total free energy of the system (G_t) can be expressed as the sum of the adhesion free energy (G_a), elastic energy (G_{el}) stored in the cantilever and the entropic free energy (G_{en}) of the detached polymer chain⁹⁵:

$$G_t = G_a + G_{el} + G_{en}$$

$$= -\varepsilon * (n - n_i) + \frac{1}{2} * K * \left(\frac{F_p}{K}\right)^2 + L * \int_0^{\frac{x}{L}} \frac{K_B T}{L_p} \left[\frac{1}{4} \left(1 - \frac{x}{L}\right)^{-2} - \frac{1}{4} + \frac{x}{L} \right] d\frac{x}{L} \quad (1)$$

where K_B is Boltzmann constant, T is temperature, L_p is the persistence length of the chain and L is the contour length of the desorbed and extended component of the chain, which increases continually as the chain is peeled off. Meanwhile, x is the end-to-end distance of the desorbed portion of the polymer chain. In this study, it represents the vertical distance along the vertical-axis between the cantilever and the substrate based on the frictionless assumption⁵⁰⁻⁵¹. In the SMFS measurement, the value of x is provided by AFM as the extension or retraction of the piezo can be accurately controlled by the applied voltage. And ε is the adhesion energy per monomer that includes intermolecular interaction and hydration free energy of the system. n is the total number of the monomers in the polymer; n_i is the number of monomers that are already detached from the substrate. K is the spring constant of the cantilever and F_p (equals to F_{WLC}) is the force needed to

peel a single polymer chain from the substrate. The work done by the cantilever for a x change by an infinitesimal amount dx can be expressed as:

$$F_p dx = dG_a + dG_{en} = \varepsilon * dn_i + \frac{K_B T}{L_p} * f(\varphi) * dL \quad (2)$$

$$f(\varphi) = \int_0^\varphi \left[\frac{1}{4} (1-t)^{-2} - \frac{1}{4} + t \right] dt \quad (3)$$

where $\varphi = \frac{x}{L}$. Since $L = n_i * a$, we have:

$$dn_i = \frac{1}{a} dL \quad (4)$$

Thus, we have the following relationship:

$$F_{WLC} dx = \varepsilon \frac{1}{a} dL + \frac{K_B T}{L_p} * f(\varphi) * dL \quad (5)$$

As mentioned previously, $F_p = F_{WLC}$. In the SMFS experiment, plateau is observed, which illustrates that the force keeps constant as the polymer is gradually peeled off from the substrate. To keep F_p and F_{WLC} constant, the value of $\frac{x}{L}$ must be a constant. Then we have:

$$d\left(\frac{x}{L}\right) = \frac{1}{L} dx - \frac{x}{L^2} dL = 0 \quad (6)$$

$$dx = \frac{x}{L} dL \quad (7)$$

When equation 7 is applied, then we have:

$$F_{WLC} dx = F_{WLC} \frac{x}{L} dL \quad (8)$$

Thus, we have the mathematical relationship by combining equations 5 and 8:

$$F_{WLC} = \frac{L}{x} \left[\varepsilon * \frac{1}{a} + \frac{K_B T}{L_p} * f(\varphi) \right] \quad (9)$$

In order to determine the value of $\frac{x}{L}$, the adhesion force was derived as follows (the detailed derivation can be found in Appendix A):

$$F_p = \frac{L}{x} [\varepsilon * \frac{1}{a} + \frac{K_B T}{L_p} * f(\varphi)] = F_{WLC} = \frac{K_B T}{L_p} [\frac{1}{4} (1 - \frac{x}{L})^{-2} - \frac{1}{4} + \frac{x}{L}] \quad (10)$$

where a is the length of monomer along the backbone of the polymer chain. By setting $F_p = F_{WLC}$ (Figure 3-5A), the value of $\frac{x}{L}$ for each NaCl concentration was determined, as well as the corresponding value of ε . The value of $f(\varphi)$ can be calculated using the relationship described in eq. 3. Since $\frac{x}{L}$ is more or less constant for all salt concentrations which changed from 0.87 for 1mM NaCl solution to 0.89 when 2M NaCl electrolyte solution was used, $f(\varphi)$ which determined by $\frac{x}{L}$ and was found to be insensitive to NaCl concentration as the desorbed portion of the copolymer was significantly stretched. Although the assumption that no segment-segment interaction was made to derive this model as such that this model may not be suitable for the systems with inter- or intra molecule interactions³⁴, good agreements reported with the experimental data in low force range (<100 pN)^{34, 100} suggests that we could use it as an approximation. With the experimental obtained SFMS results, the contributions of the adhesion energy per monomer and the entropic free energy of the stretched polymer chain on the total polymer-MoS₂ single-molecule adhesion force were calculated using the above equations and shown in Figure 3-5C. Though the curve represents the contribution of entropic free energy on total single-molecule adhesion force seems constant over the NaCl concentration range studied, its value was found increased by 20% when NaCl concentration was increased from 1 mM to 2M.

3.5 Adhesion energy per monomer

Based on the previous discussion, eq. 4 can be modified and used to estimate the adhesion energy per monomer (ε) by:

$$\varepsilon = F_p * \frac{x}{L} * a - \frac{K_B T}{L_p} * f(\varphi) * a \quad (11)$$

With the conversion in hand, the adhesion energy per monomer at each condition was calculated using the experimental data and the results are shown in Figure 3-5C. Assuming an L_p value of 1.2 nm^{34, 149-152}, an order of magnitude estimation, and a value of 0.25 nm which corresponds to the length of a C-C-C chemical bond length with an bond angle of 109.5°, the calculated adhesion energy per monomer ranges from 2.5 to 3.75 $K_B T$, that is, 6.2 to 9.2 kJ/mol.

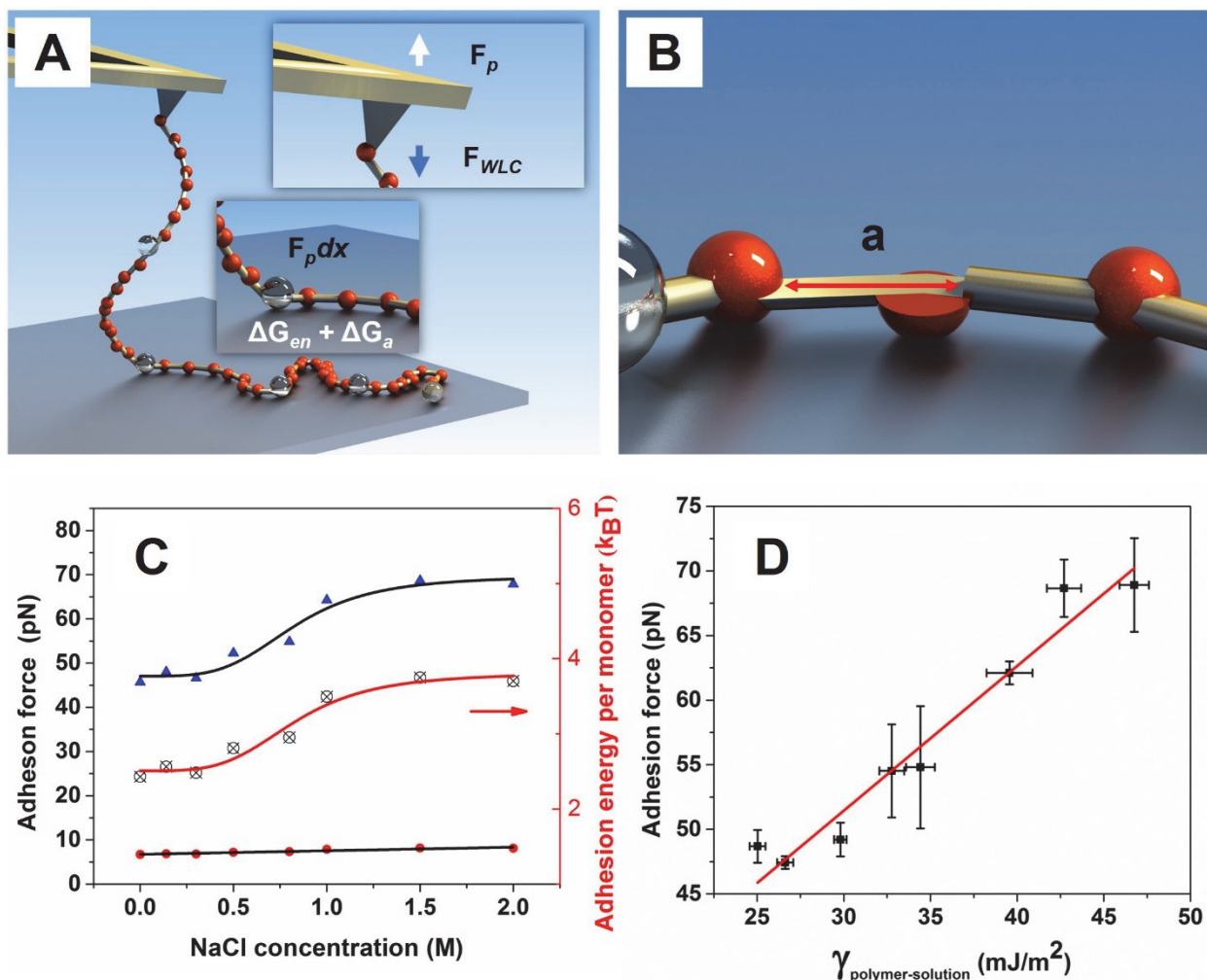


Figure 3-5 (A) Illustration of the force balance when the polymer chain is peeling from the MoS₂ substrate. (B) Geometric parameters of the monomer and (C) Dependence of adhesion force and adhesion energy on NaCl concentration. Red dots represent the adhesion force originating from the entropic free energy of the chain, the blue triangles denote the contribution of monomer-substrate interaction on the total measured adhesion force. The empty circles show the adhesion energy per monomer on the substrate. Trend lines were drawn to guide the eyes (using black trend lines for adhesion force and red color for adhesion energy). (D) relationship between the adhesion force contributed by adhesion energy per monomer and the polymer-solution interfacial tension.

In this study, the energy stored as the entropic free energy only accounts for 10-11% of the total energy. Although higher entropic contribution is observed at lower NaCl concentration, overall the dependence of the entropic free energy on salt concentration is negligible as shown by an increase in its contribution to total adhesion force from 6.7 pN at 1 mM NaCl concentration to 8.1

pN at 2 M NaCl concentration. It is evident that the higher single-molecule adhesion force in electrolyte solution with elevated NaCl concentration was resulted from the higher adhesion energy per monomer ε .

3.6 Origin of the increased polymer-substrate interaction

In general, the overall adhesion energy per monomer ε could arise from several interactions: van der Waals interaction, electric double layer interaction and hydrophobic attraction. Within the scope of this study, the electric double layer interaction was ruled out since the polymer does not contain any chargeable chemical groups.

The van der Waals interactions are universal among all kinds of matters and bodies in vacuum and liquids. There are several contributions to van der Waals interactions. Two non-dispersion portion contributions of the van der Waals interaction are dipole-dipole and dipole induced dipole interactions which are regarded as the zero-frequency contribution to the total van der Waals interactions. Both suffer from a significant screening effect in aqueous solutions containing high concentrations of free ions. This is because they are basically electrostatic interaction in nature and the electric field is significantly screened due to the polarization of free charges in solution¹⁵³. The screened zero-frequency was previously systematically studied and a mathematical relationship was developed¹⁵⁴. The zero-frequency components of van der Waals forces decay roughly exponentially with the inverse value of Debye Screening length. Macroscopic investigations confirmed the screening effect on the total van der Waals interaction. Thus, the progressively reduced van der Waals interaction could not be the reason for the higher adhesion force between the oligo (ethylene glycol) methacrylate copolymer and hydrophobic MoS₂ basal plane surface in high salt solution observed in this study.

The hydrophobic attraction has been investigated for decades using AFM and Surface Force Apparatus (SFA)¹⁵⁵ and was believed to be the driving force for the protein folding in aqueous solution to form functional complexes¹⁰³. However, the obtained data were found to be influenced by the surface preparation techniques which give rise to secondary effects such as bubble adsorption¹⁵⁶, cavitation¹⁵⁶⁻¹⁵⁷ and compositional rearrangement¹⁵⁸. These secondary effects were excluded by using SMFS which probes the interaction between a single polymer chain and an interested stable substrate in contact⁶⁶. In this work, as the electric double layer interaction is ruled out and van der Waals interaction do not play a major role, the experimental data clearly

demonstrated that the hydrophobic attraction between single oligo (ethylene glycol) methacrylate copolymer chain and MoS₂ is important and becomes more dominant with increasing NaCl concentrations. Previous single polymer study on pulling a single polymer chain out of its collapsed globule demonstrated that the free energy of the hydrophobic attraction is the difference of hydration free energies before and after the interaction^{100, 144}. Therefore, when the length scale of the polymer perpendicular to the backbone is larger than the crossover region (1 nm), the strength of the hydrophobic attraction can be assessed by the hydrophobic hydration of the hydrophobic species which scales with the macroscopic interfacial free energy^{100, 104, 159}. Based on the calculation on the simple geometry, the size of the studied polymer here were estimated to be larger than 1 nm due to the presence of the side chain. Thus, if the claim of the important role of hydrophobic attraction is correct, the single-molecule force should show clear linear dependence on the interfacial free energy. The adhesion force contributed from adhesion energy per monomer was plotted as a function of interfacial tension of polymer-solution (Figure 3-5D) as MoS₂-solution barely changed (Appendix) and polymer-MoS₂ interfacial tension is a constant in our study. The obvious linear relationship supports the claim that the hydrophobic attraction plays an important role here. These single-molecule adhesion force measurement results provide molecular mechanism on the critical role of hydrophobicity on the molecular interaction between polymer and solid substrate.

Meanwhile, this work also provides updated single-molecule results on the Hofmeister effect¹⁶⁰⁻¹⁶¹ which describes the systematic effect of salt on the solubility of macromolecules and the most common phenomena are the salting-in/salting-out or folding/unfolding of proteins¹⁶². The analysis of the dependence of single-molecule adhesion force on salt concentration provided in this study illustrates that the hydrophobic attraction is the main contribution responsible for the higher single-molecule force in high salt concentration between the stimuli-responsive polymer and hydrophobic surface of MoS₂. This demonstrated that the Hofmeister effect and hydrophobic effect are closely related, which agrees with the previous investigation^{103, 155}. Although the detailed underlying mechanism remains to be explored¹⁰³, the results might be partially explained in the perspective of Hofmeister effect by the molecular hypothesis proposed before¹⁶³⁻¹⁶⁴, which claimed that the kosmotropic salts can affect the solubility of polymer in two ways: 1) polarize the water molecules that directly hydrogen bonded with the polymer; 2) raise the surface tension of the polymer/water interface to increase the cost of the hydrophobic hydration.

3.7 Conclusions

In this work, the single-molecule adhesion force of oligo (ethylene glycol) methacrylate copolymer on MoS₂ basal plane surface was found in the range of 50 – 75 pN increasing with increased NaCl concentration. The results indicated that the oligo (ethylene glycol) methacrylate copolymer is a promising building blocks in aqueous solution for proper modification of MoS₂ sheets. Furthermore, the adhesion force shows a clear dependence on the hydrophobicity of polymer which increases linearly with polymer-solution interfacial free energy. The fundamental analysis elucidated that the adhesion energy per monomer is the main contribution that governs the single-molecule adhesion force since the percentage that the entropic free energy accounted for is less than 11%. With screened electrostatic interaction, the hydrophobic attraction, one component that determines the adhesion energy per monomer in our system, is believed to be even more dominant in high salt concentration rather than being suppressed. The salt concentration dependent interaction between the oligo (ethylene glycol) methacrylate copolymer and MoS₂ basal plane surface indicates that hydrophobic segments/polymer chains are good candidate for noncovalent functionalization of MoS₂ as it shows considerable stronger binding affinity compared with those of more hydrophilic ones. The experimental results in single-molecule level also shed light on the origin of hydrophobic attraction and its dependence on electrolyte, which is still under debate.

Chapter 4

The Contribution of Hydrophobic Attraction to Molecular Adhesions on Hydrophobic Surface in Water

4.1 Introduction

The hydrophobic attraction (HA), defined as the interaction between apolar objects/molecules in aqueous environment¹⁶⁵, is widely accepted nowadays to be closely related with water structures^{102-103, 132, 134, 166-167}. It is responsible for a variety of phenomena, from the micellization of cleaning process in laundry, to the emulsions for preparation of novel functional materials, to the precise assemble of proteins into functional 3D complexes^{100, 104, 144}.

The measurements of the hydrophobic attraction using AFM and Surface Force Apparatus (SFA) were sought-after in the past several decades^{21, 155, 168}. Valuable updates were provided to decipher the mechanism of hydrophobic attraction. However, the long-lasting debate on the existence of long-range hydrophobic interaction after its first publication¹⁶⁹ plagues the whole society. One possible reason for the discovery of long-range hydrophobic attraction might be attributed to the defective surface preparation techniques, which induce notorious secondary effects such as bubble adsorption, surface composition rearrangement¹⁵⁸. These effects bring in other forms of forces, which complicated or were counted as hydrophobic attraction¹⁶⁵. Ducker and his coworkers reported¹⁶⁵ that only limited experimental results between extended hydrophobic surfaces provide convincing evidence of hydrophobic attraction, which exponentially decays in range of 3-12 Å^{18-21, 170}. This is because the preparation of clean hydrophobic surface that free of ambiguous attribution of forces to the measurement is extremely difficult.

To eliminate the influence of secondary effects and get clean experimental data, measurements in smaller scale is highly desired¹⁵⁵. In molecular scale, the quantification of hydrophobic attraction without influence of secondary effects is probable⁶⁶.

Moving forward, the partitioning of the vdW interactions and hydrophobic attraction in total interactions is important. The quantification of hydrophobic attraction in nanometer or above is based on the extended DLVO theory. The hydrophobic attraction is quantified by deducting the contributions of van der Waals (vdW) and electric double layer interaction (EDL) from experimental data^{140, 165}. However, this widely accepted approach is no longer applicable in single-molecule scale. The utilization of macroscopic Lifshitz theory requires the system to be macroscopic and homogeneous⁵⁹, which is not satisfied by SMFS investigations. Though the experimental studies capable of probing the dispersion forces in molecular scale are highly sought-after¹⁷¹⁻¹⁷³, the direct measurement in solution remains difficult¹⁷⁴⁻¹⁷⁵. Furthermore, the modelling

of van der Waals/dispersion forces involving single organic molecule remains a great computational challenge in vacuum, let alone in solution¹⁷⁶. Thus, questions remain-how to quantify the hydrophobic attraction at the molecular scale and how much does hydrophobic attraction contribute to the single-molecule adhesion in solution.

To access the investigation at the molecular scale and eliminate the annoying secondary effects⁶⁶, single molecule force spectroscopy (SMFS) was utilized. By peeling the polymer chain from interested solid-liquid interface¹⁰², force curves with plateau feature were readily collected in the experiment. The height of each plateau was statistical analyzed to give the mean equilibrium desorption force³⁴. In common with other SMFS studies⁹⁵, the contributions for the total single-molecule adhesion force can be divided into two categories: The entropic free energy of the stretched polymer chain (conformational free energy) and the adhesion free energy per monomer (ϵ). In detail, ϵ can be split into several fundamental portions: the vdW interactions, the electric double layer (EDL) interactions and hydrophobic attractions^{67-68, 95}.

The unambiguous assignment of each individual interaction contributing to the single-molecule adhesion requires careful design of the experiment. Therefore, anisotropic crystalline substrate (MoS₂) was used as substrate in this study. The probing of the single-molecule adhesion force on MoS₂ provides one possible approach for dissecting-out the contribution of EDL interaction on single-molecule adhesion by varying solution pH. The feasibility of this approach relies on the intrinsic property of MoS₂ basal surface, which offers pH dependent surface potential¹⁴⁰. The determination of the individual contribution of vdW interaction and hydrophobic attraction can be performed by probing the SMFS experiment on hydrophobic basal and hydrophilic edge surfaces. The validity of this method is supported by the fact that the hydrophobic attraction does not exist on hydrophilic surface¹⁴⁰ and the vdW interaction on different surfaces of same material is identical or in the same magnitude^{140, 177-182}. Recent DFT study confirmed that the vdW promoting the adsorption of organic molecules on basal and edge surfaces of layered materials is in same magnitude¹⁸².

4.2 Materials, characterization and methods

4.2.1 Materials

The water used in the experiment was particle free and purified with Milli-Q system. (3-Aminopropyl) triethoxysilane (APTES), N-(3-Dimethylaminopropyl)-N'-ethylcarbodiimide hydrochloride(EDC), N-Hydroxysuccinimide (NHS), dioxane, di(ethylene glycol) methyl ether methacrylate (MEO₂MA, MW188.22), poly(ethylene glycol) methyl ether methacrylate (PEGMA, Mn=500), 4,4'-Azobis(4-cyanovaleric acid) (ACVA) and the RAFT agent 2-(Dodecylthiocarbonothioylthio)-2-methylpropionic acid were purchased from Aldrich.

4.2.2 Synthesis of oligo (ethylene glycol) methacrylate based copolymer

The polymers were synthesized via RAFT polymerization and the details can be found elsewhere³⁴. Before experiment, the monomers were purified by passing through a neutral aluminum oxide column to remove the inhibitors. In a typical experiment, 3.2 g di(ethylene glycol) methyl ether methacrylate and 0.8 g poly(ethylene glycol) methyl ether methacrylate (Mn=500) were mixed with 8 mL dioxane. After that, 3 mg of 2-(Dodecylthiocarbonothioylthio)-2-methylpropionic acid and 1.1 mg of ACVA were added into the flask. The flask was then sealed and purged with nitrogen for 1 h to remove the oxygen inside. After polymerized for 24 h at 75 °C, the polymerization was stopped by exposing to air. The polymer was then purified by dialysis against water and obtained by lyophilization.

4.2.3 Polymer Analysis.

THF phase size-exclusion chromatography was performed in a GPC system equipped with Styragel HR1 GPC column and a light scattering detector (ELSD 2000). A series of polystyrene standards were used for the GPC calibration. The polymer was dissolved in 5 mg/L and 10 µL was injected at a flow rate of 0.5 mL min⁻¹. The design molecular weight of all the studied polymer is 330 kDa. The measured molecular weight of polymer A is 118 kDa (Mn) with a PDI=1.85. The molecular weight of copolymer B is 200 kDa (Mn) with a PDI=1.7. The molecular weight of copolymer C is 94 kDa (Mn) with a PDI=1.8. The molecular weight of polymer D is 61 kDa (Mn) with a PDI=2.7. ¹H NMR was performed in 10 mg/mL in CDCl₃ on a 200 MHz NMR spectrometer (Bruker).

4.2.4 Cantilever Modification.

Rectangular silicon nitride cantilevers purchased from Bruker (MSCT) were used in the experiments. The cantilevers were functionalized with (3-Aminopropyl)triethoxysilane (APTES) according to the well-developed procedure³⁴. The amine-silanized cantilevers were deprotonated by immersing in sodium borate buffer solution (150 mM, pH 8.5) for 30 min. Next, 0.5 mL of a 4 mg/mL poly(oilgo(ethylene glycol)) copolymer solution was mixed with 0.5 mL of sodium phosphate buffer (10 mM phosphate, 137 mM NaCl, pH 7.4). After that, 50 mg EDC and 50 mg NHS were added. The coupling reaction of the polymer and cantilever proceeds for 1 h at room temperature. To be noted, the chemical linkage (amide group) that links the polymer chain to APTES modified AFM cantilever tend to hydrolyze when is exposed to water. Thus, the polymer linked cantilever was used immediately after the modification process. The shelf life can be extended to 2 days if shored in chloroform.

4.2.5 Single Molecular Force Spectroscopy (SMFS).

The SMFS measurement was performed on Multimode 8 AFM using piconnector with a fluid cell. The spring constant of the cantilever was calibrated before or after each experiment using the equipartition theorem⁴⁹. The cantilevers used in the experiments were bought from Bruker (MSCT) and the typical spring constant was around 0.03 nN/nm with a mean resonance frequency of 10 kHz. The MoS₂ was peeled with Scotch tape to expose the clean surface before each experiment. The sampling rate was 6 kHz and various pulling velocity and surface delay time were used. Data was then baseline corrected and analyzed. Each experiment was repeated at least 3 times with different cantilevers in different days.

4.3 SMFS results of oligo (ethylene glycol) methacrylate copolymer with surfaces of MoS₂

AFM probes were chemically modified by polymer prior to the SMFS experiments. The plateau feature observed in the collected force curves signifies the equilibrium desorption¹⁴³. The representative equilibrium single-molecule adhesion force was obtained by statistical analysis of the plateau heights relative to the baseline and fitting with Gaussian equation^{28, 34, 67-68}.

The layered structure of MoS₂ crystal leads to the presence of two distinctively different surfaces-basal and edge surfaces. The anisotropic property facilitates the dissection-out of the magnitude of each individual contribution. The characteristic surface morphologies of these two surfaces were

characterized by AFM and are shown in Figure 4-1A and 4-1B. Typical distance between adjacent molecular smooth layers were determined to be close to typical value of 0.6 nm^{183} . Smooth MoS_2 edge surface for SMFS was prepared using Ultra microtome technique following our reported method¹⁴⁰. As a typical anisotropic material, the basal surface is hydrophobic in nature while the edge surface is highly hydrophilic. The contact angle on the basal surface is usually in the range of $90 - 100^\circ$ depending on the freshness of the sample surface¹⁸⁴. For the edge surface, the contact angle is as low as 18° ¹⁴⁰.

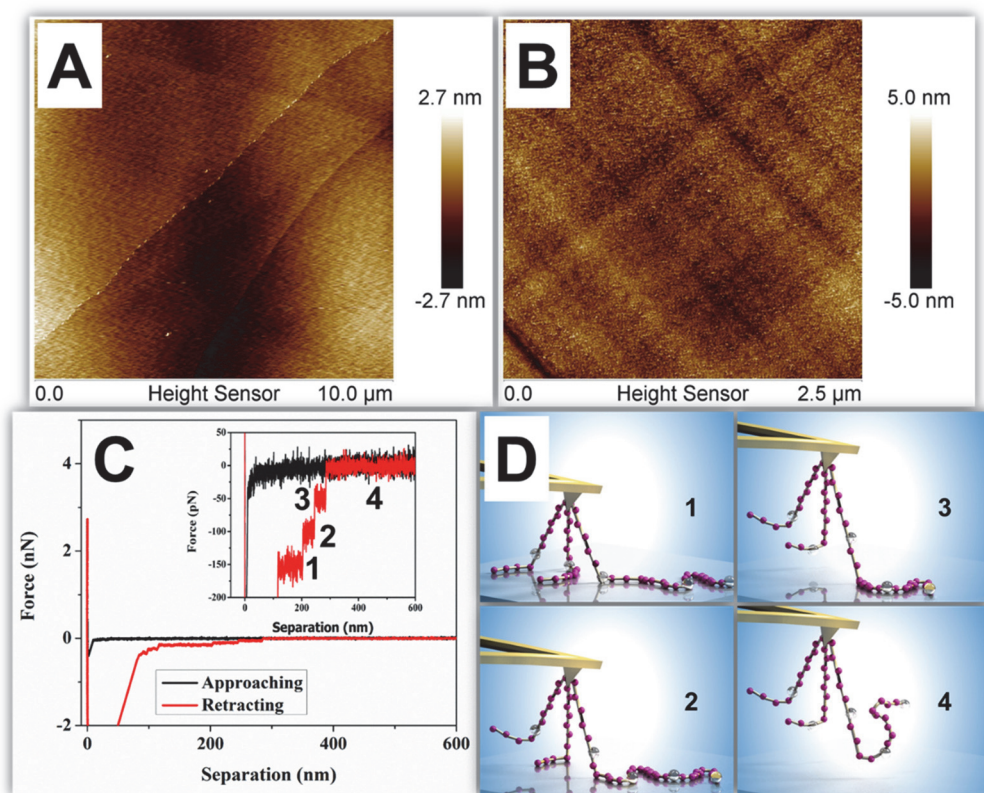


Figure 4-1 AFM images of basal surface (A) and edge surface (B). Typical force curves obtained in experiment for oligo ethylene glycol copolymer on MoS_2 basal surface in presence of 1 mM NaCl with pH around 3.3 (C). Schematics showing multiple polymer chains being probed during experiment (D).

Representative force curves obtained in experiment between polymer B (please refer to supporting information for details) and basal plane surface of MoS_2 in the presence of 1 mM NaCl aqueous solution (pH 3.3) is shown in Figure 4-1C. Multiple polymer chains were probed simultaneously since triple plateaus were observed in force-extension curve. The peeling events were described

schematically in Figure 4-1D. Though peeling events involves multiple polymer chains were frequently encountered in the experiment, only the last plateau representing single-polymer peeling event was analyzed to partition the individual contributions of EDL interaction, vdW interactions and hydrophobic attraction.

4.3.1 Contribution of electric double layer interaction

The electric double layer interaction (EDL) is one of the fundamental contributions for interbody or intermolecular interactions^{58, 185}. Previous investigation had shown that the surface potential on the basal surface of MoS₂ is dependent on the solution pH¹⁸⁶. For example, the typical surface potential in pH 3 was around -28 mV and decreased to -44 mV when the pH is increased to 11¹⁴⁰. Thus, the presence of EDL interaction would outshine itself by a highly pH dependent single-molecule adhesion force. However, no such dependence on solution pH was observed (Figure 4-2). Possible explanations for this could be attributed to the uncertainty of the SMFS measurement (around 10%) and the relatively small change on the surface potential. However, both of them were excluded as possible explanations because obvious pH dependent single-molecule adhesion force was detected for a cationic polymer on MoS₂ basal surface (please see Figure B-2 in supporting information for details). This demonstrated that even though the change on the surface potential of MoS₂ is not huge, the influence on the molecular EDL interaction is significant. The non-dependence of single-molecule adhesion force on the surface potential illustrated that the EDL interaction does not play a role between studied polymer and charged MoS₂ basal surface. This is reasonable as the studied polymer is electric neutral in nature. Similarly, we can safely extend this conclusion to MoS₂ edge surface.

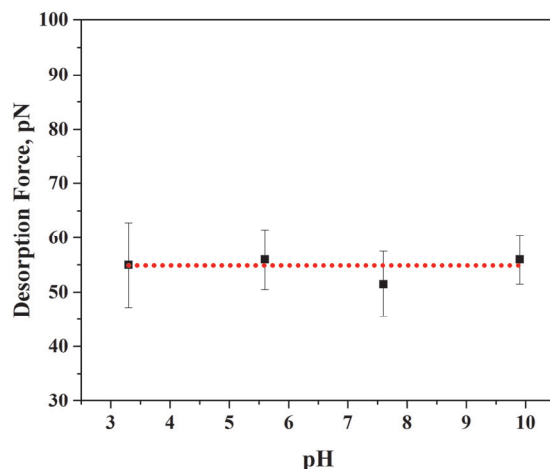


Figure 4-2 Single-molecule adhesion force of a single oligo (ethylene glycol) copolymer chain on basal surface of MoS₂ as a function of pH in presence of 1 mM NaCl background solution (A).

4.3.2 Contribution of van der Waals interaction

The vdW interaction plays ubiquitous roles among molecules, surfaces and bodies. When EDL is excluded, the isolation and determination of vdW was achieved by probing single-molecule interaction on anisotropic surfaces of MoS₂. Since the same substrate and polymer are used, the vdW interaction interacting between single polymer chain and substrates on contact should be identical or similar on the hydrophobic basal or hydrophilic edge surfaces^{140, 177-182}. It is notes that the Sulphur atoms on basal surface of MoS₂ is the main reason that the basal surface is hydrophobic in nature. Meanwhile, the broken bonds on the edge surface is responsible for the charging mechanism and intrinsic hydrophilicity of the edge surface¹⁴⁰. Furthermore, the hydrophobic attraction by definition describes the force between apolar objects/molecules in aqueous environment. Thus, it ceases to play a role when a hydrophilic MoS₂ edge surface is encountered. Thus, anisotropic properties of MoS₂ offers a facile approach to reasonably estimate the contribution of each specific interactions on the total single-molecule adhesion force between polymer and MoS₂ surfaces.

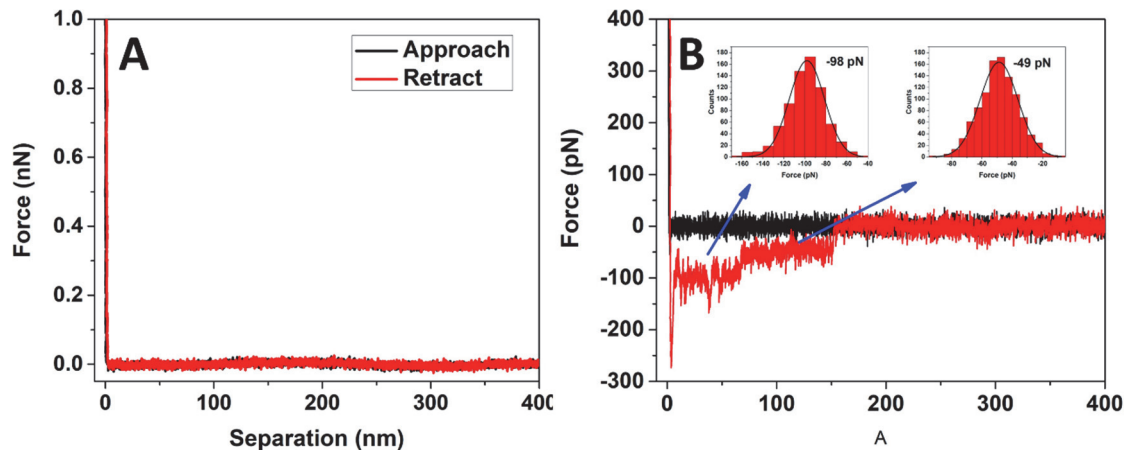


Figure 4-3 Typical force curves obtained in a SMFS experiment between polymer and hydrophilic edge surface of MoS₂ in the presence of 1 mM NaCl with pH around 5.5: (A) oligo (ethylene glycol) copolymer and (B) poly (vinylbenzyl trimethyl ammonium chloride) (PVBTA). The insets shows the histogram of adhesion forces corresponding to double and single chain peeling events in a single force curve.

The none-detectable single-molecule interaction between polymer and MoS₂ edge surface (Figure 4-3A) can be attributed to two possible reasons: the single-molecule interaction is too small to be probed or the setup of the experiment did not allow the quantification of single-molecule adhesion on the edge surface. The second possibility was excluded because strong single-molecule adhesion force of cationic poly (vinylbenzyl trimethyl ammonium chloride) on edge surface was readily probed (Figure 4-3B). Reasonable analysis of the experiment data requires a clarification on the lower detection limit of SMFS before any conclusion is reached. As a technique build on AFM platform, the minimum force that can be detected by SMFS is determined by the spring constant of cantilever. After careful analysis of the power spectrum density of the thermal fluctuations⁴², the spring constant of AFM cantilever used in our study was found around 0.03 nN/nm. This gives rise to a lower detection limit around 9 pN ($F_{det} = (k_B T * K)^{0.5}$)¹⁶⁵ in this study. Therefore, the vdW interaction between the studied neutral copolymer and hydrophobic MoS₂ basal surface was illustrated to be small and its contribution on the single-molecule adhesion force was less than 9 pN.

4.3.3 Contribution of hydrophobic attraction

The aforementioned results have excluded the contribution of EDL interaction and illustrated that vdW interactions played a minor role in governing the single-molecule interactions. Intuitively, these results elucidated that the most likely dominant contribution for the single-molecule adhesion of polymer on hydrophobic surface is hydrophobic attraction.

To determine the contribution of hydrophobic effect, we borrowed the experimental method developed by Walker and his coworkers¹⁰⁰. From their work, we see that the dependence of single-molecule force on ethanol addition can be used as a criterion to judge if the hydrophobic attraction is the main driving force^{100, 104}. Therefore, the influence of ethanol on the probed single-molecule adhesion force was investigated. As is shown in Figure 4-3, two polymers with different compositions (polymer A and polymer B) were studied. The quantified single-molecule adhesion force was plotted as a function of the molar ratio of ethanol. The graph clearly shows that the probed single-molecule adhesion force is sensitive to the addition of ethanol. The single-molecule adhesion force decreased sharply upon addition of ethanol even though the molar ratio (χ) of the added ethanol was as low as 0.008. Furthermore, the force continued to decrease when increasing amount of ethanol was added. The clear dependence on the ethanol addition for the single-molecule adhesion illustrated that the hydrophobic attraction is a nontrivial contribution here.

To further confirm the role of hydrophobic attraction on the single-molecule interaction between polymers with MoS₂ basal surface, the composition of the studied polymer was varied. By doing this, the vdW interaction between each repeating unit of polymer and hydrophobic MoS₂ basal surface was kept comparable as similar chemical structure was maintained. However, due to the change on the molar ratio of monomers, the hydrophobicity of polymers were systematically varied. Based on their increasing hydrophilicity, these polymers were named as polymer A, polymer B, polymer C and polymer D, respectively (please refer to the supporting information for chemical structures).

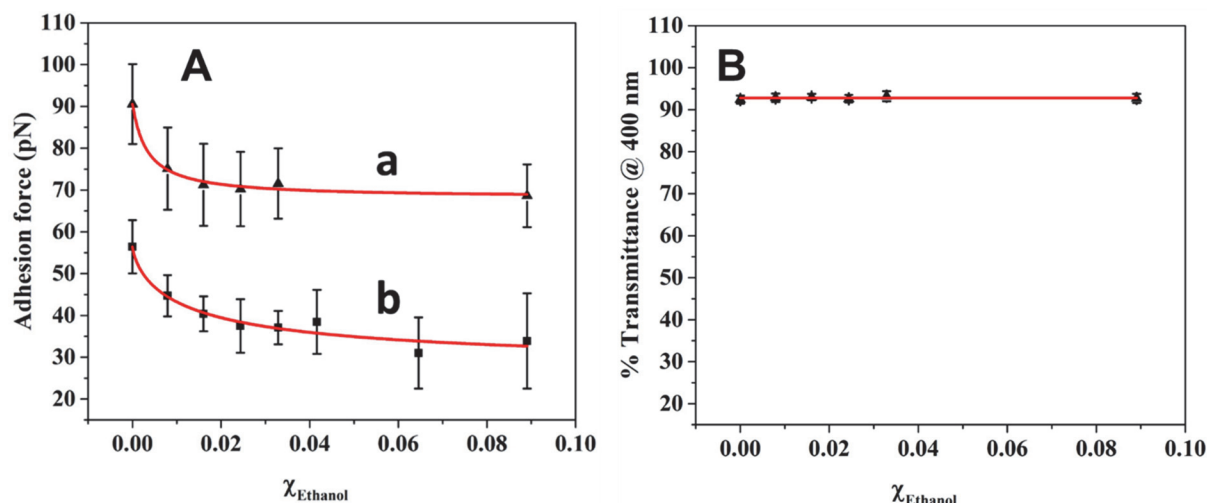


Figure 4-4 The adhesion force of a single polymer chain on the basal surface of MoS₂ as a function of ethanol addition: adhesion forces of polymer A (a) and polymer B (b). The transmittance of aqueous solution of polymer B (4 mg/ml in 1 mM NaCl) as a function of ethanol addition (B).

The probed statistical mean equilibrium single-molecule adhesion force of the synthesized polymers (A, B, C, D) on the MoS₂ basal surface is shown in Figure 4-5. The most hydrophobic polymer (polymer A) showed the highest single-molecule adhesion force. As reported in our previous publication¹⁶⁷, the single-molecule adhesion force of polymer B on basal surface of MoS₂ is around 53 pN. Thus, a significant decrease in the single-molecule adhesion force was observed when the molar ratio of hydrophilic MEO₈MA in polymer was increased. Furthermore, single-molecule adhesion force between PMEO₈MA and MoS₂ basal surface was determined around 30 pN. Such difference is statistically significant. The most immediate observation arising from these SMFS results was that the hydrophobicity of polymer was critical on the magnitude of single-molecule interaction.

However, such claim is only convincing when the influence of the size of monomer on the strength of vdW interaction is clarified. Recently, it has been reported that the single-molecule vdW interaction in vacuum linearly grows with the molecule size⁵⁹. The linear relationship was attributed to the increased deconfinement of electrons in the π -conjugated poly-naphthalene derivatives. However, the polymers we studied here were oligo ethylene glycol methacrylate based polymers. They lack the π -conjugated chemical structure that is necessary for the effective deconfinement of electrons. Even if this conclusion can be applied to our system to a certain extent,

the lower single-molecule adhesion force probed using polymer with larger monomer size is still unexplainable. Furthermore, the validity of extending the conclusion from vacuum to liquid environment is plausible. As is reported recently, the presence of solvent molecules complicate the whole system and greatly reduces the strength of dispersion interactions¹⁸⁷⁻¹⁸⁹. Thus, the results demonstrated that the hydrophobic attraction was the main contribution in determining the single-molecule adhesion force between oligo ethylene glycol methacrylate based polymer and MoS₂ basal surface. These experimental results supported and provided updated quantified results to the previous proposition that solvophobic effects have a dominant role for the attractive interaction between apolar solutes in liquid medium¹⁹⁰.

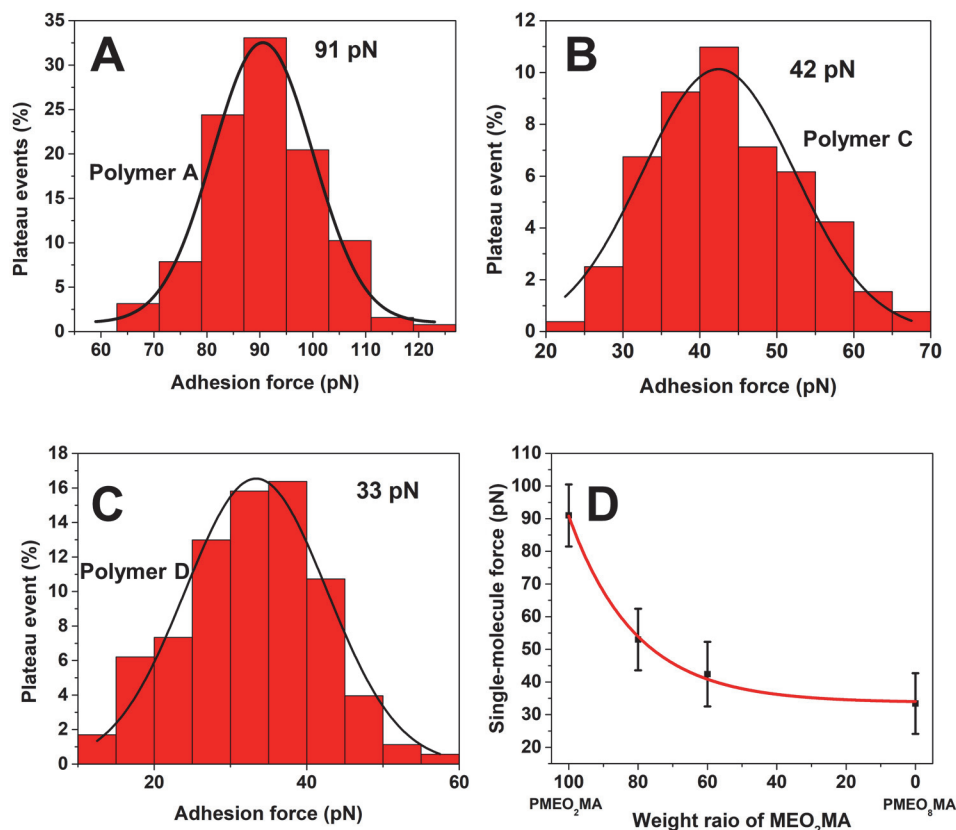


Figure 4-5 The adhesion force of a single oligo (ethylene glycol) methacrylate based polymer on the basal surface of MoS₂ in the presence of 1 mM NaCl background solution: (A): polymer A; (B): polymer C; (C): polymer D. The single-molecule adhesion forces as a function of polymer composition (D).

4.4 Discussions

The unraveling of the hydrophobic attraction relies on the in-depth understanding of experimental data that truly reflects the hydrophobic effect. Thus, the deconvolution of its contribution to total interactions needed to be carefully performed. Up to now, it is still difficult to do so because the determination of vdW interactions at the molecular scale is challenging. Although theoretical descriptions for single atom and homogeneous macroscopic bodies have been established^{42, 191-192}, systematic descriptions for intermediate-sized objects such as organic molecules are remain to be explored. Furthermore, the modeling of vdW interactions using first-principles are very difficult because the correlation between interacting electrons need to be appropriately treated¹⁹³⁻¹⁹⁶.

Therefore, experimental approaches capable of precise quantification of vdW interactions are highly desired to partitioning the contribution of hydrophobic attraction with acceptable accuracy. Recently, general experimental procedures were proposed for studying single-molecule interaction between a π -conjugated organic molecule and extended substrate in vacuum⁵⁹. However, this method is not applicable in solution. Besides that, indirect measurements using molecular torsion balance to determine the molecular vdW interactions in solution was reported recently^{176, 189, 197}. The free energy is determined by comparing the areas of characteristic peaks in ¹H NMR spectra corresponding to folded and unfolded conformations. A simple linear regression is conducted to determine the contribution of vdW interactions¹⁸⁹. However, the regression process introduces uncertainty in the determination of vdW interactions. Meanwhile, the physical meaning of the coefficients used during regression need to be clarified as both negative and positive values are obtained.

Alternatively, by taking the advantage of the anisotropic properties of MoS₂, the individual contributions of these two interactions were reasonably estimated for the first time in direct force study in solution. Before reaching the above conclusion, it is important to clarify the feasibility and uncertainty of this method. It is noted that both of them originate from the assumption made in the experiment. In the analysis, it is assumed that the vdW interaction between polymer and hydrophobic basal surface on contact is identical or similar to that on hydrophilic edge surface. Support for the approximate identical vdW on both surfaces can be found from previous investigations¹⁴⁰. Meanwhile, even if there is certain difference in vacuum, the difference is greatly

reduced and might be small enough to be neglected in solution. This is supported by recent publication reported that the presence of solvent decreases the dispersion interactions by 90%¹⁷⁶.

Considering the single-molecule adhesion force for polymer A was around 90 pN, the contribution of vdW interaction in solution was smaller than 10% of the total interactions. It is not surprising as previous publication has reported that van der Waals interactions are ‘weak’ in solution. Cockroft and his coworkers studied the interaction of apolar alkyl chains in solution and advocated that the molecular vdW interactions are one order of magnitude smaller than that estimated using vaporization enthalpies. The highly suppressed molecular vdW dispersing interaction was attributed to the competitive dispersion interactions with the solvent^{176, 189, 197}.

The reasonable determination of vdW interactions leads to the quantification of hydrophobic attraction with satisfactory accuracy. In general, it accounted for more than 90% in the total single-molecule interactions. The validity of this was supported by the probed influence of ethanol on single-molecule adhesion. Compared with the reported investigation¹⁰⁰, both systems show significant dependence of the probed force on the addition of ethanol. It is important as the strength of hydrophobic attraction is sensitive to the presence of ethanol in aqueous solution^{100, 104}. With the continuous addition of ethanol in the background solution, the polar component of surface tension of solution is significantly changed¹⁰⁰. As a result, interfacial free energy between solutes and solvent contributed by the polar component, which is regarded as the main reason for hydrophobic effect¹⁰⁰, is significantly reduced. One more evidence that is supportive for the partitioning of the hydrophobic attraction at the molecular scale is the probed dependence of single-molecule adhesion force on polymer composition. The probed forces were highly sensitive to hydrophobicity of studied polymer. Meanwhile, all the polymers showed no detectable interactions on hydrophilic edge surfaces of MoS₂.

As advocated recently, only the data collected at separation < 20 nm, especially at separation < 1 nm contains valuable information on true hydrophobic attraction¹⁶⁵. This requires that the force measurement to be performed in ultra-short range and the individual contribution of each interaction needs to be determined. The first requirement was successfully satisfied by the emergence of SMFS. However, due to the lack of appropriate method to deconvolute the individual contributions, the way that the SMFS data analyzed was not consistent. Hugel and his coworkers claimed that the water-structure-force and vdW interactions are individual contributions for the

interaction between peptides and hydrophobic surfaces^{66, 198}. However, in a recent published work¹⁹⁹, the hydrophobic attraction was referred to the total interaction between solvated hydrophobes. With the individual contributions of vdW interactions and hydrophobic attractions determined, a big step forward is achieved as the clear deconvolution would boost the deciphering process of hydrophobic attraction.

4.5 Conclusions

In summary, we have presented experimental measurements of single-molecule interaction on surfaces of MoS₂, which demonstrated that the contribution of vdW interaction on total single-molecule adhesion force of polymer on hydrophobic MoS₂ basal surface is less than the lower detection limit (9 pN) of the equipment. The results are consistent with the previous postulation that the dispersion force is largely cancelled due to the complete interaction with solvent molecules. Furthermore, the results elucidate that the hydrophobic attraction is the main driving force for the interaction between polymer and hydrophobic surface and account for more than 90% of total interactions. The updated data provide new insights into the polymer-solid interaction in presence of water and is beneficial for the further development of fundamental theories of hydrophobic attraction.

Chapter 5

Underwater Adhesion of a Stimuli-Responsive Polymer on Highly Oriented Pyrolytic Graphite (HOPG): A Single-Molecule Force Study

5.1 Introduction

Robust interfacial adhesion in aqueous environment is of great importance for a variety of industrial and bio-related applications. Examples of such applications are bone sealing²⁰⁰, dental and medical transplants²⁰¹, coronary artery coatings²⁰², under water adhesives¹⁵, to name a few. Meanwhile, smart adhesion systems that offer controllable adhesion properties by environmental stimulus are highly desirable in cases where controllable attachment/detachment is longing for. Up to now, a great deal of efforts have been devoted to overcome the influence of surrounding water, which undermines the interfacial adhesion and reduces strengths of various molecular interactions¹⁸⁷. However, the performance of synthesized underwater adhesives requires further optimization to develop novel underwater adhesive systems¹⁵⁻¹⁶.

One efficient strategy for developing advanced, underwater adhesive is to investigate and mimic existing natural sticky systems. Previous research of adhesive proteins in marine organisms²⁰³⁻²⁰⁴ revealed the essential role of 3,4-dihydroxyphenethylamine (Dopa) in interfacial adhesion by its capability of forming bidentate coordination and/or hydrogen bonding^{57, 205-209}. Later on, it was found that Dopa is not the only important parameter that determines the wet adhesion⁹⁻¹¹. Hydrophobic domains in mussel adhesive protein was revealed to provide an extra attractive interaction when interacting with hydrophobic surfaces²¹⁰⁻²¹¹. Though these findings open a new direction in understanding the naturally occurring adhesion systems and offer a new strategy in improving the performance of synthetic adhesive systems, the quantitative influence of polymer hydrophobicity on interfacial adhesion and the insights into single-molecule level remains elusive.

Recently, growing interests in controllable attachment/detachment⁷⁸⁻⁸⁰ and self-cleaning⁸¹ has led to the development of smart polymer surfaces for desired applications. These systems rely on the stimuli-responsive behavior of a special category of polymer upon environmental stimulus. Adhesion on the polymer modified solid surfaces is promoted by the presence of hydrophobic attraction when temperature is above lower critical solution temperature (LCST) of the polymer⁸⁰. The surface properties of the polymer are altered drastically and creates a steric-osmosis layer after the restoration of the hydrophilic nature of the polymer⁸¹ when the temperature is decreased and below LCST. The repulsive interaction this is responsible for the detachment or self-cleaning property originate from the suppression of available conformations for polymer, which lead to large osmosis/entropic free energy penalty. The interaction between polymer and the foreign

surface is also important as it provides negative enthalpic contribution that promotes the adhesion²¹². Therefore, understanding the polymer-foreign surface interaction before and after the polymer is switched is imperative for improving performance of the smart systems.

The aforementioned macroscopic results and practical applications call for insights of interfacial adhesion of stimuli-responsive polymer in aqueous environment, as well as its dependence on polymer hydrophobicity. Results at the single-molecule level are highly desirable as it provides fundamental information for interfacial adhesion while other interactions contributing to cohesion can be excluded. These clean results are valuable for deepening understanding of polymer-substrate interaction, deciphering the macroscopic results and clarifying the key molecular parameters that determine the strength of macroscopic adhesion. However, the quantification of single-molecule hydrophobic polymer-surface interaction in aqueous solution is challenging. The relative unfavorable interaction between water and hydrophobic monomers compared with monomer-monomer interaction would promote the hydrophobic collapse of the polymer in aqueous solution. The collapsed globule conformation minimizes the contact area of polymer with substrate and aqueous solution which effectively precludes the measurement of polymer-substrate interaction¹⁰⁴. Nevertheless, we have demonstrated in our previous study that the quantification of single-molecule interaction of a hydrophobic polymer on a hydrophobic surface was possible by tailoring the right polymer-substrate pair¹⁶⁷. The peeling of polymer chains from solid-water interface during SMFS experiments was realized by the catalytic role of hydrophobic surface, which promotes the direct contact of monomers in polymer with hydrophobic surface¹⁴⁵.

In this study, oligo ethylene glycol copolymer was used as a model stimuli-responsive polymer. Its responsive behavior to environmental stimulus (NaCl) was studied by quantifying the single-molecule adhesion force as a function of NaCl concentration. As the polymer undergoes a transition from hydrophilic to hydrophobic state in response to the NaCl concentration, the influence of the hydrophobicity of the polymer on single-molecule adhesion force was elucidated. A molecular smooth surface (HOPG) with natural hydrophobicity was used as model hydrophobic surface in this study.

The quantification of equilibrium single-molecule adhesion force was based on peeling a single/few polymer chain from the solid-water interface. The validity of this approach relies on the fact that the plateau features in the collected force curves represents frictionless scenario^{34, 50-51}. It

means that the macromolecule on the surface cannot support a net horizontal friction force and be peeled off from the substrate at an average angle of 90° with respect to the substrate⁵¹. As a result, the equilibrium single-molecule adhesion forces in various solution conditions were determined by the analysis of plateau heights relative to baseline and the following statistical treatment in this work.

5.2 Materials, characterization and methods

5.2.1 Materials

The water used in the experiment was particle free and purified with Milli-Q system. (3-Aminopropyl)triethoxysilane (APTES), N-(3-Dimethylaminopropyl)-N'-ethylcarbodiimide hydrochloride(EDC), N-Hydroxysuccinimide (NHS), dioxane, di(ethylene glycol) methyl ether methacrylate (MEO₂MA, MW188.22), poly(ethylene glycol) methyl ether methacrylate (PEGMA, average Mn 500), 4,4'-Azobis(4-cyanovaleric acid) (ACVA) and the RAFT agent 2-(Dodecylthiocarbonothioylthio)-2-methylpropionic acid were purchased from Aldrich. The silica wafer was purchased from nanoFAB in University of Alberta. The highly oriented pyrolytic graphite (HOPG) sample was purchased from hqgraphene.

5.2.2 Synthesis of oligo (ethylene glycol) copolymer.

The copolymer was synthesized using RAFT polymerization following a published procedure³⁴. The monomers were purified by passing through a neutral aluminum oxide column to remove the inhibitors prior to polymerization. Generally, 3.2 g di(ethylene glycol) methyl ether methacrylate and 0.8 g poly(ethylene glycol) methyl ether methacrylate (average Mn 500) were mixed with 8 mL dioxane. Then, 3 mg 2-(Dodecylthiocarbonothioylthio)-2-methylpropionic acid and 1.1 mg ACVA were added into the flask. The flask was sealed and purged with nitrogen for 1 h. After polymerized for 24 h in 75°C , the system was exposed to air to quench the polymerization. The gel like polymer solution was dissolved and purified by dialysis against Milli-Q water. Then, the polymer was dried by lyophilization.

5.2.3 Polymer Analysis.

THF phase size-exclusion chromatography was performed in GPC system equipped with Styragel HR1 GPC column and light scattering detector (ELSD 2000). A series of polystyrene standards

were used for GPC calibration. The polymer was dissolved in 5 mg/L and 10 μ L was injected at a flow rate of 0.5 mL min⁻¹. The design molecular weight of the polymer is 330 kDa while the measured M_w = 200 kDa with PDI = 1.7. ¹H NMR was performed in 10 mg/mL in CDCl₃ on a 400 MHz NMR spectrometer (Bruker). The actual composition of the polymer was determined based on the NMR results. The polymer was found composed of 94.9% MEO₂MA and 5.1% MEO₈MA.

5.2.4 Cantilever Modification.

Rectangular silicon nitride cantilevers purchased from Bruker (MLST) were used in the experiments. The cantilevers were functionalized with (3-Aminopropyl)triethoxysilane (APTES) according to the reported procedure³⁴. The amine-silanized cantilevers were deprotonated by immersing in sodium borate buffer solution (150 mM, pH 8.5) for 30 min. Next, 0.5 mL 4 mg/mL poly(oilgo(ethylene glycol)) copolymer solution was mixed with 0.5 mL sodium phosphate buffer (10 mM phosphate, 137 mM NaCl, pH 7.4). After that, 50 mg EDC and 50 mg NHS were added. The coupling reaction of the polymer and cantilever proceeds for 1 h in room temperature. To be noted, the chemical linkage (amide group) that links the polymer chain to APTES modified AFM cantilever tend to hydrolyze when is exposed to water. Thus, the polymer linked cantilever was used immediately after the modification process. The shelf life can be extended to 2 days if stored in chloroform.

5.2.5 Single Molecule Force Spectroscopy (SMFS).

The SMFS measurement was performed on Multimode 8 AFM using picoforce scanner with a fluid cell. The spring constant of the cantilever was calibrated before or after each experiment using equipartition theorem⁴⁹. The cantilevers used in the experiment were bought from Bruker (MLCT) and the spring constant was around 0.03 nN/nm with a mean resonance frequency of 10 kHz. The HOPG surface was peeled with Scotch tape to expose the fresh clean surface prior to each experiment. The sampling rate was 6 kHz. Data was then baseline corrected and analyzed. Each experiment was repeated at least for 3 times with different cantilevers in different days.

5.2.6 Contact angle measurement.

Fresh HOPG surface was exposed by applying the Scotch tape prior to the contact angle measurement. The HOPG surface was placed on the stage and a water droplet with various concentration of NaCl (approx. 5 μ L) was generated at the tip of metal needle. The droplet was

brought in contact with the sample surface and the contact angle was quantified when the needle was retracted. Contact angle measurement was repeated at least for 5 times for each NaCl concentration on fresh HOPG surface.

5.3 SMFS Investigation of oligo (ethylene glycol) copolymer on HOPG surface

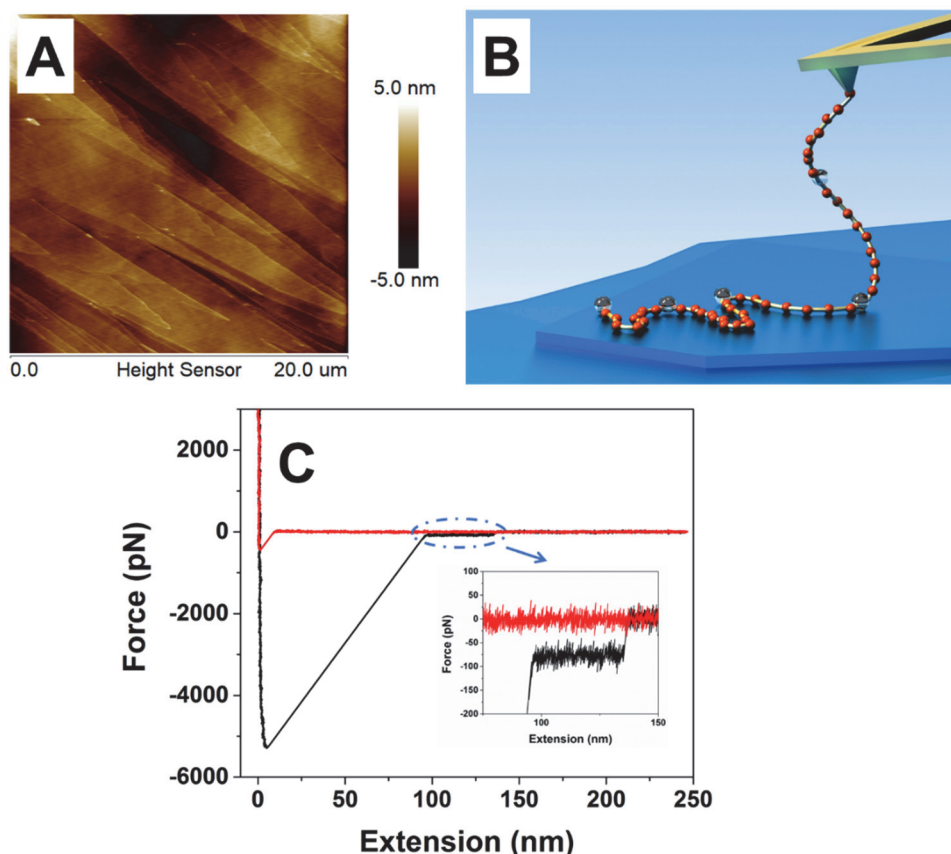


Figure 5-1 (A) An Atomic Force Microscope (AFM) image of HOPG surface in air. (B) Schematic representation of peeling a polymer chain from substrate in aqueous solution. (C) Typical approaching (red) and retracting force (black) curves obtained in the experiment representing a polymer chain peeling event.

Finding a model surface representative of hydrophobic surfaces is important to answer or partially answer the previous stated questions. Therefore, the selected substrate should possess general properties that stands for hydrophobic surfaces and the obtained SMFS results on this surface is reliable so that the conclusions can be extended to various hydrophobic surfaces. In this study, HOPG was used as model surface as it outshines other counterparts for its natural hydrophobicity^{184, 213-214}, homogeneity²¹⁵, stability²¹⁶ and reliable/reproducible sample

preparation²¹⁷. Moreover, its surface roughness is less than 0.2 nm within the same layer as calculated from the AFM image (Figure 5-1A). The SMFS experiment is delicate, as it requires one or several polymer chains to be probed in the experiment. In this study, to increase the possibility of observing polymer peeling event, as well as to control the number of polymer chains that are probed, the Si₃N₄ AFM cantilevers were modified with oligo (ethylene glycol) copolymer prior to the experiments. In detail, experiments were conducted by approaching an oligo (ethylene glycol) copolymer functionalized AFM tip onto the HOPG surface in water at constant velocity (500 nm/s) under a maximum load of 2-4 nN and retracting with the same rate after a certain period of dwelling time (1-2 seconds).

A schematic drawing representing the polymer peeling process during SMFS experiment is shown in Figure 5-1B. The key point of successful observation of polymer detachment event is the adsorption of polymer chain on the solid-liquid interface in trains conformation^{70, 142}. The presence of the trains conformation is promoted by the attractive interaction between polymer and studied substrate¹⁰². Meanwhile, certain period of dwell time was given during SMFS experiment for chain conformational rearrangement. The force curve with plateau feature obtained in the experiment is shown in Figure 5-1C, indicating that the adsorbed polymer chain is highly mobile on the interface⁵⁰⁻⁵¹. The height of the plateaus can be interpreted as the molecular adhesion force between the studied polymer and substrate³⁴. In our experiment, at least 30% of the force curves showed plateau events by using appropriate polymer modified AFM probes. The retracting force curves recorded in the experiment were baseline corrected and the plateau heights were quantified in the following data analysis to obtain the molecular interaction between polymer and HOPG surface. As shown in Figure 5-2A and 5-2B, the fluctuation of the force curves complicated the data processing so that the statistical fitting was used to obtain plateau height for each force curve. Though force curves with three or more plateaus were also readily collected in the experiments, only the last plateau was analyzed in our study as it represents the single-molecule adhesion event. The probing of the single-molecule peeling event was influenced by the noise of the environment and instability of the equipment, which resulted in a distribution of single-molecule adhesion forces (Figure 5-3). The Gaussian equation was then applied to provide a typical statistical description on the mean single-molecule adhesion force for each condition (Figure 5-3).

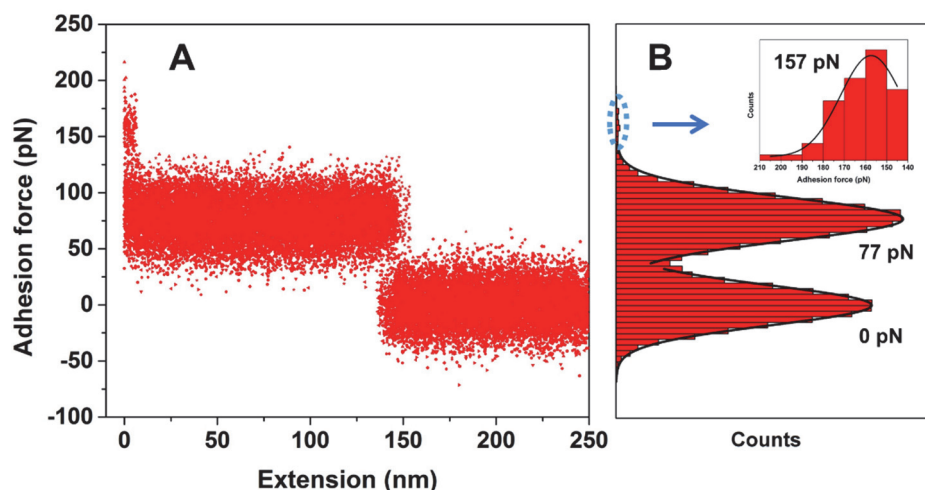


Figure 5-2 Analysis of SMFS results: (A) Retracting force curve after baseline correction and inversion. (B) Histogram shows the distribution of data points in force curves. The bottom peak represents the baseline. The second and the third peaks indicate the forces required to peel single or double polymer chains from the HOPG surface.

The transition/switching of the polymer from hydrophilic to hydrophobic state was manipulated gradually by elevating the NaCl concentration while keeping the environmental temperature constant (23 °C). The determined critical NaCl concentration for the transition of the polymer at 23°C by UV-Vis cloud-point characterization was reported between 0.5 M and 1.0 M¹⁶⁷. This was consistent with the results of this SMFS study. As can be seen in Figure 5-3, the single-molecule adhesion force is almost constant below 0.5 M while it starts to increase sharply at a NaCl concentration around 0.5 M. A similar trend was also observed in our previous investigation when the MoS₂ surface was used (see Figure C-1 in Appendix C). The single-molecule adhesion force of the polymer on the HOPG surface increased by 75% when the NaCl concentration was increased from 1 mM to 2M. This increase in adhesion force is statistically significant as it was larger than any deviation due to the uncertainty of the AFM force measurement (10%). These results demonstrated that the higher single-molecule adhesion force in electrolyte solution with higher NaCl concentration was due to the sensation of environment changes by polymer and its corresponding response to it.

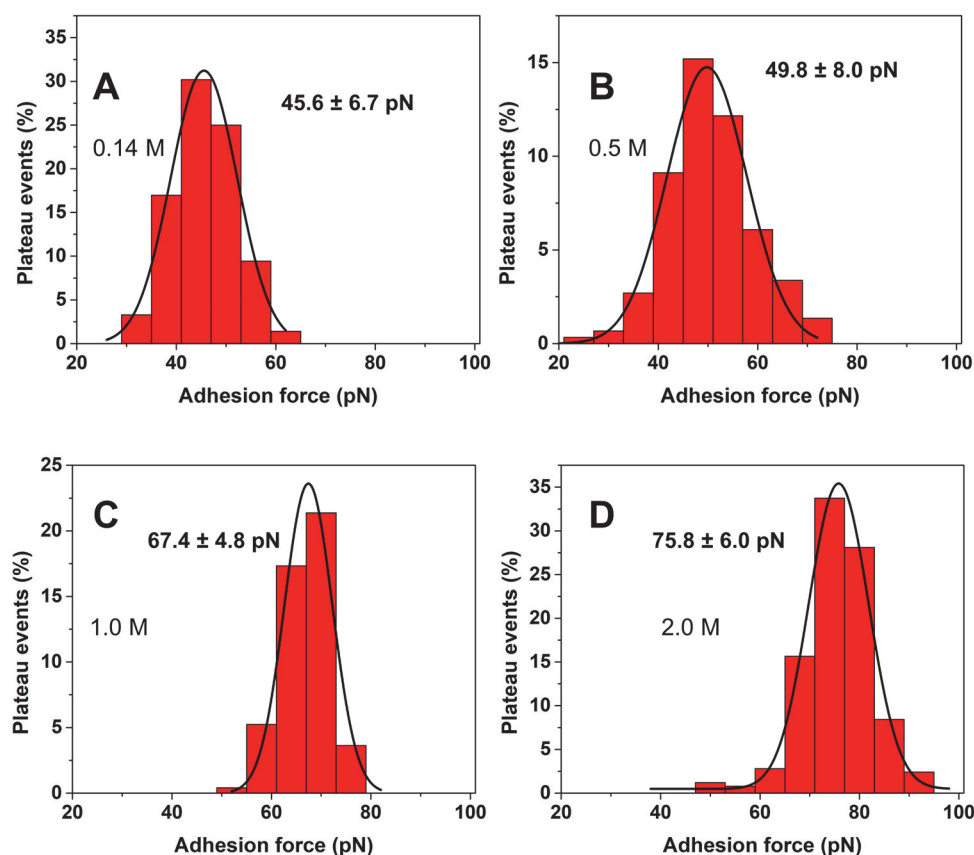


Figure 5-3 Single molecule adhesion forces of oligo (ethylene glycol) copolymer on the HOPG surface in electrolyte solutions with different NaCl concentrations: (A) 0.14 M; (B) 0.5 M; (C) 1.0 M and (D) 2.0 M.

5.4 Theory of polymer desorption in SMFS experiment

The continuous investigation on single molecule mechanics has led to the development of theories that capture the underlying physics. Hugel and his colleagues⁹⁵ developed a model that correlates the single-molecule adhesion force with adhesion energy per monomer and entropic free energy of the desorbed portion of polymer chain. Meanwhile, Walker and his coworkers¹⁰⁰ also proposed a model for polymer globule unfolding in poor solvent and confirmed that the single-molecule hydration/solvation free energy scales with the change of the surface area and interfacial tension. In our experiment, forced hydration of the polymer chain and substrate occurred when the polymer chain was peeled from HOPG surface, which is similar to the case described by Walker's mode¹⁴⁴. Thus, in our model, we combine the aforementioned models together and replace the adhesion

energy per monomer (ε_{adh}) by hydration/solvation free energy per monomer. It is worth emphasizing that in our previous work¹⁶⁷, we used ε_{adh} to relate the peeling force to the adhesion (i.e., the hydration/solvation free energy of the polymer molecule and the substrate is lumped into the parameter ε_{adh}). However, in the present work, we are in an attempt to deconvolute such contributions to the peeling force.

As shown in Figure 5-4A, the peeling starts as the driving force equals the attractive interactions holding the polymer on the substrate when performed in equilibrium desorption condition. The polymer chain between the cantilever and the substrate acts as a spring while the force-distance follows a much more complicate relationship rather than the simple Hooke's law. The entropic-elastic property of the single polymer chain can be described by the well-known worm-like-chain model^{95, 147-148}:

$$F_{WLC} = \frac{K_B T}{L_p} \left[\frac{1}{4} \left(1 - \frac{x}{L} \right)^{-2} - \frac{1}{4} + \frac{x}{L} \right] \quad (1)$$

where K_B is the Boltzmann constant, T is temperature, L_p is the persistence length of the chain and L is the contour length of the extended segment of the chain which varies continually as the chain is peeled from substrate (Figure 5-4A). It is noted that the extended desorbed portion of the chain is surrounded by water. Meanwhile, x is the end-to-end distance of the desorbed polymer chain. In this experiment, it is defined as the vertical distance along the vertical-axis between the cantilever and substrate based on the frictionless assumption (Figure 5-4A)⁵⁰⁻⁵¹.

The total free energy of the system (G_t) can be expressed as the sum of the adhesion free energy (G_a), elastic energy (G_{el}) stored in the cantilever and the entropic free energy (G_{en}) of the desorbed portion of polymer chain⁹⁵. The entropic free energy were quantified by integrating the force over distances. The adhesion free energy (G_a) was obtained by multiplying the hydration/solvation energy per monomer by the numbers of adsorbed monomers. The hydration free energy of hydrophobic molecules/surfaces is size-dependent. Studies on this topic have shown that the hydration in the microscopic scale (< 1 nm) differs fundamentally from the macroscopic scenario¹⁰³. Detailed theoretical and experimental results demonstrated that the free energy of the hydrophobic hydration scales with the surface area and surface tension when the dimension of the solute is larger than the cross-over length scale (1 nm)¹⁰³. Due to the presence of the oligo ethylene

glycol (OEG) side chain, the size perpendicular to the backbone of the polymer is estimated to be larger than the crossover length-scale. Thus, inspired by the model developed by Walker^{100, 104, 159}, hydration/solvation free energy per monomer is described as:

$$\varepsilon_{adh} = a * b * (\gamma_{ps} + \gamma_{ss} - \gamma_{sub.p}) \quad (2)$$

Where γ_{ps} and γ_{ss} are polymer-solution and substrate-solution (i.e., HOPG-solution or MoS₂-solution) interfacial tension, respectively. $\gamma_{sub.p}$ is substrate-polymer interfacial tension. As shown in Figure 5-4A, a and b are the dimensions of monomer. As the probed force corresponding to peeling of a single chain from substrate kept constant, the elastic free energy stored in the cantilever was a constant as a result. Thus, based on an energy balance, the work done by the cantilever if x changes by an infinitesimal amount dx can be expressed as:

$$\begin{aligned} F_{WLC} dx &= dG_a + dG_{en} \\ &= a * b * (\gamma_{ps} + \gamma_{ss} - \gamma_{sub.p}) dn_i + \frac{K_B T}{L_p} * f(\varphi) * dL \end{aligned} \quad (3)$$

Where n_i is the number of monomers that have already been detached from the substrate and $f(\varphi) = \int_0^{\frac{x}{L}} [\frac{1}{4} (1 - \varphi)^{-2} - \frac{1}{4} + \varphi] d\varphi$. Eqn. 3 is then simplified to (please refer to the Appendix C for detailed derivation):

$$F_{WLC} * \frac{x}{L} = b * (\gamma_{ps} + \gamma_{ss} - \gamma_{sub.p}) + \frac{K_B T}{L_p} * f(\varphi) \quad (4)$$

Eqn. 4 describes the force (F_{WLC} or F_p) needed to peel a single polymer chain from the substrate and its dependence on the total free energy of the system. The first term is the contribution of solvation/hydration on the single-molecule adhesion force. The second term shows the influence of entropic free energy of the desorbed chain on adhesion force. Considerable energy is stored as entropic free energy when the desorbed polymer chain is stretched during the experiment. In this study, the end-to-end distance to contour length ratio ($\frac{x}{L}$) changed from 0.87 to 0.89 when NaCl concentration increased from 1 mM to 2M which contributed 6-8 pN to the total single-molecule adhesion force. Higher peeling leads to a higher degree of polymer chain stretching. In our analytical model, $\gamma_{sub.p}$ is a fitting parameter, the values for polymer-HOPG and polymer-MoS₂

were determined to be 22 and 12 mN/m, respectively. The parameters used in the theoretical model was shown in Table 1 and interfacial energies obtained in experiments (see Appendix C for details), the adhesion force was calculated using the derived model (eq. 4) which is shown as the solid line in Figure 5-4B.

Table 5-1 List of parameters used in the Model

Parameter	Value
L_p^a	1.2 nm
b	1.23 nm
T	296.2 K

^aThe persistence length L_p was given to show the approximate order of magnitude¹⁶⁷. The width value of monomer b was estimated based on the bond length and simple geometry of the monomers.

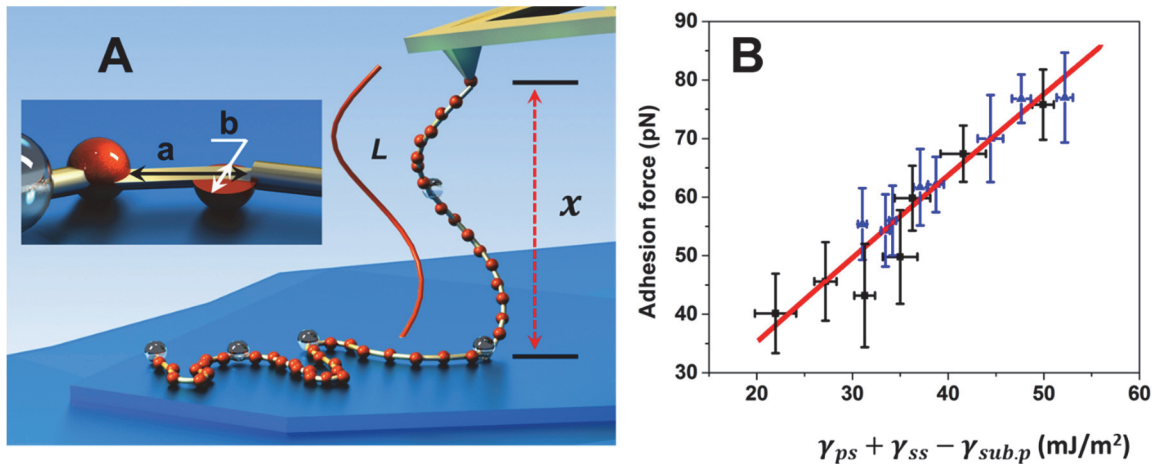


Figure 5-4 (A) Illustration of the force balance when the polymer chain is peeling off from the substrate and (B) Single-molecule adhesion force plotted against the total interfacial energy. The dots are experimental results and the solid line is the adhesion force calculated by the model. The squares and triangles represent the single-molecule adhesion forces of HOPG-polymer and MoS₂-polymer, respectively. The data on HOPG-polymer were obtained in this study and the data of MoS₂-polymer interaction were taken from our previous work¹⁶⁷.

The contribution of the entropic free energy on single-molecule adhesion force changed from 5.6 pN to 7.6 pN when the NaCl concentration increased from 1 mM to 2M. Though the relative change is large in percentage (36%), the absolute value compared to the total single-molecule force is small and negligible. Therefore, the single-molecule adhesion force was plotted as a function of interfacial tension (Figure 5-4B). The data taken from our previous paper was also included in the analysis¹⁶⁷. All the single-molecule adhesion force data show good linearity with interfacial energy and agree well with the derived model when an appropriate fitting parameter $\gamma_{sub,p}$ was utilized. The good agreement demonstrated that the model captured most of the underlying physics of the single-polymer detachment. Besides the experiment conducted by Walker and his coworkers, other experiments also reached the same conclusion that the probed force in microscale is linearly dependent on the surface free energy²¹⁸. This verifies that the good agreement between our model and experimental results is reflecting the true underlying mechanism of polymer chain peeling.

As has been reported that the interaction of macromolecule with substrate results from the interplay of solvation, surface and intermolecular force⁶⁶, the result here reveals that the macroscopic interfacial free energy is an essential fundamental parameter because it describes not only the water-water interaction, but also the other two important interactions in interfacial adhesion: polymer-water and polymer-substrate interaction. As the bulk water-water interaction²¹⁹⁻²²¹ and polymer-substrates interaction are almost constant among all the solution conditions, the hydration free energy illustrates the influence of solvent condition on the detachment of single polymer chain from hydrophobic surface in aqueous solution. The results demonstrated that the stimuli-responsive behavior of the polymer was mainly due to the decreased solvent quality of the polymer by the presence of environmental stimulus. The suppressed polymer-water interaction leads to a much higher polymer-water interfacial tension, thus, a much higher polymer hydrophobicity. This poses higher free energy penalty for the detachment of the polymer from the substrate as higher hydrophobic attraction energy barrier (hydration/solvation energy) is encountered.

5.5 Discussions

Our single-molecule force study revealed how a single polymer chain interacted with the HOPG surface in aqueous environment and its response to environmental stimulus on the adhesion force. The results demonstrated that the stimuli-responsive polymer studied here showed considerable interaction with hydrophobic surfaces before and after switch. The adhesion force per single

polymer is around 45 pN when the polymer is effectively hydrated in aqueous solution and increased to 75 pN when the hydration is suppressed. The results advocate that the polymer-interface interaction should be considered when designing smart polymer surfaces for application in controlled attachment/detachment as the interaction is not negligible.

The previous publication and this study have shown that the strength of the interaction between a single polymer and substrate is determined by the interplay of monomer and the substrate surface⁶⁶. Meanwhile, the strength of macroscopic interfacial adhesion relies on the collective results of the numerous fundamental single-molecule adhesions. Scaling law was found applicable for impermeable surfaces between the macroscopic adhesion and the single-molecule adhesion⁴⁻⁵. Based on the scaling law, the wet interfacial adhesion force contributed only by hydrophobic attraction per 1 cm² was estimated to be 91 to 152 N (i.e., 0.91 to 1.52 MPa) depending on the solution condition assuming the size perpendicular to the backbone of the polymer is 1.23 nm and the length of each polymer chain on substrate is 40 nm. It is huge compared to the strength of underwater adhesion for commercial adhesives which was reported to be less than 1 MPa¹⁵. As the traditional macroscopic characterization of the bonding strength of adhesive is combined results of interface adhesion and bulk cohesion, the fundamental investigations in this study may shed light on the optimization of adhesive systems since a clear picture on solely the interfacial adhesion was provided.

Furthermore, the maximization of the total adhesion force calls for the optimization of the number of single-molecule adhesion events and the corresponding force for it. A high population of polymer chain end can be beneficial since it increases the available number of the single-molecule adhesion events. However, as indicated by this study, intimate contact between the polymer and substrate is needed for the effective interaction. Thus, the glass transition temperature (*T_g*) of the polymer in water should be appropriately designed to ensure the proper mobility of the polymer chain. It is necessary to ensure that the monomers are in direct contact with the substrate.

For underwater adhesives, previous investigation on the single-molecule adhesion of Dopa on hydrophilic surface revealed that the magnitude of force required to break the bidentate/hydrogen bonding is around 800 pN per Dopa molecule⁵⁷. The results here showed that the single-molecule force due to the hydrophobic effect is one order of magnitude lower (75 pN). However, the effective bidentate H-bonding requires that the distance between hydroxyl groups on surface

matches with that of Dopa (i.e., 0.29 nm)²¹¹. Meanwhile, Dopa's interfacial adhesion is sensitive to solution pH^{6-7, 210}, which oxidized to quinone at pH above 5.5. Inspired by the approach that mussel adapts itself to various substrates to maintain adequate adhesion strength²¹¹, the synthetic underwater adhesives can expand its applicable substrate scope by introducing the hydrophobic monomers in the polymer chain. The experimental single-molecule results and theoretical analysis quantitatively demonstrated that higher single-molecule force can be obtained by increasing the solvation free energy. It can be used as a guideline in optimizing the molecular structure of novel adhesives though other facts such as the chain mobility that influence the intimate contact between the polymer and substrates should also be considered.

5.6 Conclusions

In summary, results on the underwater single-molecule adhesion force of stimuli responsive polymer on HOPG surface are reported. It was demonstrated here that the neutral polymer-hydrophobic surface interaction was not negligible even in the case that the polymer was effectively hydrated. Detailed thermodynamic analysis confirmed that the single-molecule adhesion force of the smart polymer on hydrophobic surface is dependent on the entropic free energy and hydrophobic solvation/hydration free energy. The single-molecule results and thermodynamic analysis quantitatively illustrated how hydrophobic attraction determines the interfacial adhesion of a single polymer on the hydrophobic solid-water interface. These insights are helpful for proper designing or optimization of current smart surface for controlled attachment/detachment and the mussel-inspired underwater adhesives. Using our approach, these systems may be improved or regulated in molecular scale to improve the performance at the macroscopic scale.

Chapter 6

Noncovalent Functionalization of MoS₂: Single-Molecule MoS₂-Polymer Interactions and Efficient Aqueous Exfoliation of MoS₂ into Single-Layer

6.1 Introduction

As a typical layered metal dichalcogenide, MoS₂ has received strong academic interests due to its ability to remove sulphur from crude oil in the hydrodesulphurization (HDS) process¹¹⁵. Recent discovery of its unique properties expanded its application scope to many other interesting fields such as nanotribology¹⁰⁹, photocatalysis²²², drug delivery¹¹², solar cells²²³⁻²²⁴ and catalysis of hydrogen evolution reactions (HER)²²⁵⁻²²⁶.

The stacking of adjacent 2D MoS₂ layers into 3D bulk structure is common due to the ubiquitous van der Waals interactions²²⁷. By breaking the van der Waals forces, single or few layered exfoliated MoS₂ nanosheets can be obtained for much more interesting properties due to the much higher surface areas¹¹² and higher bandgaps²²⁸⁻²²⁹ as compared with the bulk materials. The pursuit on controlling the thickness of MoS₂ nanosheets led to the development of chemical vapor deposition (CVD)¹⁰⁵ or epitaxial growth⁷⁵. However, the aforementioned approaches have size limitations on the resultant product and relatively high requirement on the equipment¹⁰⁶.

To realize important applications of MoS₂ nanosheets, many simple MoS₂ exfoliation methods have been proposed and developed in the past few years^{107, 121, 125, 230-232}. Among the existing methods, aqueous phase exfoliation is most desirable as it is convenient and environmentally friendly. Appropriate functionalization of MoS₂ by organic chemicals during aqueous exfoliation process is critical to facilitate the production of nanosheets in the required large scale. The addition of organic agents modifies the physical properties of the MoS₂ nanosheets and minimizes the energy cost while stabilizing the resultant exfoliated MoS₂ nanosheets during exfoliation process. Gaurdia and his co-workers demonstrated that ethylene oxide and propylene oxide based block copolymer (P123) can significantly increase the efficiency of MoS₂ solution exfoliation²³³. Furthermore, the addition of poly(vinyl pyrrolidone) (PVP) was found to be beneficial for the exfoliation of MoS₂ in the aqueous phase²³⁴. Bovine serum albumin (BSA), a well-known natural macromolecule, was recently utilized to functionalize and stabilize the exfoliated MoS₂ nanosheets¹²⁸. The addition of BSA promotes the exfoliation and enables the production of single-layer MoS₂ sheets.

The introduction of macromolecules effectively increases the efficiency of the exfoliation process and is beneficial for the scaled production. Meanwhile, proper modification of MoS₂ by polymers is found critical for many applications in which the stability of the exfoliated MoS₂ nanosheets in

aqueous solution with different water chemistry is needed¹¹². Though tremendous progresses have been made in this area, rare synthetic polymers are found to be capable of exfoliating MoS₂ into single-layer nanosheets in aqueous environments¹²⁸. The modification of MoS₂ relies on certain functional groups or chains that are capable of adsorbing/binding at the MoS₂-water interface, which significantly alters the surface properties of MoS₂. So far, the facile preparation of highly stable single-layer MoS₂ nanosheets in aqueous solution remains a major challenge. Thus, deep understanding of the interactions between the interfacial active polymer and MoS₂ surfaces in aqueous solutions of variable water chemistry is highly desired. It is critical to improve present systems or design of new polymers for effective exfoliation.

In this research, the single-molecule force spectroscopy (SMFS) was used as a tool to discover appropriate functionalizing polymers for a large-scale production of single-layer MoS₂ nanosheets. Experimentally, the interactions between three types of polymers and two MoS₂ surfaces (basal and edge surfaces) were determined to reveal the fundamental single-molecule interaction. The strength of the single-molecule interactions with the basal and edge surfaces of MoS₂ was quantified by SMFS experiments as a function of water chemistry. To link the measured single molecule interaction forces with functionalization and exfoliation of MoS₂, the exfoliation of MoS₂ by corresponding candidate polymers was conducted. As indicated by the SMFS results, cationic poly (vinylbenzyl trimethyl ammonium chloride) (PVBTA) was applied in the following mechanical exfoliation experiment. The reliable and scale-up production of single-layered MoS₂ nanosheets in aqueous environment demonstrated the capability of the selected polymer in efficient MoS₂ exfoliation. More importantly, the importance and benefit of probing single-molecule interaction using SMFS to optimize the practical applications were also elucidated.

6.2 Materials, characterization and methods

6.2.1 Materials

The water used in the experiment was particle free and purified with Milli-Q system. (3-Aminopropyl)triethoxysilane (APTES), N-(3-Dimethylaminopropyl)-N'-ethylcarbodiimide hydrochloride(EDC), N-Hydroxysuccinimide (NHS), dioxane, di(ethylene glycol) methyl ether methacrylate (MEO₂MA, MW188.22), poly(ethylene glycol) methyl ether methacrylate (PEGMA, average Mn 500), 4,4'-Azobis(4-cyanovaleric acid) (ACVA), vinylbenzyl trimethyl ammonium

chloride and the RAFT agent 2-(Dodecylthiocarbonothioylthio)-2-methylpropionic acid were purchased from Aldrich.

6.2.2 MoS₂ preparation for SMFS

Bulk crystalline MoS₂ was exfoliated with Scotch tape to expose a fresh hydrophobic and molecular smooth basal surface immediately prior to the experiment. Usually, the tape was pressed with finger to fully contact with the MoS₂. The aged contaminated MoS₂ layer was removed when tape was gently pulled away, thereby exposing a fresh surface on the bulk sample. The edge surface of bulk MoS₂ was prepared by embedding in epoxy resin and cut by diamond knife using Ultramicrotome technique.

6.2.3 Synthesis of oligo (ethylene glycol) polymer/copolymer and Poly (vinylbenzyl trimethyl ammonium chloride)

All polymers were synthesized via Reversible addition–fragmentation chain-transfer (RAFT) polymerization and the details can be found in published procedure³⁴. Before the experiment, di(ethylene glycol) methyl ether methacrylate (MEO₂MA) and poly(ethylene glycol) methyl ether methacrylate (MEO₈MA) were purified by passing through a neutral aluminum oxide column to remove the inhibitors. Crystal (vinylbenzyl trimethyl ammonium chloride) was used as received since no inhibitor was added. In a typical experiment, 3.2 g MEO₂MA and 0.8 g MEO₈MA (average Mn 500) were mixed with 8 mL dioxane. After that, 3 mg 2-(Dodecylthiocarbonothioylthio)-2-methylpropionic acid and 1.1 mg ACVA were added into the flask. The flask was then sealed and purged with argon for 1 h. After polymerized for 24 h in 75 °C, the polymerization was stopped by exposing to air. Milli-Q water was added and the polymer was further purified by dialysis against Milli-Q water. Finally, the polymer was dried by lyophilization. Homopolymer polymer (PMEO₂MA) was synthesized and purified in the same way. Poly (vinylbenzyl trimethyl ammonium chloride) was synthesized in the same way except that water was used as polymerization medium.

6.2.4 Polymer analysis

Tetrahydrofuran (THF) phase size-exclusion chromatography was performed in Gel permeation chromatography (GPC) equipped with Styragel HR1 GPC column and light scattering detector (ELSD 2000). A series of polystyrene standards were used for GPC calibration. The neutral

polymers were dissolved in 5 mg/L and 10 μ L was injected at a flow rate of 0.5 mL min⁻¹. The design molecular weight of the polymer is 330 kDa while the measured Mw= 200 kDa with PDI=1.7 for oligo ethylene glycol copolymer. ¹H NMR was performed in 10 mg/mL in CDCl₃ or D₂O on a 400 MHz NMR spectrometer (Bruker).

6.2.5 Transmission Electron Microscopy (TEM) Characterization

TEM analysis was performed on a JEOL JEM-ARM200cF S/TEM, which is equipped with a cold Field-Emission Gun (cFEG) and a probe Cs corrector. High resolution TEM (HR-TEM) images were acquired at an acceleration voltage of 200 kV.

6.2.6 Cantilever modification

The cantilevers were functionalized with (3-Aminopropyl)triethoxysilane (APTES) according to the well-developed procedure³⁴. The amine-silanized cantilevers were deprotonated by immersing in sodium borate buffer solution (150 mM, pH 8.5) for 30 min. Next, 0.5 mL 4 mg/mL polymer solution was mixed with 0.5 mL sodium phosphate buffer (10 mM phosphate, 137 mM NaCl, pH 7.4). After that, 50 mg EDC and 50 mg NHS were added. The coupling reaction of the polymer and cantilever proceeds for 1 h in room temperature. To be noted, the chemical linkage (amide group) that links the polymer chain to APTES modified AFM cantilever tend to hydrolyze when is exposed to water. Thus, the polymer linked cantilever was used immediately after the modification process. The shelf life can be extended to 2 days if stored in chloroform.

6.2.7 Single Molecular Force Spectroscopy (SMFS)

The SMFS measurement was performed on Multimode 8 AFM using picoforce scanner with a fluid cell. The spring constant of the cantilever was calibrated before or after each experiment using equipartition theorem⁴⁹. The cantilevers used in the experiment were bought from Bruker (MSCT) and the typical spring constant was around 0.03 nN/nm with a mean resonance frequency of 10 kHz. The sampling rate of 6 kHz, pulling velocity of 500 nm/s and surface delay of 2 s to 4s were used. Each experiment was repeated at least for 3 times using different cantilevers in different days.

6.2.8 Aqueous solution exfoliation of MoS₂ in the presence of polymer

In a typical experiment, 5 g of MoS₂, 1 g of polymer and 120 g of DI water was added to a grinding mortar. 300 g of grading beads (1.2-2 mm) was added afterwards and the system was operated in 1800 rpm using an agitator manufactured by Union Process. The aqueous phase was collected and centrifuged using 8000 rpm for 30 min after 2 h grinding. The final product was collected by centrifuge in 11500 rpm after tip sonication for 2 h in 0 °C. The resultant supernatant was dialyzed against DI water to remove impurities.

6.2.9 UV-Vis characterization of produced exfoliated MoS₂ sheets

UV-vis absorption spectra was recorded on a Shimadzu UV-3150 spectrophotometer. The sample was centrifuged with 8000 rpm for 30 min and the supernatant was then diluted by 4 times for the following UV-Vis characterization.

6.3 Study of MoS₂-polymer interaction by single molecule force spectroscopy

Single Molecule Force Spectroscopy (SMFS) is a powerful technique for quantifying polymer-substrate interaction with resolution down to the single-molecule level^{27-28, 66-68}. In a typical SMFS experiment, the cantilever is continuously brought close to and retracted from the surface at various locations. During most of the measurement cycles, the polymer(s) is peeled from the substrate, which results in a plateau representing equilibrium detachment in the obtained force curves¹⁶⁷. The plateaus illustrate that the polymer chain can move and slide freely on the surface, and the binding and rebinding of the polymer chain on the substrate occurs much faster than the experimental time scale³⁴. The force corresponding to single-molecule peeling event can be quantified by analyzing the plateau heights relative to the baseline in the retracting force curves. In general, the measured statistical average value of peeling (adhesion) force from each plateau representing the interaction between single/multiple polymer chain/chains and MoS₂ surfaces is obtained by fitting the histograms of adhesion forces of at least 500 peeling events with Gaussian equation. In this study, the polymer is covalently anchored onto the cantilever prior to the experiment so that the possibility of picking up pre-adsorbed polymer chain(s) on the substrate using a raw AFM cantilever is very low⁹⁷.

Experimentally, two neutral and one cationic polymers were studied using the SMFS technique. One neutral homopolymer was synthesized using di(ethylene glycol) methyl ether methacrylate (MEO₂MA) as monomer and is referred to as polymer N1 in the remainder of the paper. The other

neutral polymer (polymer N2) was an oligo ethylene glycol methacrylate based copolymer that was composed of MEO₂MA and oligo ethylene glycol methyl ether methacrylate (MEO₈MA). These two monomers are almost identical in the chemical structure, except for the length of the ethylene glycol (EG) side chain, which gives rise to different degrees of hydrophobicity of the monomers. Polymer N1 was found relatively hydrophobic and not soluble in 1 mM NaCl solutions at room temperature while the polymer N2, which is more hydrophilic, was reported to dissolve well under the same condition³⁴. For comparison, the cationic polymer used in this study was poly (vinylbenzyl trimethyl ammonium chloride) (polymer C1) (Please refer to Table S1 in supporting information for detailed chemical structure and molecular weight of the studied polymers).

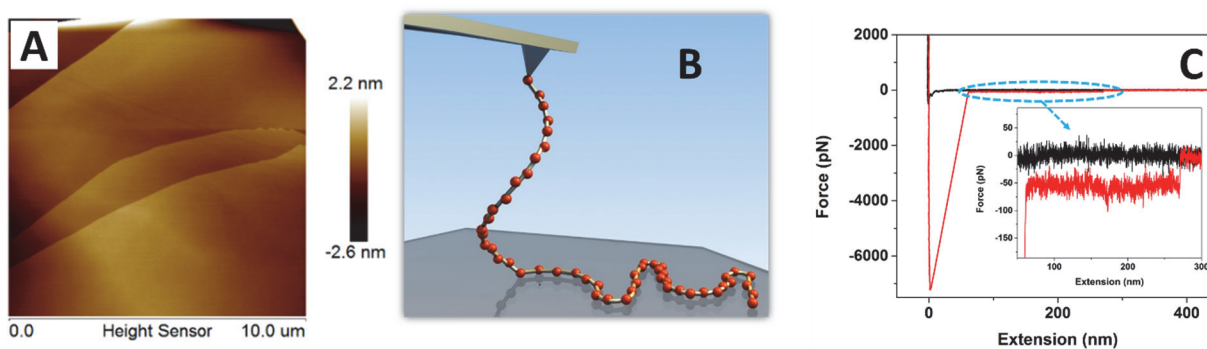


Figure 6-1 AFM image of MoS₂ basal surface (A), schematic representation showing the SMFS experiment on basal surface of MoS₂ (B) and typical force curves obtained in a SMFS experiment when a chain of Polymer C1 was peeled from basal surface of MoS₂ in 1 mM NaCl aqueous solutions of pH around 5.5 (C).

Figure 6-1 C shows SMFS force curves obtained in a typical experiment after baseline correction. Only the retraction force curves were relevant to this investigation. The single plateau in the force curve indicates that only one polymer chain was probed in this system. Force curves with multiple plateaus could also be observed under the same experimental conditions due to statistically nature of the binding events inherent in this type of measurements. The statistical distribution of the first and second plateaus of the collected force curves between oligo ethylene glycol copolymer and MoS₂ basal surface in 1 mM NaCl aqueous solutions is shown in Figure 6-2B. The mean adhesion forces obtained by statistical analysis were found around 52 pN for the first peak and 105 pN for the second. The fact that the force for the second peak was twice the first indicated that multiple polymer chains were probed simultaneously when two or more plateaus were observed. However,

only the first plateau was analyzed in the rest of the paper as it represents the single-molecule peeling event.

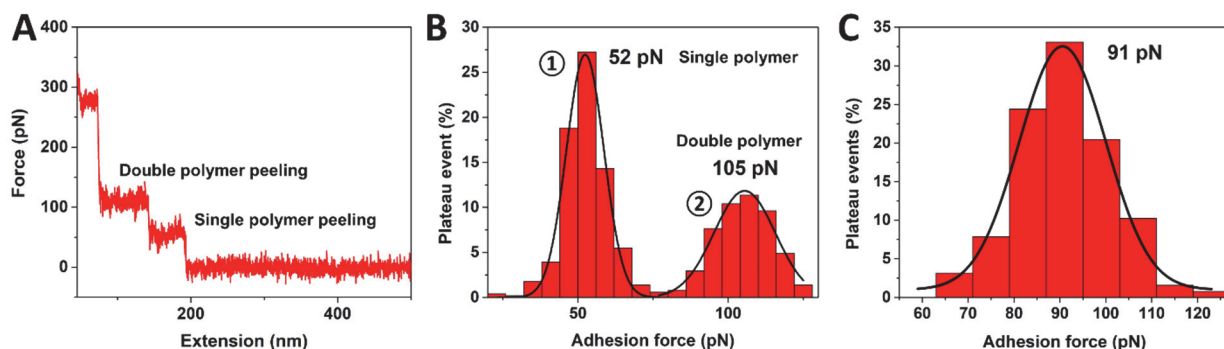


Figure 6-2 Representative force curve obtained in the SMFS experiment when a chain of Polymer N2 was peeled from basal surface of MoS₂ (A). The statistical SMFS results obtained between MoS₂ basal surface and polymer N2 (B) or polymer N1 (C). The experiments were carried out in the presence of 1 mM NaCl (pH 5.5) background solution.

The single-molecule adhesion force of neutral oligo ethylene glycol copolymer on MoS₂ basal plane surface was around 52 pN. It was insensitive to the pulling rate though the level of background noise in the force curves were clearly increased (see Figure D-2 in supplementary information). In this study, the single-molecule adhesion force of polymer N1 on MoS₂ basal surface was also probed. The statistical average single-molecule adhesion force was around 91 pN for polymer N1, which was much higher than that of the oligo ethylene glycol copolymer (52 pN). The differences of the adhesion force per single-polymer for these two neutral polymers exceeded any deviation due to the uncertainty of the AFM force measurement which was around 10%. The results confirmed that the hydrophobicity of the polymer and hydrophobic attraction were important in determining the single-molecule polymer-substrate interaction. The results of the interaction between Polymer C1 and MoS₂ basal surface are shown in Figure 6-3B. At the same pH (5.5), the single-molecule force was around 59 pN when a single cationic Polymer C1 chain was peeled from the MoS₂-water interface.

Meanwhile, the influence of solution pH on single-molecule interaction of Polymer C1 on MoS₂ basal surface was probed as well since the stability of surface functionalization by polymer is important. The SMFS experiments were performed in 1 mM NaCl background solution to ensure

that the electric double layer (EDL) interaction is not effectively screened. Detailed investigation on the surface property of MoS₂ basal surface has confirmed that the surface potential is pH dependent¹⁴⁰. Typical surface potential value of MoS₂ basal surface when pH = 3 is around - 28 mV and decreased to - 44 mV when the pH is increased to 11. As the salt concentration was too low to effectively screen the electric double layer interaction, the significant dependence of single-molecule adhesion force between polymer C1 and MoS₂ basal surface on solution pH was observed. The single-molecule adhesion force increased from 50 pN when pH was around 3.3 to 78 pN when the pH was high (pH = 9.9) (Figure 6-3C). The change on the surface potential led to the change of adhesion force as the polymer chain was positively charged.

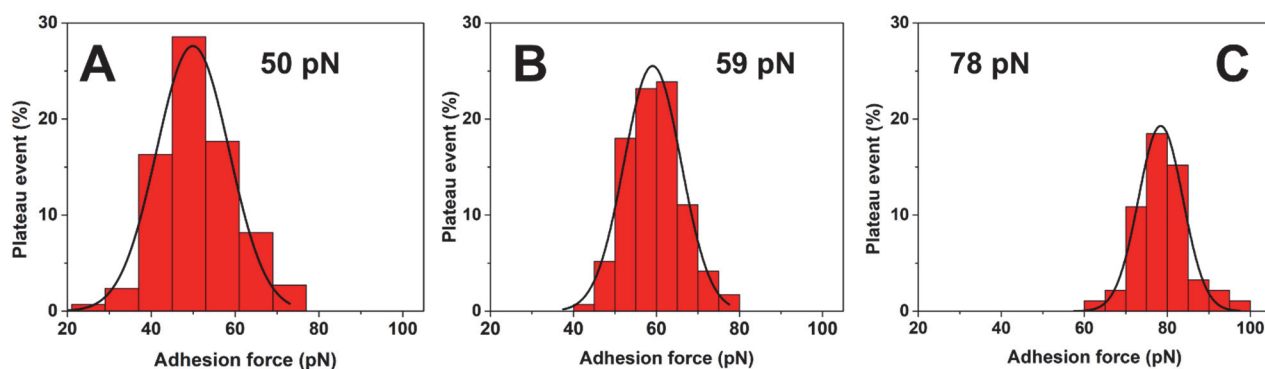


Figure 6-3 Influence of the solution pH on the strength of the single-molecule adhesion force on MoS₂ basal surface for Polymer C1. (A) pH = 3.3, (B) pH = 5.5 and (C) pH = 9.9.

The SMFS experiments revealed the magnitude of the single-molecule adhesion force for the three polymers on MoS₂ basal surface and the dependence on the solution pH. However, the anisotropic properties of the MoS₂ calls for SMFS investigations on the edge surface to fully characterize the system. Thus, in this study, the interaction of polymer-MoS₂ edge surface was studied for the first time with resolution into single-molecule level. The edge surface was prepared according to our previous reported procedures¹⁴⁰. In detail, the ultramicrotome was used with diamond knife to obtain smooth edge surface (Please refer to Figure D-3 in supporting information for detailed information).

The interaction between MoS₂ edge surface and neutral polymers (polymer N1 and N2) was studied first. Figure 6-4A schematically shows the measurement of single-molecule interaction between polymers and edge surface of MoS₂. Surprisingly, only baseline was observed as shown

in Figure 6-4B. On the contrary, the single-molecule adhesion force of polymer C1 on the hydrophilic edge surface in 1 mM NaCl background solution of pH = 5.5 was determined to be 51 pN (Figure 6-4B). The results illustrated that the non-detectable single-molecule interaction between neutral polymers and hydrophilic edge surface was due to the ultra-weak interactions.

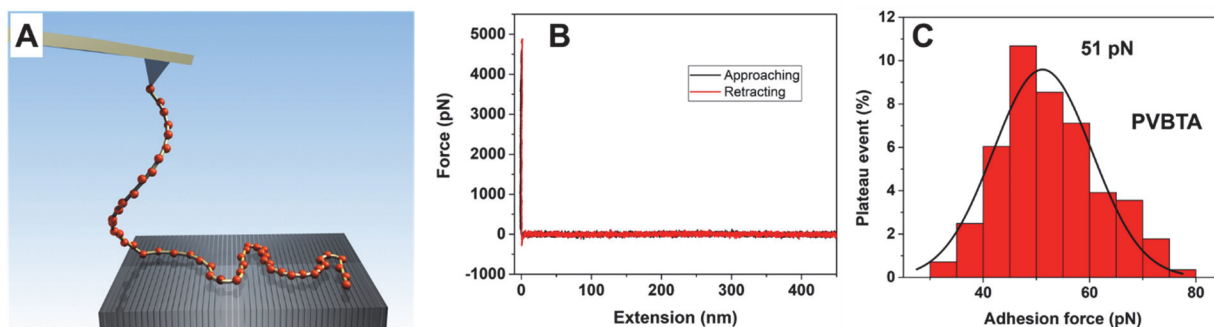


Figure 6-4 (A) Schematic representation showing the SMFS experiment probing single-molecule adhesion force on hydrophilic edge surface of MoS₂, (B) typical force curve showing no single-molecule interaction of polymer N2 on hydrophilic edge surface and (C) histogram of single-molecule adhesion forces of positively charged polymer C1 on negatively charged hydrophilic edge surface of MoS₂ in the presence of 1 mM NaCl with a pH around 5.5.

Based on the fundamental understanding of the molecular interaction, it is reasonable to conclude that polymer C1 was more promising compared to polymer N2 for effective exfoliation of bulk MoS₂ crystals as it interacts with both surfaces of MoS₂ and highly water soluble. When the polymer C1 is added to the aqueous suspension of MoS₂ crystals/particles, the polymer adsorbs on both basal and edge surface of MoS₂. However, since the polymer-edge and polymer-basal interactions are relatively close in magnitude, it is not likely that the polymer would adsorb preferentially on basal or edge surfaces. The polymer N1 was not considered to be a good candidate as it was not soluble in water. Therefore, polymer C1 is used as exfoliation agent in the next section to prepare single-layered MoS₂ nanosheets.

6.4 Polymer assisted exfoliation of MoS₂ in aqueous solution

To illustrate the role of single molecule forces measured by SMFS in exfoliating MoS₂, the exfoliation experiment using selected polymer (Polymer C1) was conducted. Meanwhile, the performance of neutral polymer N2 was also studied for comparison. After grinding for 2h in water using polymer C1 as exfoliation agent, MoS₂ sheets dispersion was obtained after centrifuge in

8000 rpm. The UV-Vis absorption spectrum of the obtained exfoliated MoS₂ sheets clearly exhibited two peaks at 607 and 666 nm (Figure 6-5A), which can be attributed to the direct excitonic transition at K point of Brillouin zone for single-layer MoS₂ sheets^{128, 235}. The blue shift of the absorption peak from 687 for bulk MoS₂¹²⁸ to 666 nm in this study confirmed that the number of layers was greatly reduced. The polymer C1-dispersed MoS₂ nanosheets were stable after storing for 6 months without any noticeable aggregation or precipitation. Moreover, it was stable over the entire pH range (0 -14) studied. In addition, in a control experiment, transparent supernatant was obtained after grinding treatment without adding polymer C1 (Figure 6-5A). For polymer N2, the exfoliation performance was found to be poor (Figure 6-5A). As shown in Figure 6-5A, the production of exfoliated MoS₂ in unit time using polymer N2 was much lower than that of C1. Meanwhile, optical pictures were also provided in Figure D-4 in supplementary information. Moreover, compared with those of polymer C1, the size of the exfoliated MoS₂ after 2 h grinding was large and thicker (see Figure D-5 in supporting information). Here, one can see that polymer C1 was an effective functionalization and exfoliating agent for preparing highly dispersed single-layer nanosheets in water. Thus, polymer C1 was utilized for the scaled production of single-layer MoS₂ nanosheets.

When exfoliating bulk MoS₂ powder via aqueous phase grinding, the resulted dispersion was monitored using UV-Vis absorption spectrum at predetermined time interval. The adsorption intensity of the dispersions quickly increased in the first 100 min and then leveled off, reaching an equilibrium state. Figure 6-5A clearly shows the linear relationship of the spectrum intensity with processing time during the early stage of grinding. The amount of the exfoliated MoS₂ nanosheets grew linearly with the grinding time in the first 100 min. However, only grinding was found not enough for the readily production of single-layer MoS₂ since only MoS₂ sheets with 2-3 layers with size around 500 nm were obtained (Figure D-5). Thus, tip sonication (2 h) was combined with the grinding procedures. The obtained MoS₂ nanosheets were first characterized by TEM to show the presence of thin 2D flakes. The size of the flakes was less than 50 nm. The high-resolution TEM image clearly shows the hexagonal lattice structure of prepared single-layer MoS₂ nanosheets (Figure 6-5C). The obtained lattice spacing is 0.27 nm and can be assigned to the (100) atomic plane of MoS₂^{193, 236}. The Fast Fourier Transform (FFT) in Figure 6-5B shows perfect hexagonal spot pattern. Though previous investigation indicated that the crystal structure of MoS₂ is prone to be destroyed during sonication²³⁰, our results indicated that the obtained MoS₂ flakes

retained the single crystal structure^{117, 195} and were free of damage. The HR-TEM on the edge of MoS₂ nanosheet (Figure 6-5C) was also observed and revealed that the obtained MoS₂ flakes were in single-layer. Atomic force microscopy imaging confirmed the production of single-layer MoS₂ nanosheets with thickness centered around 0.7 nm (Figures 6-5D and 6-5E)²³⁷. The efficient exfoliation of MoS₂ into single-layer was further confirmed using X-ray diffraction (XRD) (Figure D-6). The XRD pattern of the exfoliated MoS₂ nanosheets did not show any reflection peaks that is typical for bulk MoS₂, indicating that there was no stacking of MoS₂ layers due to effective exfoliation and formation of single-layer nanosheets^{117, 195}. Raman characterization of the prepared sample is shown in Figure D-7 of supporting information. The single-layer MoS₂ nanosheets exhibit bands at 381 and 405 cm⁻¹, which can be attributed to the in-plane vibration (E_{12g}) and out-of-plane vibration (A_{1g}) modes, respectively. The concentration of prepared single-layer MoS₂ nanosheets in water was determined to be 6.7 mg/mL, which was an order of magnitude higher than that of the other methods using N-methylpyrrolidone (0.3 mg/mL)²³⁶, surfactant (0.5 mg/mL)²³¹ or poly(ionic liquid) (0.5 mg/mL)²³. The exfoliation rate was determined to be 4.6 x 10¹⁴ layers per hour, which is two orders of magnitude higher than previous reported values¹²⁸. The mass measurement of polymer adsorbed on MoS₂ nanosheet surface was quantified using Thermal Gravimetric Analysis (TGA) and found that 2.2 mg of polymer C1 was absorbed on 1.69 mg MoS₂ basal and edge surfaces (see Figure D-8 in supplementary information).

Through the SMFS investigation and experimental exfoliation, a simple hypothesis was proposed for the formation of single-layer and two-layered MoS₂ nanosheets (Figure 6-6). After adding polymer C1 in to MoS₂ aqueous dispersion, polymer C1 molecules spontaneously interact with the exposed basal and edge surfaces of MoS₂ via electric double layer interaction (refer to SMFS investigation part). Meanwhile, the hydrophobic attraction between the hydrophobic phenyl ring on the chemical structure of the polymer and the basal surface may also plays a role. Upon grinding, the surface layers of MoS₂ crystals could slide gradually upon mechanical shear and collision forces. It was irreversible as the freshly exposed surfaces were immediately covered by free polymer C1, eventually leading to the exfoliation of bulk MoS₂ into single-layer MoS₂ nanosheets in water. This cycle was repeated for many times to produce high concentration of single-layer MoS₂ nanosheets in water.

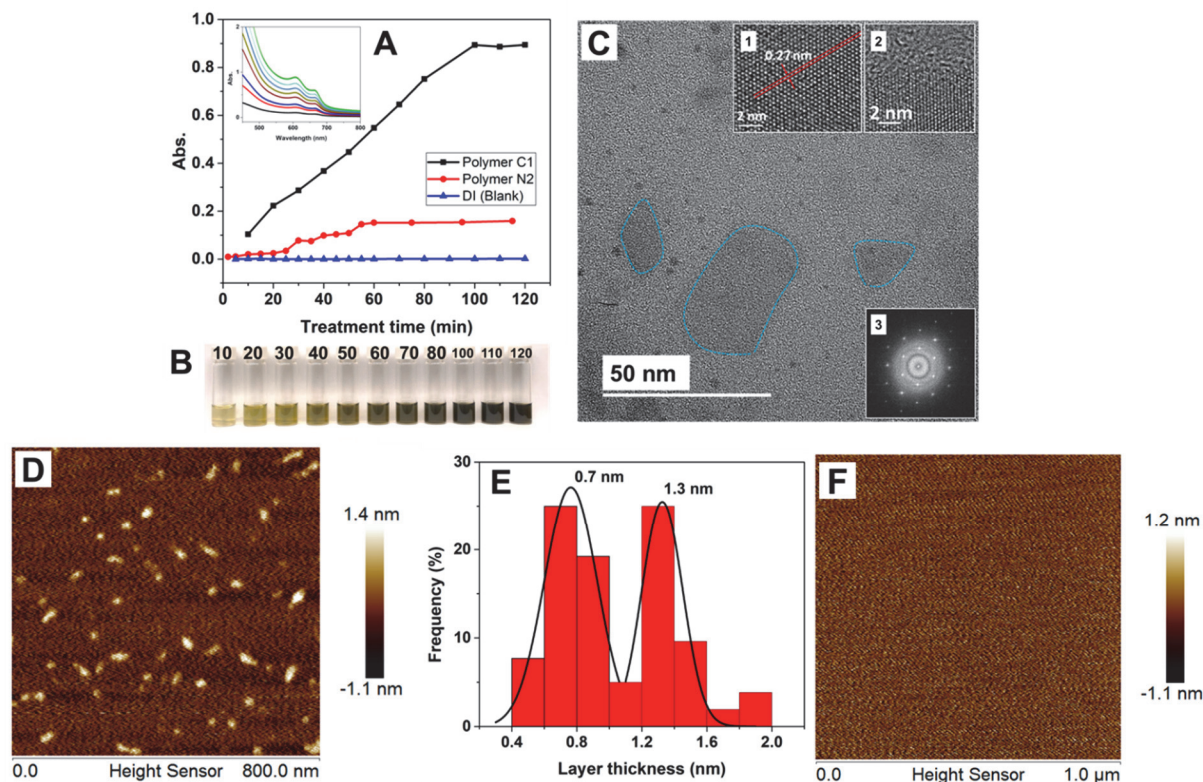


Figure 6-5 (A) Temporal evolution of the absorption intensity at 666 nm with the increase of treatment time (The raw dispersion was diluted for 4 times). The inset is UV-vis spectra of the obtained exfoliated MoS₂ nanosheets in water after treatment for different time. (B) Optical images of the obtained exfoliated MoS₂ nanosheets dispersion using polymer C1 as exfoliation agent. (C) TEM image of the MoS₂ nanosheets exfoliated by using polymer C1 as functionalization agent. The insets are the high-resolution TEM images showing the lattices structure of single-layer MoS₂ nanosheet (1), the edge of nanosheet (2) and the Fast Fourier Transform (FFT) pattern (3). (D) AFM image of single-layer MoS₂, (E) statistical analysis of layer thickness of the obtained exfoliated MoS₂ nanosheets showing the thickness of a single-layer is around 0.7 nm and (F) AFM image of raw mica.

In this study, we performed a SMFS investigation of polymer with basal and edge surfaces of MoS₂. The quantification of single-molecule adhesion force allowed us to quantify the strength of the polymer-MoS₂ interaction, which determines the performance/stability of the non-covalent functionalization by polymer. Meanwhile, this technique also allowed the quantification of polymer on the edge surface of MoS₂ which is difficult to realize using other techniques. The fundamental understanding of single-molecule interaction facilitated the selection of appropriate

polymer for effective functionalization of MoS₂ bulk powders for efficient exfoliation. However, one must be careful when selecting the polymer candidate for functionalization based on SMFS results if stabilization of desired particles/nanosheets in certain liquid is desired. Previous theoretical investigation concluded that the adsorption of polymer chain on the interface would lead to the presence of loops, trains and tails¹⁰². The presence of tails and loops is responsible for stabilization²³⁸, which in general relies on repulsive interactions between polymer segments on opposite surfaces. It can be attributed to osmotic interactions that arises in a good solvent. The overlap of the polymer chains on approaching surfaces suppress the available conformation for polymer chains (entropy in origin), which results in repulsive steric interactions. Thus, the selected polymer must have good compatibility with solvent when adsorption stabilization is desired. Otherwise, attractive forces would be dominant between the surfaces, which leads to the presence of large aggregates. Therefore, functionalization performance of polymer N1 was not tested in this study though it showed the highest single-molecule adhesion force on basal surface. Furthermore, for polyelectrolytes, beside the osmotic repulsion, the electric double layer repulsion plays a significant role as well. The charges on the polymer chain can be beneficial for stabilization as they offer extra strong repulsive electric double interaction. The zeta potential of the obtained exfoliated single-layer MoS₂ after combined grinding and tip sonication using polymer N2 and C1 as exfoliation agent was determined to be -5.5 and +37.9 mV, respectively (please see Table S2 in supporting information). This huge difference leads to distinctively different electric double layer interactions experienced by the dispersed MoS₂ nanosheets. This might be another reason why the selected PVBTA (polymer C1) is much more superior to neutral polymer N2 in stabilizing and exfoliating MoS₂ bulk material into single-layer nanosheets.

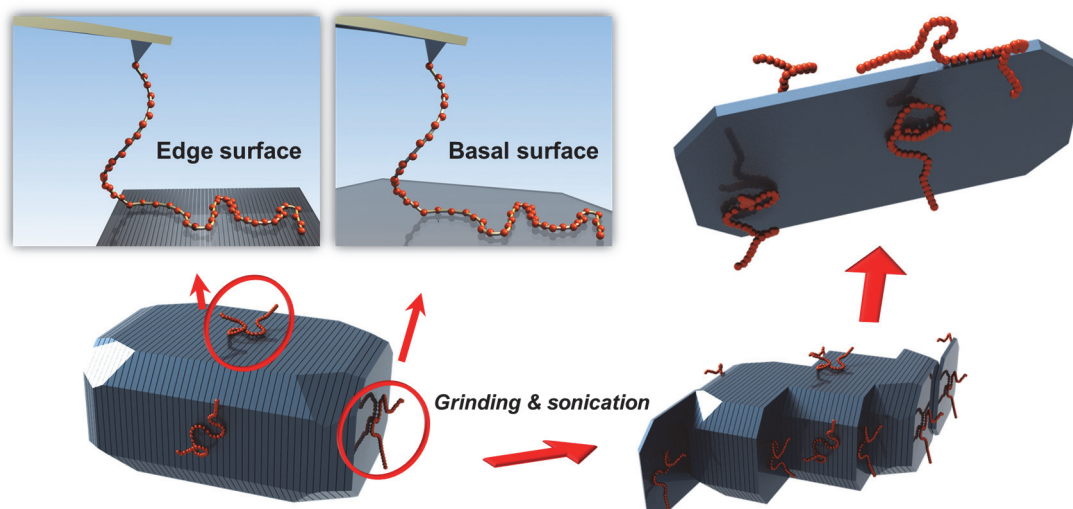


Figure 6-6 Schematics for the exfoliation of bulk MoS₂ nanosheets into single-layer using Polymer C1 as a functionalization/exfoliation agent.

6.5 Conclusions

In summary, we managed to quantify the single-molecule interaction between polymer and MoS₂ surfaces using SMFS. The comparison of different polymers for stable functionalization of MoS₂ became possible as quantified SMFS experimental results in single-molecule level were provided. The selected poly (vinylbenzyl trimethyl ammonium chloride) showed high performance in functionalizing, stabilizing and exfoliating MoS₂ crystals into single-layer, which is the first time that MoS₂ was exfoliated into single-layer using synthetic polymer in aqueous phase exfoliation with concentration above 5 mg/ml while the treatment time was decreased by one magnitude. We have shown here that the investigation of the fundamental polymer-MoS₂ interaction using SMFS can be beneficial for the materials science as guideline for the selection of appropriate functionalization agents was given by the fundamental results. We hope this systematic approach may shed light on finding suitable functionalization agent for other materials, where breakthrough is needed.

Chapter 7

Conclusions and Recommendations for Future Work

The conclusions of this thesis and the recommendations for future research are summarized in this chapter.

7.1 Conclusions

Firstly, the general experimental approach for the quantification of the single-molecule interaction between polymer and solid-liquid interface was established. By utilizing this technique, the interaction between stimuli-responsive oligo ethylene glycol methacrylate copolymer and hydrophobic basal surface of MoS₂ was quantified. Based on the dual stimuli-responsive properties of the studied copolymer, the single-molecule adhesion force of copolymer on the MoS₂ surface was monitored as a function of NaCl concentration, or in other words, as a function of the hydrophobicity of the polymer. The results provided in-depth understanding of the interaction between a stimuli-responsive polymer and hydrophobic surface during the switching process. The probed single-molecule adhesion force that was dependent on the concentration of environmental stimuli (NaCl) revealed the magnitude of the fundamental single-molecule adhesion force (50-80 pN) and indicated that hydrophobic attraction was important in governing the strength of polymer-solid interaction in water. Theoretical analysis demonstrated that the contribution of entropic free energy to the single-molecule adhesion force was minor (~11%) and the magnitude of the adhesion energy per monomer was around 2-4 $k_B T$. Moreover, it was found that polymers adopt similar conformations on hydrophobic MoS₂ basal surfaces in water when they exhibited hydrophilic coil or hydrophobic collapsed globule states in bulk solutions.

Secondly, the anisotropic properties of MoS₂ crystal were utilized for the determination of the individual contribution of van der Waals interaction, electric double layer interaction and hydrophobic attraction. The probed single-molecule adhesion force that was independent on the surface potential of MoS₂ basal surface excluded the presence of electric double layer interactions. The strong single-molecule adhesion force on hydrophobic basal and non-detectable force on hydrophilic edge surface demonstrated that the van der Waals interaction was weak, and its contribution to the total single-molecule adhesion force was smaller than the lower detection limit of the equipment (9 pN). The experimental results elucidated that the hydrophobic attraction played a dominant role in determining the strength of single-molecule adhesion force. Further experiments probing the influence of ethanol addition and polymer composition confirmed the significant role of hydrophobic attraction.

Thirdly, the single-molecule adhesion force as a function of the concentration of environmental stimuli (NaCl) was probed on another molecularly smooth hydrophobic surface of highly oriented pyrolytic graphite (HOPG). The similar single-molecule adhesion behavior as a function of NaCl revealed that the probed trend of polymer-solid interaction in water was not substrate dependent and represented the general interplay between stimuli-responsive polymer and hydrophobic surfaces. The good agreement between the experimental results and derived theoretical model further confirmed the aforementioned claim that hydrophobic attraction drove the interplay between neutral oligo ethylene glycol methacrylate copolymer and hydrophobic surfaces in water. Furthermore, this study presented a mathematical relationship between the hydrophobic hydration free energy and single-molecule force, which provided guidelines for the optimization or designing of underwater adhesive systems or non-covalent functionalization agent.

Finally, relying on the ultra-high force sensitivity and space resolution of single molecule force spectroscopy (SMFS), high performance polymeric functionalization agent was discovered for scaled production of single-layered MoS₂ nanosheets. The setup of the SMFS experiment allowed the quantification of single polymer adhesion force on both basal and edge surfaces. Among the studied polymers, the cationic poly (vinylbenzyl trimethyl ammonium chloride) (PVBTA) was indicated to be the promising candidate polymer because it interacted strongly with both basal and edge surfaces of MoS₂ and was highly water soluble. Mechanical exfoliation of MoS₂ was performed and single-layered nanosheets were obtained with record high concentration. The combined SMFS and exfoliation experiments demonstrated that the optimization of current material preparation processes calls for in-depth understanding of the fundamental interactions between polymers and interested materials. More importantly, the approach provided in this study that probing quantitative single-molecule interaction by SMFS for reasonable estimation and comparison of the potential performance is highly effective. This method can be applied to a variety of practical applications where polymer-solid interaction is important for system improvement.

7.2 Recommendations for future work

Future work should address the following issues:

1 In Chapter 3, the single-molecule interaction of oligo ethylene glycol methacrylate copolymer on hydrophobic basal surface of MoS₂ was probed, which is in the range of 50-75 pN. However,

the physical picture that the location of polymer chain on the hydrophobic interface is not clear. Meanwhile, it is also desired to know if the oligo ethylene glycol side chain of the adsorbed polymer lays flat on the substrate or stretched into the solution. Rigorous simulation work combined with systematic SMFS experiments are recommended for the future work.

2 In Chapter 4, the contribution of the van der Waals interaction to the total single-molecule adhesion force of studied polymer on MoS₂ surfaces is lower than the lower detection limit of the SMFS, which is 9 pN. However, the exact number of the contribution is not able to be determined based on the current studied polymer-solid pair. Future work should address this problem by either using cantilevers with lower spring constant or change the setup of the SMFS experiment.

3 In Chapter 5, theoretical model was developed relating the single-molecule adhesion force with hydrophobic hydration free energy. This mathematical relationship provides quantitative understanding on how Mussel adopt themselves to a variety of environmental conditions for safe, secure and adequate underwater adhesion. However, no application of the proposed theoretical model was performed to improve the performance of synthetic underwater adhesives in this study. It is highly recommended that such application should be done in the future work.

4 In Chapter 6, the single-molecule interaction between cationic poly (vinylbenzyl trimethyl ammonium chloride) (PVBTA) and basal surface of MoS₂ was probed as a function of pH. The obvious dependence of single-molecule adhesion force on pH reveals the significant contribution of electric double layer interaction. It is interesting for the further work to deconvolute the individual contribution of van der Waals, electric double layer and hydrophobic interactions between this cationic polymer and hydrophobic surfaces.

Bibliography

1. Alagha, L.; Wang, S. Q.; Yan, L. J.; Xu, Z. H.; Masliyah, J., Probing Adsorption of Polyacrylamide-Based Polymers on Anisotropic Basal Planes of Kaolinite Using Quartz Crystal Microbalance. *Langmuir* **2013**, *29* (12), 3989-3998.
2. Zhao, Q.; Lee, D. W.; Ahn, B. K.; Seo, S.; Kaufman, Y.; Israelachvili, J. N.; Waite, J. H., Underwater contact adhesion and microarchitecture in polyelectrolyte complexes actuated by solvent exchange. *Nat Mater* **2016**, *15* (4), 407-412.
3. Levine, Z. A.; Rapp, M. V.; Wei, W.; Mullen, R. G.; Wu, C.; Zerze, G. H.; Mittal, J.; Waite, J. H.; Israelachvili, J. N.; Shea, J. E., Surface force measurements and simulations of mussel-derived peptide adhesives on wet organic surfaces. *P Natl Acad Sci USA* **2016**, *113* (16), 4332-4337.
4. Utzig, T.; Raman, S.; Valtiner, M., Scaling from Single Molecule to Macroscopic Adhesion at Polymer/Metal Interfaces. *Langmuir* **2015**, *31* (9), 2722-2729.
5. Raman, S.; Utzig, T.; Baimpos, T.; Shrestha, B. R.; Valtiner, M., Deciphering the scaling of single-molecule interactions using Jarzynski's equality. *Nat Commun* **2014**, *5*, 1-7.
6. Ashkin, A.; Dziedzic, J. M.; Bjorkholm, J. E.; Chu, S., Observation of a Single-Beam Gradient Force Optical Trap for Dielectric Particles. *Opt Lett* **1986**, *11* (5), 288-290.
7. Tskhovrebova, L.; Trinick, J.; Sleep, J. A.; Simmons, R. M., Elasticity and unfolding of single molecules of the giant muscle protein titin. *Nature* **1997**, *387* (6630), 308-312.
8. Wang, M. D.; Schnitzer, M. J.; Yin, H.; Landick, R.; Gelles, J.; Block, S. M., Force and velocity measured for single molecules of RNA polymerase. *Science* **1998**, *282* (5390), 902-907.
9. Dame, R. T.; Noom, M. C.; Wuite, G. J. L., Bacterial chromatin organization by H-NS protein unravelled using dual DNA manipulation. *Nature* **2006**, *444* (7117), 387-390.

10. Liphardt, J.; Onoa, B.; Smith, S. B.; Tinoco, I.; Bustamante, C., Reversible unfolding of single RNA molecules by mechanical force. *Science* **2001**, 292 (5517), 733-737.
11. Strick, T.; Allemand, J. F.; Croquette, V.; Bensimon, D., Twisting and stretching single DNA molecules. *Prog Biophys Mol Bio* **2000**, 74 (1-2), 115-140.
12. Charvin, G.; Strick, T. R.; Bensimon, D.; Croquette, V., Tracking topoisomerase activity at the single-molecule level. *Annu Rev Bioph Biom* **2005**, 34, 201-219.
13. Gore, J.; Bryant, Z.; Stone, M. D.; Nollmann, M. N.; Cozzarelli, N. R.; Bustamante, C., Mechanochemical analysis of DNA gyrase using rotor bead tracking. *Nature* **2006**, 439 (7072), 100-104.
14. Bausch, A. R.; Moller, W.; Sackmann, E., Measurement of local viscoelasticity and forces in living cells by magnetic tweezers. *Biophys J* **1999**, 76 (1), 573-579.
15. Koster, D. A.; Croquette, V.; Dekker, C.; Shuman, S.; Dekker, N. H., Friction and torque govern the relaxation of DNA supercoils by eukaryotic topoisomerase IB. *Nature* **2005**, 434 (7033), 671-674.
16. Hinterdorfer, P.; Dufrene, Y. F., Detection and localization of single molecular recognition events using atomic force microscopy. *Nat Methods* **2006**, 3 (5), 347-355.
17. Grandbois, M.; Beyer, M.; Rief, M.; Clausen-Schaumann, H.; Gaub, H. E., How strong is a covalent bond? *Science* **1999**, 283 (5408), 1727-1730.
18. Fernandez, J. M.; Li, H. B., Force-clamp spectroscopy monitors the folding trajectory of a single protein. *Science* **2004**, 303 (5664), 1674-1678.
19. Lee, G. U.; Chrisney, L. A.; Colton, R. J., Direct Measurement of the Forces between Complementary Strands of DNA. *Science* **1994**, 266 (5186), 771-773.
20. Carrion-Vazquez, M.; Li, H. B.; Lu, H.; Marszalek, P. E.; Oberhauser, A. F.; Fernandez, J.

M., The mechanical stability of ubiquitin is linkage dependent. *Nat Struct Biol* **2003**, *10* (9), 738-743.

21. Dietz, H.; Berkemeier, F.; Bertz, M.; Rief, M., Anisotropic deformation response of single protein molecules. *P Natl Acad Sci USA* **2006**, *103* (34), 12724-12728.

22. Binnig, G.; Quate, C. F.; Gerber, C., Atomic Force Microscopy. *Physical Review Letters* **1986**, *56* (9), 930-933.

23. Jalili, N.; Laxminarayana, K., A review of atomic force microscopy imaging systems: application to molecular metrology and biological sciences. *Mechatronics* **2004**, *14* (8), 907-945.

24. Rief, M.; Oesterhelt, F.; Heymann, B.; Gaub, H. E., Single molecule force spectroscopy on polysaccharides by atomic force microscopy. *Science* **1997**, *275* (5304), 1295-1297.

25. Liu, N. N.; Zhang, W. K., Feeling Inter- or Intramolecular Interactions with the Polymer Chain as Probe: Recent Progress in SMFS Studies on Macromolecular Interactions. *Chemphyschem* **2012**, *13* (9), 2238-2256.

26. Wang, C.; Shi, W. Q.; Zhang, W. K.; Zhang, X.; Katsumoto, Y.; Ozaki, Y., Force spectroscopy study on poly(acrylamide) derivatives: Effects of substitutes and buffers on single-chain elasticity. *Nano Lett* **2002**, *2* (10), 1169-1172.

27. Hugel, T.; Grosholz, M.; Clausen-Schaumann, H.; Pfau, A.; Gaub, H.; Seitz, M., Elasticity of Single Polyelectrolyte Chains and Their Desorption from Solid Supports Studied by AFM Based Single Molecule Force Spectroscopy. *Macromolecules* **2001**, *34* (4), 1039-1047.

28. Kienle, S.; Gallei, M.; Yu, H.; Zhang, B. Z.; Krysiak, S.; Balzer, B. N.; Rehahn, M.; Schluter, A. D.; Hugel, T., Effect of Molecular Architecture on Single Polymer Adhesion. *Langmuir* **2014**, *30* (15), 4351-4357.

29. Reis, L. A.; Rocha, M. S., DNA interaction with DAPI fluorescent dye: Force spectroscopy

decouples two different binding modes. *Biopolymers* **2017**, *107* (5), 1-8.

30. Nevzorova, T. A.; Zhao, Q.; Lomakin, Y. A.; Ponomareva, A. A.; Mukhitov, A. R.; Purohit, P. K.; Weisel, J. W.; Litvinov, R. I., Single-Molecule Interactions of a Monoclonal Anti-DNA Antibody with DNA. *Bionanoscience* **2017**, *7* (1), 132-147.

31. Bao, Y.; Qian, H. J.; Lu, Z. Y.; Cui, S., Revealing the Hydrophobicity of Natural Cellulose by Single-Molecule Experiments. *Macromolecules* **2015**, *48* (11), 3685-3690.

32. Luo, Z. L.; Zhang, A. F.; Chen, Y. M.; Shen, Z. H.; Cui, S. X., How Big Is Big Enough? Effect of Length and Shape of Side Chains on the Single-Chain Enthalpic Elasticity of a Macromolecule. *Macromolecules* **2016**, *49* (9), 3559-3565.

33. Yu, M.; Qian, L.; Cui, S. X., Reentrant Variation of Single-Chain Elasticity of Polyelectrolyte Induced by Monovalent Salt. *Journal of Physical Chemistry B* **2017**, *121* (16), 4257-4264.

34. Nash, M. A.; Gaub, H. E., Single-Molecule Adhesion of a Stimuli-Responsive Oligo(ethylene glycol) Copolymer to Gold. *Acs Nano* **2012**, *6* (12), 10735-10742.

35. Wang, C. Z.; Hu, R.; Morrissey, J. J.; Kharasch, E. D.; Singamaneni, S., Single Molecule Force Spectroscopy to Compare Natural versus Artificial Antibody-Antigen Interaction. *Small* **2017**, *13* (19), 1-7.

36. Dai, P.; Wang, S. K.; Taub, H.; Buckley, J. E.; Ehrlich, S. N.; Larese, J. Z.; Binnig, G.; Smith, D. P. E., X-Ray-Diffraction and Scanning-Tunneling-Microscopy Studies of a Liquid-Crystal Film Adsorbed on Single-Crystal Graphite. *Phys Rev B* **1993**, *47* (12), 7401-7407.

37. Binnig, G.; Garcia, N.; Rohrer, H., Conductivity Sensitivity of Inelastic Scanning Tunneling Microscopy. *Phys Rev B* **1985**, *32* (2), 1336-1338.

38. <https://www.brukerafmprobes.com/p-3419-msct.aspx>.

39. APractical Guide to SPM scanning Probe Microscopy. *Veeco Instruments Inc.* **2005**.
40. MULTIMODE 8 INSTRUCTION MANUAL-B. *Bruker Corporation* **2011**.
41. Burnham, N. A.; Chen, X.; Hodges, C. S.; Matei, G. A.; Thoreson, E. J.; Roberts, C. J.; Davies, M. C.; Tendler, S. J. B., Comparison of calibration methods for atomic-force microscopy cantilevers. *Nanotechnology* **2003**, *14* (1), 1-6.
42. Casimir, H. B. In *On the attraction between two perfectly conducting plates*, Proceedings of the KNAW, 1948; pp 793-795.
43. Butt, H. J.; Jaschke, M., CALCULATION OF THERMAL NOISE IN ATOMIC-FORCE MICROSCOPY. *Nanotechnology* **1995**, *6* (1), 1-7.
44. <http://main.spsj.or.jp/c5/kobunshi/kobu2009/hottopics0909.html>.
45. Kienle, S.; Liese, S.; Schwierz, N.; Netz, R. R.; Hugel, T., The Effect of Temperature on Single-Polypeptide Adsorption. *Chemphyschem* **2012**, *13* (4), 982-989.
46. Neuman, K. C.; Nagy, A., Single-molecule force spectroscopy: optical tweezers, magnetic tweezers and atomic force microscopy. *Nat Methods* **2008**, *5* (6), 491-505.
47. Noy, A., Force spectroscopy 101: how to design, perform, and analyze an AFM-based single molecule force spectroscopy experiment. *Curr Opin Chem Biol* **2011**, *15* (5), 710-718.
48. Evans, E.; Ritchie, K., Dynamic strength of molecular adhesion bonds. *Biophysical Journal* **1997**, *72* (4), 1541-1555.
49. Hutter, J. L.; Bechhoefer, J., Calibration of Atomic-Force Microscope Tips. *Rev Sci Instrum* **1993**, *64* (11), 3342-3342.
50. Paturej, J.; Dubbeldam, J. L. A.; Rostiashvili, V. G.; Milchev, A.; Vilgis, T. A., Force Spectroscopy of Polymer Desorption: Theory and Molecular Dynamics Simulations. *Soft Matter* **2014**, *10* (16), 2785-2799.

51. Manohar, S.; Mantz, A. R.; Bancroft, K. E.; Hui, C.-Y.; Jagota, A.; Vezenov, D. V., Peeling Single-Stranded DNA from Graphite Surface to Determine Oligonucleotide Binding Energy by Force Spectroscopy. *Nano Lett* **2008**, *8* (12), 4365-4372.
52. Serr, A.; Netz, R. R., Pulling adsorbed polymers from surfaces with the AFM: stick vs. slip, peeling vs. gliding. *Europhysics Letters* **2006**, *73* (2), 292-298.
53. Shi, W. Q.; Cui, S.; Wang, C.; Wang, L.; Zhang, X.; Wang, X. J.; Wang, L., Single-chain elasticity of poly(ferrocenyldimethylsilane) and poly(ferrocenylmethylphenylsilane). *Macromolecules* **2004**, *37* (5), 1839-1842.
54. Liese, S.; Gensler, M.; Krysiak, S.; Schwarzl, R.; Achazi, A.; Paulus, B.; Hugel, T.; Rabe, J. P.; Netz, R. R., Hydration Effects Turn a Highly Stretched Polymer from an Entropic into an Energetic Spring. *Acs Nano* **2017**, *11* (1), 702-712.
55. Zou, S.; Schonherr, H.; Vancso, G. J., Stretching and rupturing individual supramolecular polymer chains by AFM. *Angew Chem Int Edit* **2005**, *44* (6), 956-959.
56. Zou, S.; Schonherr, H.; Vancso, G. J., Force spectroscopy of quadruple H-bonded dimers by AFM: Dynamic bond rupture and molecular time-temperature superposition. *J Am Chem Soc* **2005**, *127* (32), 11230-11231.
57. Lee, H.; Scherer, N. F.; Messersmith, P. B., Single-molecule mechanics of mussel adhesion. *P Natl Acad Sci USA* **2006**, *103* (35), 12999-13003.
58. Israelachvili, J., Intermolecular and Surface Forces. *Academic Press: London, UK*, 1976 **2011**, 276-277.
59. Wagner, C.; Fournier, N.; Ruiz, V. G.; Li, C.; Mullen, K.; Rohlfing, M.; Tkatchenko, A.; Temirov, R.; Tautz, F. S., Non-additivity of molecule-surface van der Waals potentials from force measurements. *Nat Commun* **2014**, *5*, 1-7.

60. Li, H. B.; Zhang, W. K.; Zhang, X.; Shen, J. C.; Liu, B. B.; Gao, C. X.; Zou, G. T., Single molecule force spectroscopy on poly(vinyl alcohol) by atomic force microscopy. *Macromol Rapid Comm* **1998**, *19* (12), 609-611.
61. Li, H. B.; Zhang, W. K.; Xu, W. Q.; Zhang, X., Hydrogen bonding governs the elastic properties of poly(vinyl alcohol) in water: Single-molecule force spectroscopic studies of PVA by AFM. *Macromolecules* **2000**, *33* (2), 465-469.
62. Liu, C. J.; Cui, S. X.; Wang, Z. Q.; Zhang, X., Single-chain mechanical property of poly(N-vinyl-2-pyrrolidone) and interaction with small molecules. *Journal of Physical Chemistry B* **2005**, *109* (31), 14807-14812.
63. Liu, C.; Jiang, Z.; Zhang, Y.; Wang, Z.; Zhang, X.; Feng, F.; Wang, S., Intercalation interactions between dsDNA and acridine studied by single molecule force spectroscopy. *Langmuir* **2007**, *23* (18), 9140-9142.
64. Evans, E., Probing the relation between force - Lifetime - and chemistry in single molecular bonds. *Annu Rev Bioph Biom* **2001**, *30*, 105-128.
65. Schlierf, M.; Li, H. B.; Fernandez, J. M., The unfolding kinetics of ubiquitin captured with single-molecule force-clamp techniques. *P Natl Acad Sci USA* **2004**, *101* (19), 7299-7304.
66. Horinek, D.; Serr, A.; Geisler, M.; Pirzer, T.; Slotta, U.; Lud, S. Q.; Garrido, J. A.; Scheibel, T.; Hugel, T.; Netz, R. R., Peptide Adsorption on a Hydrophobic Surface Results from an Interplay of Solvation, Surface, and Intrapeptide Forces. *P Natl Acad Sci USA* **2008**, *105* (8), 2842-2847.
67. Pirzer, T.; Geisler, M.; Scheibel, T.; Hugel, T., Single Molecule Force Measurements Delineate Salt, pH and Surface Effects on Biopolymer Adhesion. *Phys Biol* **2009**, *6* (2), 1-8.
68. Geisler, M.; Balzer, B. N.; Hugel, T., Polymer Adhesion at the Solid-Liquid Interface Probed by a Single-Molecule Force Sensor. *Small* **2009**, *5* (24), 2864-2869.

69. Geisler, M.; Horinek, D.; Hugel, T., Single Molecule Adhesion Mechanics on Rough Surfaces. *Macromolecules* **2009**, *42* (23), 9338-9343.
70. Geisler, M.; Pirzer, T.; Ackerschott, C.; Lud, S.; Garrido, J.; Scheibel, T.; Hugel, T., Hydrophobic and Hofmeister Effects on the Adhesion of Spider Silk Proteins onto Solid Substrates: An AFM-Based Single-Molecule Study. *Langmuir* **2008**, *24* (4), 1350-1355.
71. Cui, S. X.; Liu, C. J.; Wang, Z. Q.; Zhang, X., Single molecule force spectroscopy on polyelectrolytes: Effect of spacer on adhesion force and linear charge density on rigidity. *Macromolecules* **2004**, *37* (3), 946-953.
72. Shigemitsu, H.; Hamachi, I., Design Strategies of Stimuli-Responsive Supramolecular Hydrogels Relying on Structural Analyses and Cell-Mimicking Approaches. *Accounts of Chemical Research* **2017**, *50* (4), 740-750.
73. Jeon, S. J.; Hauser, A. W.; Hayward, R. C., Shape-Morphing Materials from Stimuli-Responsive Hydrogel Hybrids. *Accounts of Chemical Research* **2017**, *50* (2), 161-169.
74. Lu, W.; Le, X. X.; Zhang, J. W.; Huang, Y. J.; Chen, T., Supramolecular shape memory hydrogels: a new bridge between stimuli-responsive polymers and supramolecular chemistry. *Chemical Society Reviews* **2017**, *46* (5), 1284-1294.
75. Tan, C. L.; Zhang, H., Epitaxial Growth of Hetero-Nanostructures Based on Ultrathin Two-Dimensional Nanosheets. *J Am Chem Soc* **2015**, *137* (38), 12162-12174.
76. Wei, M. L.; Gao, Y. F.; Li, X.; Serpe, M. J., Stimuli-responsive polymers and their applications. *Polymer Chemistry* **2017**, *8* (1), 127-143.
77. Zhu, Y. Q.; Yang, B.; Chen, S.; Du, J. Z., Polymer vesicles: Mechanism, preparation, application, and responsive behavior. *Progress in Polymer Science* **2017**, *64*, 1-22.
78. Cole, M. A.; Voelcker, N. H.; Thissen, H.; Griesser, H. J., Stimuli-responsive interfaces and

systems for the control of protein-surface and cell-surface interactions. *Biomaterials* **2009**, *30* (9), 1827-1850.

79. Yu, Q.; Cho, J.; Shivapooja, P.; Ista, L. K.; Lopez, G. P., Nanopatterned Smart Polymer Surfaces for Controlled Attachment, Killing, and Release of Bacteria. *Acs Appl Mater Inter* **2013**, *5* (19), 9295-9304.

80. Liu, H. L.; Liu, X. L.; Meng, J. X.; Zhang, P. C.; Yang, G.; Su, B.; Sun, K.; Chen, L.; Han, D.; Wang, S. T.; Jiang, L., Hydrophobic Interaction-Mediated Capture and Release of Cancer Cells on Thermoresponsive Nanostructured Surfaces. *Advanced Materials* **2013**, *25* (6), 922-927.

81. Liu, Z.; Wang, W.; Xie, R.; Ju, X. J.; Chu, L. Y., Stimuli-responsive smart gating membranes. *Chem Soc Rev* **2016**, *45* (3), 460-474.

82. Li, H.; Long, J.; Xu, Z.; Masliyah, J. H., Synergetic role of polymer flocculant in low-temperature bitumen extraction and tailings treatment. *Energy & Fuels* **2005**, *19* (3), 936-943.

83. Long, J.; Xu, Z. H.; Masliyah, J. H., Adhesion of Single Polyelectrolyte Molecules on Silica, Mica, and Bitumen Surfaces. *Langmuir* **2006**, *22* (4), 1652-1659.

84. B., H. W., Polymer Physics: A Molecular Approach. *Springer Wien Heidelberg New york Dordrecht london* **2013**.

85. Li, H. B.; Liu, B. B.; Zhang, X.; Gao, C. X.; Shen, J. C.; Zou, G. T., Single-molecule force spectroscopy on poly(acrylic acid) by AFM. *Langmuir* **1999**, *15* (6), 2120-2124.

86. Zhang, W. K.; Zou, S.; Wang, C.; Zhang, X., Single polymer chain elongation of poly(N-isopropylacrylamide) and poly(acrylamide) by atomic force microscopy. *J Phys Chem B* **2000**, *104* (44), 10258-10264.

87. Zhang, W. K.; Xu, Q. B.; Zou, S.; Li, H. B.; Xu, W. Q.; Zhang, X.; Shao, Z. Z.; Kudera, M.; Gaub, H. E., Single-molecule force spectroscopy on Bombyx mori silk fibroin by atomic force

microscopy. *Langmuir* **2000**, *16* (9), 4305-4308.

88. Zhang, W.; Zhang, X., Single molecule mechanochemistry of macromolecules. *Progress in Polymer Science* **2003**, *28* (8), 1271-1295.

89. Smith, S. B.; Cui, Y. J.; Bustamante, C., Overstretching B-DNA: The elastic response of individual double-stranded and single-stranded DNA molecules. *Science* **1996**, *271* (5250), 795-799.

90. Li, H. B.; Rief, M.; Oesterhelt, F.; Gaub, H. E.; Zhang, X.; Shen, J. C., Single-molecule force spectroscopy on polysaccharides by AFM - nanomechanical fingerprint of alpha-(1,4)-linked polysaccharides. *Chem Phys Lett* **1999**, *305* (3-4), 197-201.

91. Senden, T. J.; di Meglio, J. M.; Auroy, P., Anomalous adhesion in adsorbed polymer layers. *Eur Phys J B* **1998**, *3* (2), 211-216.

92. Kikuchi, H.; Yokoyama, N.; Kajiyama, T., Direct measurements of stretching force-chain ends elongation relationships of a single polystyrene chain in dilute solution. *Chem Lett* **1997**, (11), 1107-1108.

93. Oesterhelt, F.; Rief, M.; Gaub, H. E., Single molecule force spectroscopy by AFM indicates helical structure of poly(ethylene-glycol) in water. *New J Phys* **1999**, *1*, 1-11.

94. Doi, M. E., S. F., The theory of polymer dynamics. *Oxford university Press* **1986**.

95. Krysiak, S.; Liese, S.; Netz, R. R.; Hugel, T., Peptide Desorption Kinetics from Single Molecule Force Spectroscopy Studies. *J Am Chem Soc* **2014**, *136* (2), 688-697.

96. Schwierz, N.; Horinek, D.; Liese, S.; Pirzer, T.; Balzer, B. N.; Hugel, T.; Netz, R. R., On the Relationship between Peptide Adsorption Resistance and Surface Contact Angle: A Combined Experimental and Simulation Single-Molecule Study. *J Am Chem Soc* **2012**, *134* (48), 19628-19638.

97. Sun, W.; Long, J.; Xu, Z. H.; Masliyah, J. H., Study of Al(OH)(3)-Polyacrylamide-Induced Pelleting Flocculation by Single Molecule Force Spectroscopy. *Langmuir* **2008**, *24* (24), 14015-14021.
98. Hugel, T.; Seitz, M., The study of molecular interactions by AFM force spectroscopy. *Macromol Rapid Comm* **2001**, *22* (13), 989-1016.
99. Friedsam, C.; Gaub, H. E.; Netz, R. R., Adsorption energies of single charged polymers. *Europhysics Letters* **2005**, *72* (5), 844-850.
100. Li, I. T. S.; Walker, G. C., Interfacial Free Energy Governs Single Polystyrene Chain Collapse in Water and Aqueous Solutions. *J Am Chem Soc* **2010**, *132* (18), 6530-6540.
101. Fler, G. J.; van Male, J.; Johner, A., Analytical approximation to the Scheutjens-Fler theory for polymer adsorption from dilute solution. 1. Trains, loops, and tails in terms of two parameters: The proximal and distal lengths. *Macromolecules* **1999**, *32* (3), 825-844.
102. Scheutjens, J.; Fler, G. J., Statistical-Theory of the adsorption of interacting chain molecules .2. train, loop, and tail size distribution. *Journal of Physical Chemistry* **1980**, *84* (2), 178-190.
103. Chandler, D., Interfaces and the driving force of hydrophobic assembly. *Nature* **2005**, *437* (7059), 640-647.
104. Li, I. T. S.; Walker, G. C., Single Polymer Studies of Hydrophobic Hydration. *Accounts Chem Res* **2012**, *45* (11), 2011-2021.
105. Wu, J.; Schmidt, H.; Amara, K. K.; Xu, X. F.; Eda, G.; Ozyilmaz, B., Large Thermoelectricity via Variable Range Hopping in Chemical Vapor Deposition Grown Single-Layer MoS₂. *Nano Lett* **2014**, *14* (5), 2730-2734.
106. Biswas, Y.; Dule, M.; Mandal, T. K., Poly(ionic liquid)-Promoted Solvent-Borne Efficient

Exfoliation of MoS₂/MoSe₂ Nanosheets for Dual-Responsive Dispersion and Polymer Nanocomposites. *J Phys Chem C* **2017**, *121* (8), 4747-4759.

107. Zhang, W. T.; Wang, Y. R.; Zhang, D. H.; Yu, S. X.; Zhu, W. X.; Wang, J.; Zheng, F. Q.; Wang, S. X.; Wang, J. L., A one-step approach to the large-scale synthesis of functionalized MoS₂ nanosheets by ionic liquid assisted grinding. *Nanoscale* **2015**, *7* (22), 10210-10217.

108. Grebikova, L.; Moroni, P.; Zhang, B. Z.; Schluter, A. D.; Borkovec, M., Single-Molecule Force Measurements by Nano-Handling of Individual Dendronized Polymers. *Acs Nano* **2014**, *8* (3), 2237-2245.

109. Chhowalla, M.; Amaratunga, G. A. J., Thin Films of Fullerene-Like MoS₂ Nanoparticles with Ultra-Low Friction and Wear. *Nature* **2000**, *407* (6801), 164-167.

110. Wilcoxon, J. P.; Thurston, T. R.; Martin, J. E., Applications of Metal and Semiconductor Nanoclusters as Thermal and Photo-Catalysts. *Nanostructured Materials* **1999**, *12* (5-8), 993-997.

111. Parzinger, E.; Miller, B.; Blaschke, B.; Garrido, J. A.; Ager, J. W.; Holleitner, A.; Wurstbauer, U., Photocatalytic Stability of Single- and Few-Layer MoS₂. *Acs Nano* **2015**, *9* (11), 11302-11309.

112. Yin, W. Y.; Yan, L.; Yu, J.; Tian, G.; Zhou, L. J.; Zheng, X. P.; Zhang, X.; Yong, Y.; Li, J.; Gu, Z. J.; Zhao, Y. L., High-Throughput Synthesis of Single-Layer MoS₂ Nanosheets as a Near-Infrared Photothermal-Triggered Drug Delivery for Effective Cancer Therapy. *Acs Nano* **2014**, *8* (7), 6922-6933.

113. Wang, S. G.; Chen, Y.; Li, X.; Gao, W.; Zhang, L. L.; Liu, J.; Zheng, Y. Y.; Chen, H. R.; Shi, J. L., Injectable 2D MoS₂-Integrated Drug Delivering Implant for Highly Efficient NIR-Triggered Synergistic Tumor Hyperthermia. *Advanced Materials* **2015**, *27* (44), 7117-7122.

114. Ye, G. L.; Gong, Y. J.; Lin, J. H.; Li, B.; He, Y. M.; Pantelides, S. T.; Zhou, W.; Vajtai, R.;

- Ajayan, P. M., Defects Engineered Monolayer MoS₂ for Improved Hydrogen Evolution Reaction. *Nano Lett* **2016**, *16* (2), 1097-1103.
115. Kibsgaard, J.; Chen, Z. B.; Reinecke, B. N.; Jaramillo, T. F., Engineering the Surface Structure of MoS₂ to Preferentially Expose Active Edge Sites for Electrocatalysis. *Nat Mater* **2012**, *11* (11), 963-969.
116. Feng, J. D.; Graf, M.; Liu, K.; Ovchinnikov, D.; Dumcenco, D.; Heiranian, M.; Nandigana, V.; Aluru, N. R.; Kis, A.; Radenovic, A., Single-layer MoS₂ Nanopores as Nanopower Generators. *Nature* **2016**, *536* (7615), 197-200.
117. Eda, G.; Yamaguchi, H.; Voiry, D.; Fujita, T.; Chen, M. W.; Chhowalla, M., Photoluminescence from Chemically Exfoliated MoS₂. *Nano Lett* **2011**, *11* (12), 5111-5116.
118. Gu, W.; Yan, Y. H.; Zhang, C. L.; Ding, C. P.; Xian, Y. Z., One-Step Synthesis of Water-Soluble MoS₂ Quantum Dots via a Hydrothermal Method as a Fluorescent Probe for Hyaluronidase Detection. *Acs Appl Mater Inter* **2016**, *8* (18), 11272-11279.
119. Kis, A.; Mihailovic, D.; Remskar, M.; Mrzel, A.; Jesih, A.; Piwonski, I.; Kulik, A. J.; Benoit, W.; Forro, L., Shear and Young's Moduli of MoS₂ Nanotube Ropes. *Advanced Materials* **2003**, *15* (9), 733-736.
120. Dominko, R.; Arcon, D.; Mrzel, A.; Zorko, A.; Cevc, P.; Venturini, P.; Gaberscek, M.; Remskar, M.; Mihailovic, D., Dichalcogenide Nanotube Electrodes for Li-ion Batteries. *Advanced Materials* **2002**, *14* (21), 1531-1534.
121. Zeng, Z. Y.; Yin, Z. Y.; Huang, X.; Li, H.; He, Q. Y.; Lu, G.; Boey, F.; Zhang, H., Single-Layer Semiconducting Nanosheets: High-Yield Preparation and Device Fabrication. *Angew Chem Int Edit* **2011**, *50* (47), 11093-11097.
122. Joensen, P.; Frindt, R. F.; Morrison, S. R., Single-Layer MoS₂. *Materials Research Bulletin*

1986, *21* (4), 457-461.

123. Gopalakrishnan, D.; Damien, D.; Shaijumon, M. M., MoS₂ Quantum Dot-Interspersed Exfoliated MoS₂ Nanosheets. *Acs Nano* **2014**, *8* (5), 5297-5303.

124. Frey, G. L.; Reynolds, K. J.; Friend, R. H., Novel Electrodes from Solution-Processed Layer-Structure Materials. *Advanced Materials* **2002**, *14* (4), 265-268.

125. Yao, Y. G.; Tolentino, L.; Yang, Z. Z.; Song, X. J.; Zhang, W.; Chen, Y. S.; Wong, C. P., High-Concentration Aqueous Dispersions of MoS₂. *Advanced Functional Materials* **2013**, *23* (28), 3577-3583.

126. Liu, Y. T.; Zhu, X. D.; Duan, Z. Q.; Xie, X. M., Flexible and Robust MoS₂-Graphene Hybrid Paper Cross-Linked by a Polymer Ligand: a High-Performance Anode Material for Thin Film Lithium-ion Batteries. *Chemical Communications* **2013**, *49* (87), 10305-10307.

127. Chou, S. S.; Kaehr, B.; Kim, J.; Foley, B. M.; De, M.; Hopkins, P. E.; Huang, J.; Brinker, C. J.; Dravid, V. P., Chemically Exfoliated MoS₂ as Near-Infrared Photothermal Agents. *Angew Chem Int Edit* **2013**, *52* (15), 4160-4164.

128. Guan, G. J.; Zhang, S. Y.; Liu, S. H.; Cai, Y. Q.; Low, M.; Teng, C. P.; Phang, I. Y.; Cheng, Y.; Duei, K. L.; Srinivasan, B. M.; Zheng, Y. G.; Zhang, Y. W.; Han, M. Y., Protein Induces Layer-by-Layer Exfoliation of Transition Metal Dichalcogenides. *J Am Chem Soc* **2015**, *137* (19), 6152-6155.

129. Vancoillie, G.; Frank, D.; Hoogenboom, R., Thermoresponsive poly(oligo ethylene glycol acrylates). *Progress in Polymer Science* **2014**, *39* (6), 1074-1095.

130. Israelachvili, J., The Different Faces of Poly(ethylene glycol). *P Natl Acad Sci USA* **1997**, *94* (16), 8378-8379.

131. Tasaki, K., Poly(oxyethylene)-Water Interactions: a Molecular Dynamics Study. *J Am*

Chem Soc **1996**, *118* (35), 8459-8469.

132. Becer, C. R.; Hahn, S.; Fijten, M. W. M.; Thijs, H. M. L.; Hoogenboom, R.; Schubert, U. S., Libraries of Methacrylic Acid and Oligo(ethylene glycol) Methacrylate Copolymers with LCST Behavior. *Journal of Polymer Science Part a-Polymer Chemistry* **2008**, *46* (21), 7138-7147.

133. Roth, P. J.; Jochum, F. D.; Forst, F. R.; Zentel, R.; Theato, P., Influence of End Groups on the Stimulus-Responsive Behavior of Poly oligo(ethylene glycol) methacrylate in Water. *Macromolecules* **2010**, *43* (10), 4638-4645.

134. Hu, Z. B.; Cai, T.; Chi, C. L., Thermoresponsive oligo(ethylene glycol)-methacrylate-based polymers and microgels. *Soft Matter* **2010**, *6* (10), 2115-2123.

135. Sun, S. T.; Wu, P. Y., On the Thermally Reversible Dynamic Hydration Behavior of Oligo(ethylene glycol) Methacrylate-Based Polymers in Water. *Macromolecules* **2013**, *46* (1), 236-246.

136. Yuan, W. Z.; Wang, J. J., Oligo(ethylene glycol) and quaternary ammonium-based block copolymer micelles: from tunable thermoresponse to dual salt response. *Rsc Adv* **2014**, *4* (73), 38855-38858.

137. Lutz, J. F.; Akdemir, O.; Hoth, A., Point by point comparison of two thermosensitive polymers exhibiting a similar LCST: Is the age of poly(NIPAM) over? *J Am Chem Soc* **2006**, *128* (40), 13046-13047.

138. Sadeghi, R.; Jahani, F., Salting-In and Salting-Out of Water-Soluble Polymers in Aqueous Salt Solutions. *Journal of Physical Chemistry B* **2012**, *116* (17), 5234-5241.

139. Brown, A. A.; Khan, N. S.; Steinbock, L.; Huck, W. T. S., Synthesis of oligo(ethylene glycol) methacrylate polymer brushes. *Eur Polym J* **2005**, *41* (8), 1757-1765.

140. Lu, Z. Z.; Liu, Q. X.; Xu, Z. H.; Zeng, H. B., Probing Anisotropic Surface Properties of

Molybdenite by Direct Force Measurements. *Langmuir* **2015**, *31* (42), 11409-11418.

141. Gaur, A. P. S.; Sahoo, S.; Ahmadi, M.; Dash, S. P.; Guinel, M. J. F.; Katiyar, R. S., Surface Energy Engineering for Tunable Wettability through Controlled Synthesis of MoS₂. *Nano Lett* **2014**, *14* (8), 4314-4321.

142. Grebikova, L.; Maroni, P.; Muresan, L.; Zhang, B. Z.; Schluter, A. D.; Borkovec, M., Interactions between Individual Charged Dendronized Polymers and Surfaces. *Macromolecules* **2013**, *46* (9), 3603-3610.

143. Friedsam, C.; Gaub, H. E.; Netz, R. R., Probing Surfaces with Single-Polymer Atomic Force Microscope Experiments. *Biointerphases* **2006**, *1* (1), MR1-MR21.

144. Li, I. T. S.; Walker, G. C., Signature of Hydrophobic Hydration in a Single Polymer. *P Natl Acad Sci USA* **2011**, *108* (40), 16527-16532.

145. Patel, A. J.; Varilly, P.; Jamadagni, S. N.; Acharya, H.; Garde, S.; Chandler, D., Extended surfaces modulate hydrophobic interactions of neighboring solutes. *P Natl Acad Sci USA* **2011**, *108* (43), 17678-17683.

146. Jamadagni, S. N.; Godawat, R.; Dordick, J. S.; Garde, S., How Interfaces Affect Hydrophobically Driven Polymer Folding. *Journal of Physical Chemistry B* **2009**, *113* (13), 4093-4101.

147. Bustamante, C.; Marko, J. F.; Siggia, E. D.; Smith, S., Entropic Elasticity of Lambda-Phage DNA. *Science* **1994**, *265* (5178), 1599-1600.

148. Marko, J. F.; Siggia, E. D., Stretching DNA. *Macromolecules* **1995**, *28* (26), 8759-8770.

149. Lecommandoux, S.; Checot, F.; Borsali, R.; Schappacher, M.; Deffieux, A.; Brulet, A.; Cotton, J. P., Effect of dense grafting on the backbone conformation of bottlebrush polymers: Determination of the persistence length in solution. *Macromolecules* **2002**, *35* (23), 8878-8881.

150. Frohlich, M. G.; Zifferer, G., Atomistic Molecular Dynamics Simulation of Surface Grafted PMMA. *Macromolecular Theory and Simulations* **2011**, *20* (6), 399-410.
151. Dittmore, A.; McIntosh, D. B.; Halliday, S.; Saleh, O. A., Single-Molecule Elasticity Measurements of the Onset of Excluded Volume in Poly(Ethylene Glycol). *Physical Review Letters* **2011**, *107* (14), 1-5.
152. Kawaguchi, S.; Imai, G.; Suzuki, J.; Miyahara, A.; Kitano, T., Aqueous solution properties of oligo- and poly(ethylene oxide) by static light scattering and intrinsic viscosity. *Polymer* **1997**, *38* (12), 2885-2891.
153. Leite, F. L.; Bueno, C. C.; Da Roz, A. L.; Ziemath, E. C.; Oliveira, O. N., Theoretical Models for Surface Forces and Adhesion and Their Measurement Using Atomic Force Microscopy. *International Journal of Molecular Sciences* **2012**, *13* (10), 12773-12856.
154. Manhanty, J. N., B.W., Dispersion Forces. *Academic Press: London, UK*, 1976.
155. Meyer, E. E.; Rosenberg, K. J.; Israelachvili, J., Recent Progress in Understanding Hydrophobic Interactions. *P Natl Acad Sci USA* **2006**, *103* (43), 15739-15746.
156. Christenson, H. K.; Claesson, P. M., Direct Measurements of the Force Between Hydrophobic Surfaces in Water. *Advances in Colloid and Interface Science* **2001**, *91* (3), 391-436.
157. Carambassis, A.; Jonker, L. C.; Attard, P.; Rutland, M. W., Forces measured between hydrophobic surfaces due to a submicroscopic bridging bubble. *Physical Review Letters* **1998**, *80* (24), 5357-5360.
158. Podgornik, R.; Parsegian, V. A., An Electrostatic-Surface Stability Interpretation of the Hydrophobic Force Inferred to Occur Between Mica Plates in Solutions of Soluble Surfactants. *Chemical Physics* **1991**, *154* (3), 477-483.
159. Rajamani, S.; Truskett, T. M.; Garde, S., Hydrophobic Hydration from Small to Large

lengthscales: Understanding and Manipulating the Crossover. *P Natl Acad Sci USA* **2005**, *102* (27), 9475-9480.

160. Kunz, W.; Lo Nostro, P.; Ninham, B. W., The present state of affairs with Hofmeister effects. *Current Opinion in Colloid & Interface Science* **2004**, *9* (1-2), 1-18.

161. Bostrom, M.; Williams, D. R. M.; Ninham, B. W., Specific ion effects: Why DLVO theory fails for biology and colloid systems. *Physical Review Letters* **2001**, *87* (16), 1-4.

162. Tadeo, X.; Pons, M.; Millet, O., Influence of the hofmeister anions on protein stability as studied by thermal denaturation and chemical shift perturbation. *Biochemistry* **2007**, *46* (3), 917-923.

163. Zhang, Y. J.; Furyk, S.; Bergbreiter, D. E.; Cremer, P. S., Specific ion effects on the water solubility of macromolecules: PNIPAM and the Hofmeister series. *J Am Chem Soc* **2005**, *127* (41), 14505-14510.

164. Zhang, Y. J.; Cremer, P. S., Interactions between macromolecules and ions: the Hofmeister series. *Current Opinion in Chemical Biology* **2006**, *10* (6), 658-663.

165. Noskov, S. Y.; Lamoureux, G.; Roux, B., Molecular dynamics study of hydration in ethanol-water mixtures using a polarizable force field. *Journal of Physical Chemistry B* **2005**, *109* (14), 6705-6713.

166. Jones, R. G.; Kitayama, T.; Hellwich, K. H.; Hess, M.; Jenkins, A. D.; Kahovec, J.; Kratochvil, P.; Mita, I.; Mormann, W.; Ober, C. K.; Penczek, S.; Stepto, R. F. T.; Thurlow, K.; Vohlidal, J.; Wilks, E. S., Source-based nomenclature for single-strand homopolymers and copolymers (IUPAC Recommendations 2016). *Pure Appl. Chem.* **2016**, *88* (10-11), 1073-1100.

167. Tang, Y. C., Zhang, X. R., Choi, P., Liu, Q. X., Xu, Z. H., Probing Single-Molecule Adhesion of a Stimuli Responsive Oligo (ethylene glycol) Methacrylate Copolymer on a

Molecularly-Smooth Hydrophobic MoS₂ Basal Plane Surface. *Langmuir* **2017**, *33* (40), 10429-10438.

168. Meyer, E. E.; Lin, Q.; Israelachvili, J. N., Effects of dissolved gas on the hydrophobic attraction between surfactant-coated surfaces. *Langmuir* **2005**, *21* (1), 256-259.

169. Israelachvili, J.; Pashley, R., The Hydrophobic Interaction Is Long-Range, Decaying Exponentially with Distance. *Nature* **1982**, *300* (5890), 341-342.

170. Paul C. Hiemenz, T. P. L., Polymer chemistry, Second Edition. *CRC Press* **2007**.

171. Liu, T. J.; Schneider, H. J., Additivity and quantification of dispersive interactions-from cyclopropyl to nitro groups: Measurements on porphyrin derivatives. *Angew Chem Int Edit* **2002**, *41* (8), 1368-1370.

172. Barratt, E.; Bingham, R. J.; Warner, D. J.; Laughton, C. A.; Phillips, S. E. V.; Homans, S. W., Van der waals interactions dominate ligand-protein association in a protein binding site occluded from solvent water. *J Am Chem Soc* **2005**, *127* (33), 11827-11834.

173. Malham, R.; Johnstone, S.; Bingham, R. J.; Barratt, E.; Phillips, S. E. V.; Laughton, C. A.; Homans, S. W., Strong solute-solute dispersive interactions in a protein-ligand complex. *J Am Chem Soc* **2005**, *127* (48), 17061-17067.

174. Hunter, C. A., van der Waals interactions in non-polar liquids. *Chem Sci* **2013**, *4* (2), 834-848.

175. Cabot, R.; Hunter, C. A., Molecular probes of solvation phenomena. *Chem Soc Rev* **2012**, *41* (9), 3485-3492.

176. Yang, L. X.; Adam, C.; Nichol, G. S.; Cockroft, S. L., How much do van der Waals dispersion forces contribute to molecular recognition in solution? *Nat Chem* **2013**, *5* (12), 1006-1010.

177. Yan, L. J.; Masliyah, J. H.; Xu, Z. H., Understanding suspension rheology of anisotropically-charged platy minerals from direct interaction force measurement using AFM. *Current Opinion in Colloid & Interface Science* **2013**, *18* (2), 149-156.
178. Liu, J.; Sandaklie-Nikolova, L.; Wang, X. M.; Miller, J. D., Surface force measurements at kaolinite edge surfaces using atomic force microscopy. *J Colloid Interf Sci* **2014**, *420*, 35-40.
179. Yan, L. J.; Englert, A. H.; Masliyah, J. H.; Xu, Z. H., Determination of Anisotropic Surface Characteristics of Different Phyllosilicates by Direct Force Measurements. *Langmuir* **2011**, *27* (21), 12996-13007.
180. Yang, D. Z.; Xie, L.; Bobicki, E.; Xu, Z. H.; Liu, Q. X.; Zeng, H. B., Probing Anisotropic Surface Properties and Interaction Forces of Chrysotile Rods by Atomic Force Microscopy and Rheology. *Langmuir* **2014**, *30* (36), 10809-10817.
181. Yin, X. H.; Gupta, V.; Du, H.; Wang, X. M.; Miller, J. D., Surface charge and wetting characteristics of layered silicate minerals. *Advances in Colloid and Interface Science* **2012**, *179*, 43-50.
182. Karlicky, F.; Otyepkova, E.; Lo, R.; Pitonak, M.; Jurecka, P.; Pykal, M.; Hobza, P.; Otyepka, M., Adsorption of Organic Molecules to van der Waals Materials: Comparison of Fluorographene and Fluorographite with Graphene and Graphite. *J Chem Theory Comput* **2017**, *13* (3), 1328-1340.
183. Gao, M. R.; Chan, M. K. Y.; Sun, Y. G., Edge-terminated molybdenum disulfide with a 9.4-angstrom interlayer spacing for electrochemical hydrogen production. *Nat Commun* **2015**, *6*, 1-8.
184. Kozbial, A.; Gong, X.; Liu, H. T.; Li, L., Understanding the Intrinsic Water Wettability of Molybdenum Disulfide (MoS₂). *Langmuir* **2015**, *31* (30), 8429-8435.
185. Chan, D. Y. C., Electric Double-Layer Interaction between Dissimilar Charge-Conserved Conducting Plates. *Langmuir* **2015**, *31* (36), 9889-9892.

186. Raghavan, S.; Hsu, L. L., FACTORS AFFECTING THE FLOTATION RECOVERY OF MOLYBDENITE FROM PORPHYRY COPPER ORES. *International Journal of Mineral Processing* **1984**, *12*, 145-162.
187. Varenberg, M.; Gorb, S., A beetle-inspired solution for underwater adhesion. *J R Soc Interface* **2008**, *5* (20), 383-385.
188. Hwang, J. W.; Dial, B. E.; Li, P.; Kozik, M. E.; Smith, M. D.; Shimizu, K. D., How important are dispersion interactions to the strength of aromatic stacking interactions in solution? *Chem Sci* **2015**, *6* (7), 4358-4364.
189. Adam, C.; Yang, L. X.; Cockroft, S. L., Partitioning Solvophobic and Dispersion Forces in Alkyl and Perfluoroalkyl Cohesion. *Angew Chem Int Edit* **2015**, *54* (4), 1164-1167.
190. Otto, S., The role of solvent cohesion in nonpolar solvation. *Chem Sci* **2013**, *4* (7), 2953-2959.
191. Lifshitz, E., The theory of molecular attractive forces between solids. **1956**.
192. Ambrosetti, A.; Ferri, N.; DiStasio, R. A.; Tkatchenko, A., Wavelike charge density fluctuations and van der Waals interactions at the nanoscale. *Science* **2016**, *351* (6278), 1171-1176.
193. Bruch, L. W.; Cole, M. W.; Zaremba, E., *Physical adsorption: forces and phenomena*. Courier Dover Publications: 2007.
194. Parsegian, V. A., *Van der Waals forces: a handbook for biologists, chemists, engineers, and physicists*. Cambridge University Press: 2005.
195. Dobson, J. F.; Gould, T., Calculation of dispersion energies. *Journal of Physics-Condensed Matter* **2012**, *24* (7), 1-13.
196. Gobre, V. V.; Tkatchenko, A., Scaling laws for van der Waals interactions in nanostructured materials. *Nat Commun* **2013**, *4*, 1-6.

197. Yang, L. X.; Adam, C.; Cockroft, S. L., Quantifying Solvophobic Effects in Nonpolar Cohesive Interactions. *J Am Chem Soc* **2015**, *137* (32), 10084-10087.
198. Pirzer, T.; Hugel, T., Adsorption Mechanism of Polypeptides and Their Location at Hydrophobic Interfaces. *Chemphyschem* **2009**, *10* (16), 2795-2799.
199. Stock, P.; Monroe, J. J.; Utzig, T.; Smith, D. J.; Shell, M. S.; Valtiner, M., Unraveling Hydrophobic Interactions at the Molecular Scale Using Force Spectroscopy and Molecular Dynamics Simulations. *Acs Nano* **2017**, *11* (3), 2586-2597.
200. Winslow, B. D.; Shao, H.; Stewart, R. J.; Tresco, P. A., Biocompatibility of adhesive complex coacervates modeled after the sandcastle glue of *Phragmatopoma californica* for craniofacial reconstruction. *Biomaterials* **2010**, *31* (36), 9373-9381.
201. Long, M.; Rack, H. J., Titanium alloys in total joint replacement - a materials science perspective. *Biomaterials* **1998**, *19* (18), 1621-1639.
202. Kastrup, C. J.; Nahrendorf, M.; Figueiredo, J. L.; Lee, H.; Kambhampati, S.; Lee, T.; Cho, S. W.; Gorbatov, R.; Iwamoto, Y.; Dang, T. T.; Dutta, P.; Yeon, J. H.; Cheng, H.; Pritchard, C. D.; Vegas, A. J.; Siegel, C. D.; MacDougall, S.; Okonkwo, M.; Thai, A.; Stone, J. R.; Coury, A. J.; Weissleder, R.; Langer, R.; Anderson, D. G., Painting blood vessels and atherosclerotic plaques with an adhesive drug depot. *P Natl Acad Sci USA* **2012**, *109* (52), 21444-21449.
203. Lee, B. P.; Messersmith, P. B.; Israelachvili, J. N.; Waite, J. H., Mussel-Inspired Adhesives and Coatings. *Annu Rev Mater Res* **2011**, *41*, 99-132.
204. Brubaker, C. E.; Messersmith, P. B., The Present and Future of Biologically Inspired Adhesive Interfaces and Materials. *Langmuir* **2012**, *28* (4), 2200-2205.
205. Waite, J. H.; Tanzer, M. L., Polyphenolic Substance of *Mytilus-Edulis* - Novel Adhesive Containing L-Dopa and Hydroxyproline. *Science* **1981**, *212* (4498), 1038-1040.

206. Waite, J. H.; Tanzer, M. L., The Bioadhesive of *Mytilus Byssus* - a Protein Containing L-Dopa. *Biochem Bioph Res Co* **1980**, *96* (4), 1554-1561.
207. Waite, J. H., Marine Adhesive Proteins - Natural Composite Thermosets. *Int J Biol Macromol* **1990**, *12* (2), 139-144.
208. Holten-Andersen, N.; Harrington, M. J.; Birkedal, H.; Lee, B. P.; Messersmith, P. B.; Lee, K. Y. C.; Waite, J. H., pH-induced metal-ligand cross-links inspired by mussel yield self-healing polymer networks with near-covalent elastic moduli. *P Natl Acad Sci USA* **2011**, *108* (7), 2651-2655.
209. Ling, D.; Park, W.; Park, Y. I.; Lee, N.; Li, F.; Song, C.; Yang, S. G.; Choi, S. H.; Na, K.; Hyeon, T., Multiple-Interaction Ligands Inspired by Mussel Adhesive Protein: Synthesis of Highly Stable and Biocompatible Nanoparticles. *Angew Chem Int Edit* **2011**, *50* (48), 11360-11365.
210. Wei, W.; Yu, J.; Broomell, C.; Israelachvili, J. N.; Waite, J. H., Hydrophobic Enhancement of Dopa-Mediated Adhesion in a Mussel Foot Protein. *J Am Chem Soc* **2013**, *135* (1), 377-383.
211. Yu, J.; Kan, Y. J.; Rapp, M.; Danner, E.; Wei, W.; Das, S.; Miller, D. R.; Chen, Y. F.; Waite, J. H.; Israelachvili, J. N., Adaptive hydrophobic and hydrophilic interactions of mussel foot proteins with organic thin films. *P Natl Acad Sci USA* **2013**, *110* (39), 15680-15685.
212. Sakata, S.; Inoue, Y.; Ishihara, K., Molecular Interaction Forces Generated during Protein Adsorption to Well-Defined Polymer Brush Surfaces. *Langmuir* **2015**, *31* (10), 3108-3114.
213. Kozbial, A.; Li, Z. T.; Sun, J. N.; Gong, X.; Zhou, F.; Wang, Y. J.; Xu, H. C.; Liu, H. T.; Li, L., Understanding the intrinsic water wettability of graphite. *Carbon* **2014**, *74*, 218-225.
214. Kozbial, A.; Li, Z. T.; Conaway, C.; McGinley, R.; Dhingra, S.; Vahdat, V.; Zhou, F.; D'Urso, B.; Liu, H. T.; Li, L., Study on the Surface Energy of Graphene by Contact Angle Measurements. *Langmuir* **2014**, *30* (28), 8598-8606.

215. Okayama, S.; Haraichi, S.; Matsuhata, H., Reference sample for the evaluation of SEM image resolution at a high magnification—nanometer-scale Au particles on an HOPG substrate. *Journal of electron microscopy* **2005**, *54* (4), 345-350.
216. Demidov, D. V.; Prosvirin, I. P.; Sorokin, A. M.; Bukhtiyarov, V. I., Model Ag/HOPG catalysts: preparation and STM/XPS study. *Catalysis Science & Technology* **2011**, *1* (8), 1432-1439.
217. An, H.; Tan, B. H.; Zeng, Q.; Ohl, C.-D., Stability of Nanobubbles Formed at the Interface between Cold Water and Hot Highly Oriented Pyrolytic Graphite. *Langmuir* **2016**, *32* (43), 11212-11220.
218. Yasuda, S.; Suzuki, I.; Shinohara, K.; Shigekawa, H., Single molecular anatomy of solvophobic effects in host-guest interactions based on surface tension using atomic force microscopy. *Physical Review Letters* **2006**, *96* (22), 1-4.
219. Fournier, J. A.; Carpenter, W.; De Marco, L.; Tokmakoff, A., Interplay of Ion–Water and Water–Water Interactions within the Hydration Shells of Nitrate and Carbonate Directly Probed with 2D IR Spectroscopy. *J Am Chem Soc* **2016**, *138* (30), 9634-9645.
220. Mancinelli, R.; Botti, A.; Bruni, F.; Ricci, M. A.; Soper, A. K., Hydration of sodium, potassium, and chloride ions in solution and the concept of structure maker/breaker. *Journal of Physical Chemistry B* **2007**, *111* (48), 13570-13577.
221. Smith, J. D.; Saykally, R. J.; Geissler, P. L., The effects of dissolved halide anions on hydrogen bonding in liquid water. *J Am Chem Soc* **2007**, *129* (45), 13847-13856.
222. Zong, X.; Yan, H. J.; Wu, G. P.; Ma, G. J.; Wen, F. Y.; Wang, L.; Li, C., Enhancement of photocatalytic H₂ evolution on CdS by loading MOS₂ as cocatalyst under visible light irradiation. *J Am Chem Soc* **2008**, *130* (23), 7176-7177.

223. Tsai, M. L.; Su, S. H.; Chang, J. K.; Tsai, D. S.; Chen, C. H.; Wu, C. I.; Li, L. J.; Chen, L. J.; He, J. H., Monolayer MoS₂ Heterojunction Solar Cells. *Acs Nano* **2014**, 8 (8), 8317-8322.
224. Hao, L. Z.; Gao, W.; Liu, Y. J.; Han, Z. D.; Xue, Q. Z.; Guo, W. Y.; Zhu, J.; Li, Y. R., High-performance n-MoS₂/i-SiO₂/p-Si heterojunction solar cells. *Nanoscale* **2015**, 7 (18), 8304-8308.
225. Li, Y. G.; Wang, H. L.; Xie, L. M.; Liang, Y. Y.; Hong, G. S.; Dai, H. J., MoS₂ Nanoparticles Grown on Graphene: An Advanced Catalyst for the Hydrogen Evolution Reaction. *J Am Chem Soc* **2011**, 133 (19), 7296-7299.
226. Behranginia, A.; Asadi, M.; Liu, C.; Yasaei, P.; Kumar, B.; Phillips, P.; Foroozan, T.; Waranius, J. C.; Kim, K.; Abiade, J.; Klie, R. F.; Curtiss, L. A.; Salehi-Khojin, A., Highly Efficient Hydrogen Evolution Reaction Using Crystalline Layered Three-Dimensional Molybdenum Disulfides Grown on Graphene Film. *Chemistry of Materials* **2016**, 28 (2), 549-555.
227. O'Neill, A.; Khan, U.; Coleman, J. N., Preparation of High Concentration Dispersions of Exfoliated MoS₂ with Increased Flake Size. *Chemistry of Materials* **2012**, 24 (12), 2414-2421.
228. Mak, K. F.; Lee, C.; Hone, J.; Shan, J.; Heinz, T. F., Atomically Thin MoS₂: A New Direct-Gap Semiconductor. *Physical Review Letters* **2010**, 105 (13), 1368050-1368054.
229. Cao, T.; Wang, G.; Han, W. P.; Ye, H. Q.; Zhu, C. R.; Shi, J. R.; Niu, Q.; Tan, P. H.; Wang, E.; Liu, B. L.; Feng, J., Valley-selective circular dichroism of monolayer molybdenum disulphide. *Nat Commun* **2012**, 3, 1-5.
230. Zhou, K. G.; Mao, N. N.; Wang, H. X.; Peng, Y.; Zhang, H. L., A Mixed-Solvent Strategy for Efficient Exfoliation of Inorganic Graphene Analogues. *Angew Chem Int Edit* **2011**, 50 (46), 10839-10842.
231. Smith, R. J.; King, P. J.; Lotya, M.; Wirtz, C.; Khan, U.; De, S.; O'Neill, A.; Duesberg, G. S.; Grunlan, J. C.; Moriarty, G.; Chen, J.; Wang, J. Z.; Minett, A. I.; Nicolosi, V.; Coleman, J. N.,

Large-Scale Exfoliation of Inorganic Layered Compounds in Aqueous Surfactant Solutions. *Advanced Materials* **2011**, 23 (34), 3944-3948.

232. Zheng, J.; Zhang, H.; Dong, S. H.; Liu, Y. P.; Nai, C. T.; Shin, H. S.; Jeong, H. Y.; Liu, B.; Loh, K. P., High yield exfoliation of two-dimensional chalcogenides using sodium naphthalenide. *Nat Commun* **2014**, 5, 1-7.

233. Guardia, L.; Paredes, J. I.; Rozada, R.; Villar-Rodil, S.; Martinez-Alonso, A.; Tascon, J. M. D., Production of aqueous dispersions of inorganic graphene analogues by exfoliation and stabilization with non-ionic surfactants. *Rsc Adv* **2014**, 4 (27), 14115-14127.

234. Liu, J. Q.; Zeng, Z. Y.; Cao, X. H.; Lu, G.; Wang, L. H.; Fan, Q. L.; Huang, W.; Zhang, H., Preparation of MoS₂-Polyvinylpyrrolidone Nanocomposites for Flexible Nonvolatile Rewritable Memory Devices with Reduced Graphene Oxide Electrodes. *Small* **2012**, 8 (22), 3517-3522.

235. Quinn, M. D. J.; Ho, N. H.; Notley, S. M., Aqueous Dispersions of Exfoliated Molybdenum Disulfide for Use in Visible-Light Photocatalysis. *Acs Appl Mater Inter* **2013**, 5 (23), 12751-12756.

236. Coleman, J. N.; Lotya, M.; O'Neill, A.; Bergin, S. D.; King, P. J.; Khan, U.; Young, K.; Gaucher, A.; De, S.; Smith, R. J.; Shvets, I. V.; Arora, S. K.; Stanton, G.; Kim, H. Y.; Lee, K.; Kim, G. T.; Duesberg, G. S.; Hallam, T.; Boland, J. J.; Wang, J. J.; Donegan, J. F.; Grunlan, J. C.; Moriarty, G.; Shmeliov, A.; Nicholls, R. J.; Perkins, J. M.; Grievson, E. M.; Theuwissen, K.; McComb, D. W.; Nellist, P. D.; Nicolosi, V., Two-Dimensional Nanosheets Produced by Liquid Exfoliation of Layered Materials. *Science* **2011**, 331 (6017), 568-571.

237. Radisavljevic, B.; Radenovic, A.; Brivio, J.; Giacometti, V.; Kis, A., Single-layer MoS₂ transistors. *Nature Nanotechnology* **2011**, 6 (3), 147-150.

238. Kleshchanok, D.; Tuinier, R.; Lang, P. R., Direct measurements of polymer-induced forces. *Journal of Physics-Condensed Matter* **2008**, 20 (7), 1-25.

Appendix A

Additional information for chapter 3

1 Chemical Structure and the Stimuli-responsive Behavior of Oligo (ethylene glycol) Methacrylate Copolymer in Presence of Various Concentration of NaCl

The chemical structure of the copolymer was shown in Figure S1(A). The lower critical solution temperature (LCST) of the copolymer was characterized via the cloud point technique using a UV-Vis spectrometer (Varian Carey 50). In general, the polymer was dissolved at 4 mg/ml in NaCl aqueous solutions with different concentrations. The polymer concentration was kept constant in the characterization since the cloud point is sensitive to the polymer concentration. The solution was heated up to 52.5 °C in 30 s and the transmittance was then monitored using 400 nm during the cooling process. The transmittance curve in a 2 M NaCl solution was not obtained due to the instability of the system.

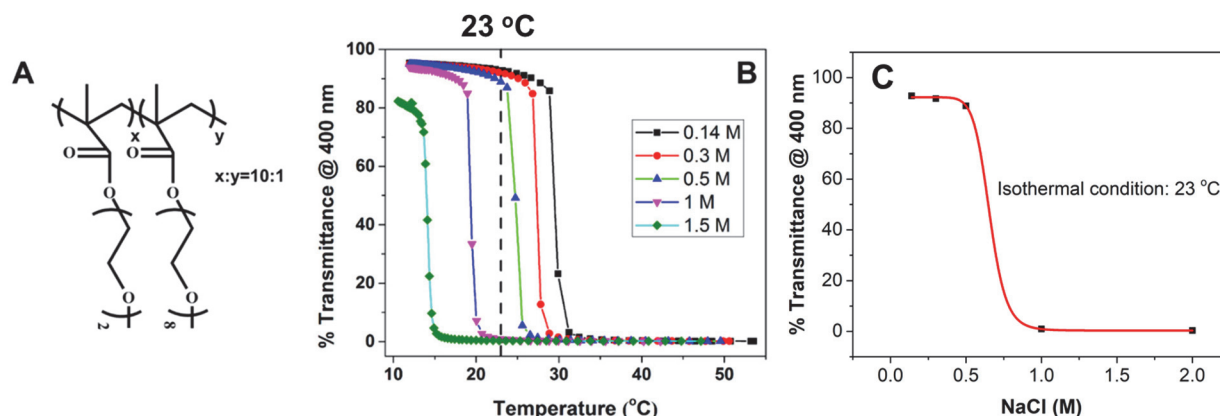


Figure A-1 Chemical structure of oligo (ethylene glycol) methacrylate copolymer (A), UV-Vis transmittance curves (cooling) measured using 400 nm in aqueous solution with various amount of NaCl (B). The transmittance as a function of NaCl concentration in isothermal condition (C)

2 GPC and ¹H-NMR Characterization of Oligo (ethylene glycol) Methacrylate Copolymer

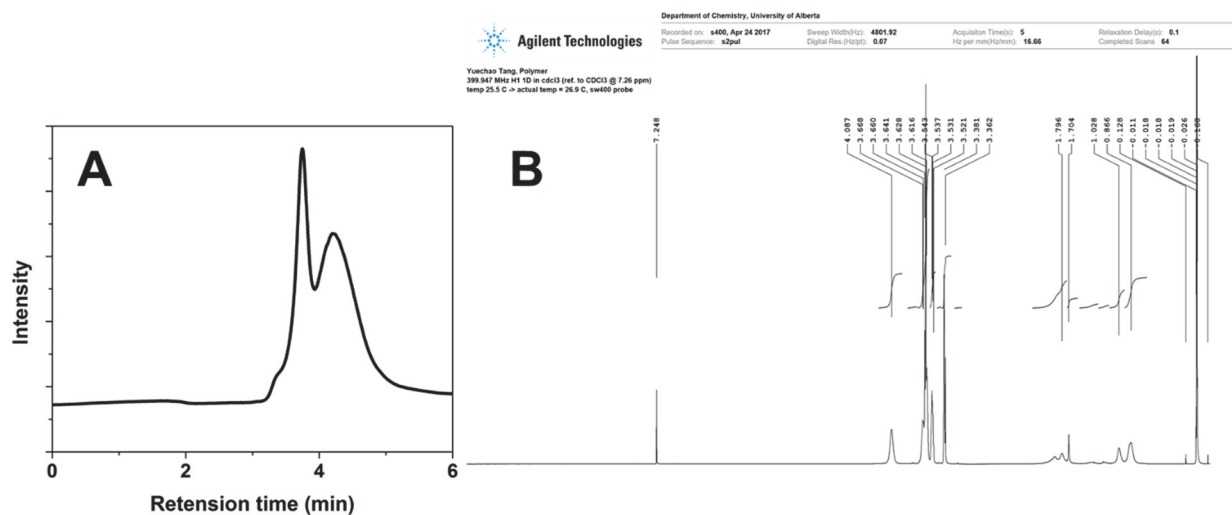


Figure A-2 GPC (A) and ¹H-NMR (10 mg/L, CDCl₃, 200 MHz) (B) characterization of synthesized oligo ethylene copolymer. The design molecule weight of the copolymer is 330 kDa. The obtained molecular weight (M_w) is 200 kDa and PDI is 1.7. As gel was formed during synthesis, broad distribution of the molecular weight was obtained due to gel acceleration.

3 SMFS Force Curves of Oligo (ethylene glycol) Methacrylate Copolymer on MoS₂ Basal Surface in Presence of NaCl Solution

The retracting force curves were baseline corrected and inverted to show the plateau feature. One typical force curve is shown in Figure 3 for each NaCl concentration. Since different polymer linked AFM tips were utilized in the experimental, different plateau length is observed.

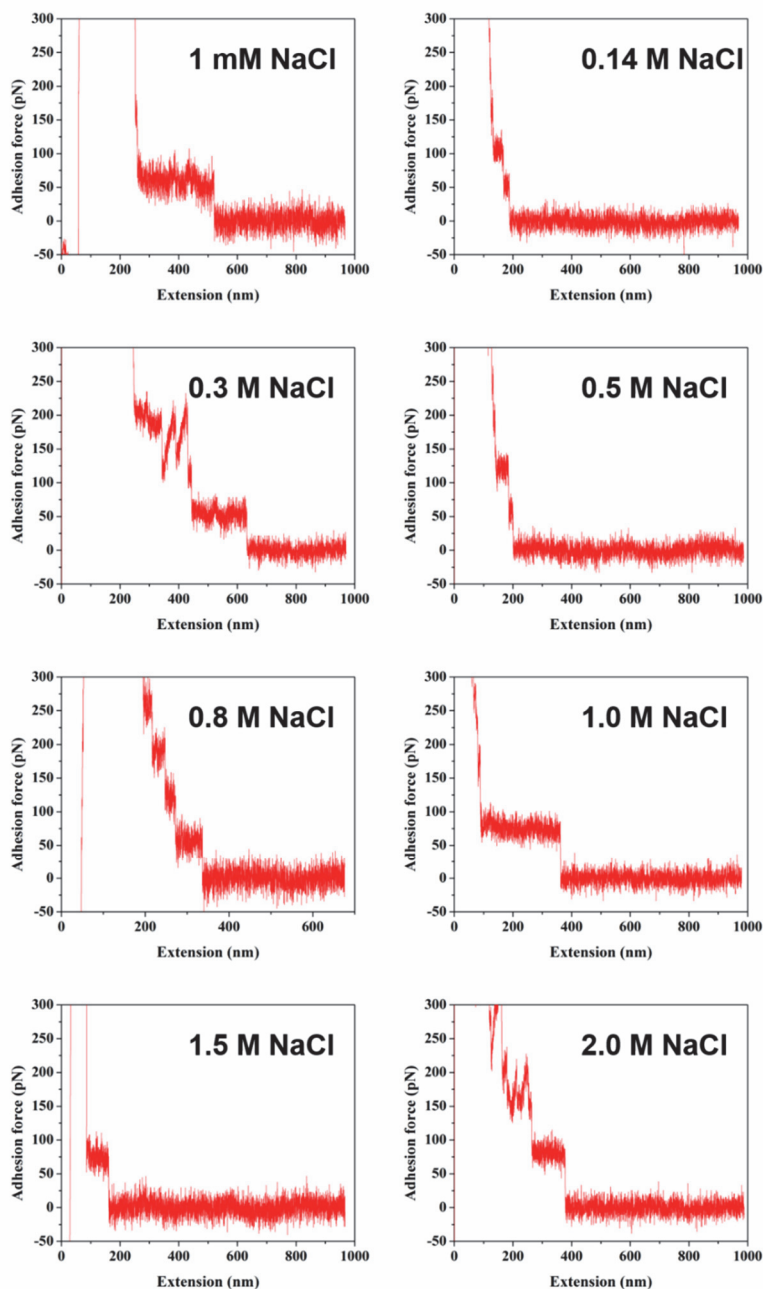


Figure A-3 The typical force curves obtained in the SMFS experiment in presence NaCl solution with different concentration.

To be noted, the chemical linkage (amide group) that links the polymer chain to APTES modified AFM cantilever tend to hydrolyze when is exposed to water. Thus, the polymer linked cantilever was used immediately after the modification process. The shelf life can be extended to 2 days if

shored in chloroform. Usually, the linking of polymer to the cantilever was performed prior to the SMFS experiment.

4 Equilibrium Contact Angle of NaCl Aqueous Solution on Oligo (ethylene glycol) Methacrylate Copolymer Brush Surface in Heptane and MoS₂/ NaCl Aqueous Solution, Polymer/ NaCl Aqueous Solution Interfacial Energy

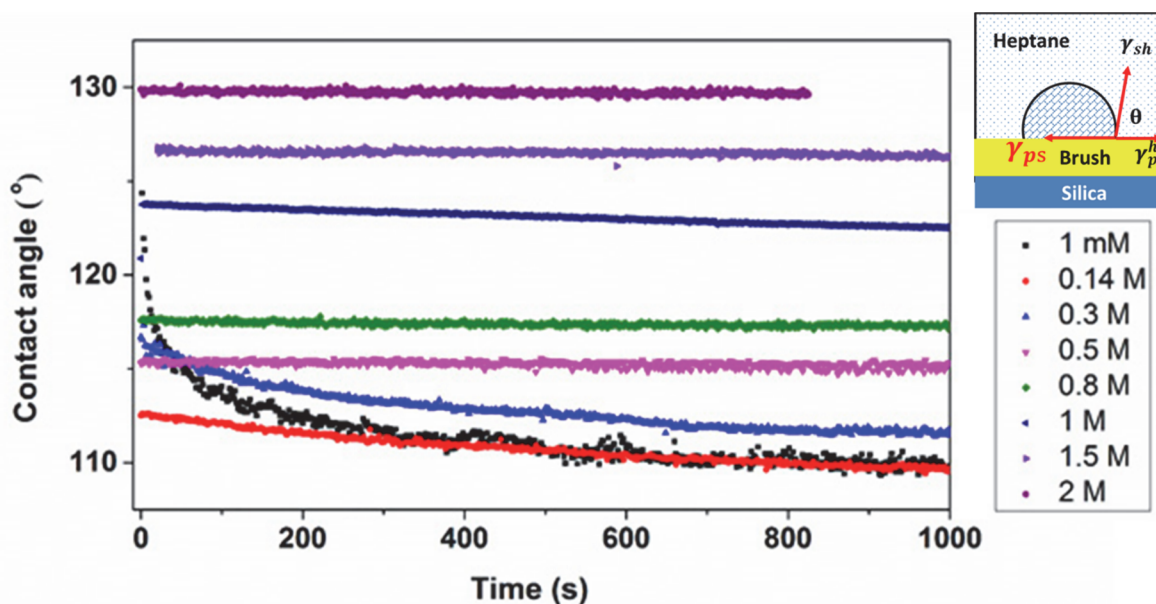


Figure A-4 Contact angle of NaCl aqueous solution on oligo (ethylene glycol) methacrylate copolymer brush in heptane

The θ_{eq} was measured on synthesized polymer brush since the polymer is water soluble. The contact angle was measured in the presence of heptane to minimize the evaporation of water in solution. To obtain the equilibrium values of contact angle, enough time was given to make sure the contact angle-time curve reaches a plateau.

The interfacial energy of polymer/NaCl aqueous solution and MoS₂/ NaCl aqueous solution was calculated with these equilibrium contact angles on brush and contact angle on MoS₂ using the equation of state proposed by Li and Neumann which:

$$\cos\theta_{eq} = -1 + 2 \sqrt{\frac{\gamma_p^h}{\gamma_s^h}} e^{-\beta(\gamma_s^h - \gamma_p^h)^2} \quad (8)$$

where γ_p^h and γ_s^h refer to the polymer/heptane and solution/heptane interfacial energy. $\beta = 0.0001247$ (m/mN) was determined by an averaging process on different surfaces. With the measured values of θ_{eq} and γ_s^h , the value of γ_p^h can be calculated by iterative method. The polymer/heptane interfacial energy was estimates using the equation of state to be 8.2 mJ/m². The surface energy of fresh MoS₂ was reported to be 54.5 mJ/m. The interfacial energy of MoS₂/solution was then calculated using the solution contact angle on MoS₂ and surface energy of MoS₂. The MoS₂/solution stays almost constant in the measured salt range while that of polymer/solution increases dramatically.

Table A-1 The measured interfacial energy of MoS₂/NaCl aqueous solution and polymer/NaCl aqueous solution

Solvent	γ_{ms} (mJ/m ²)	γ_{ps} (mJ/m ²)
1 mM NaCl	28.0	25.0
0.14 M NaCl	28.8	26.6
0.3 M NaCl	26.4	29.8
0.5 M NaCl	26.3	32.8
1.0 M NaCl	26.9	39.6
1.5 M NaCl	26.9	42.7
2.0 M NaCl	27.4	46.8

Appendix B

Additional Figures for Chapter 4

1 GPC characterization of the synthesized polymers

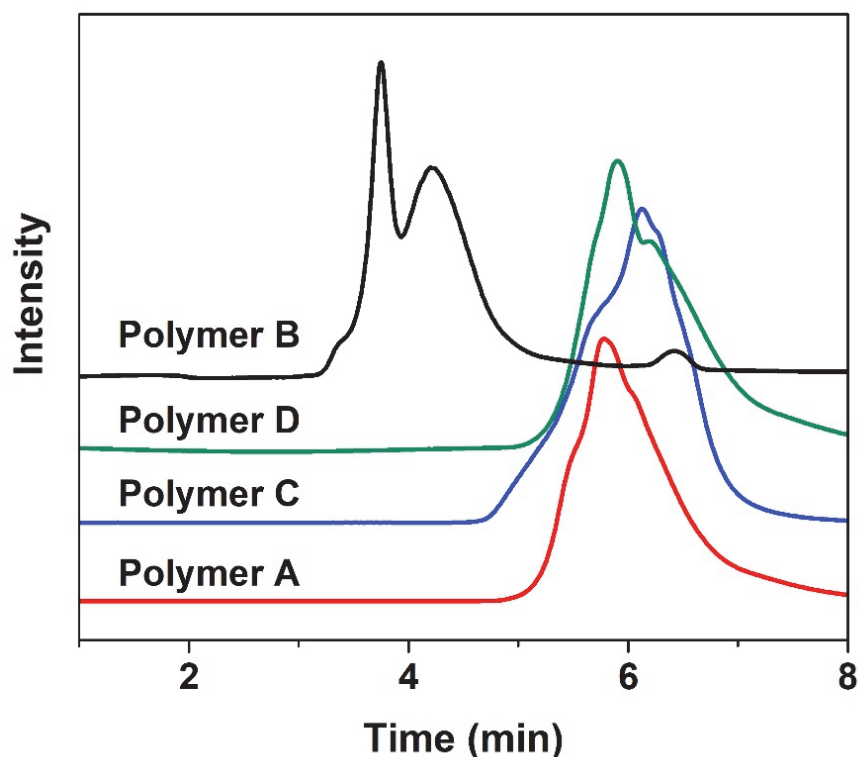
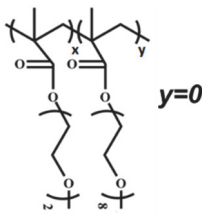
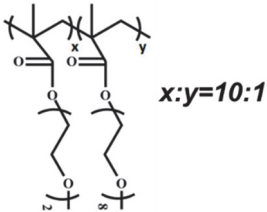
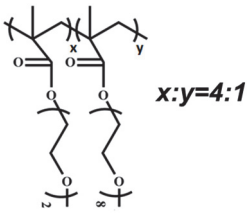
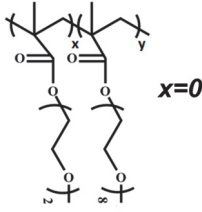


Figure B-1 GPC characterization of synthesized polymers. The designed molecule weight of all the synthesized polymer was 330 kDa. The obtained molecular weight (M_n) for Polymer A is 118 kDa with PDI close to 1.9. The M_n of polymer B is 200 kDa (PDI = 1.7). For Polymer C, the molecular weight (M_n) is 94 kDa (PDI around 1.8). The molecular weight (M_n) of polymer D is 61 kDa (PDI = 2.8).

The broad distribution of the obtained polymer can be attributed to the gel acceleration as polymer gel was formed during polymerization.

Table B-1 Chemical structures and molecular weights of the studied polymers

Polymer	Chemical structure	Mn (kDa)	PDI
Polymer A	 $y=0$	118	1.9
Polymer B	 $x:y=10:1$	200	1.7
Polymer C	 $x:y=4:1$	94	1.8
Polymer D	 $x=0$	61	2.8

2 The influence of pH on the single-molecule adhesion of polymer B and poly (vinylbenzyl trimethyl ammonium chloride) (PVBTA)

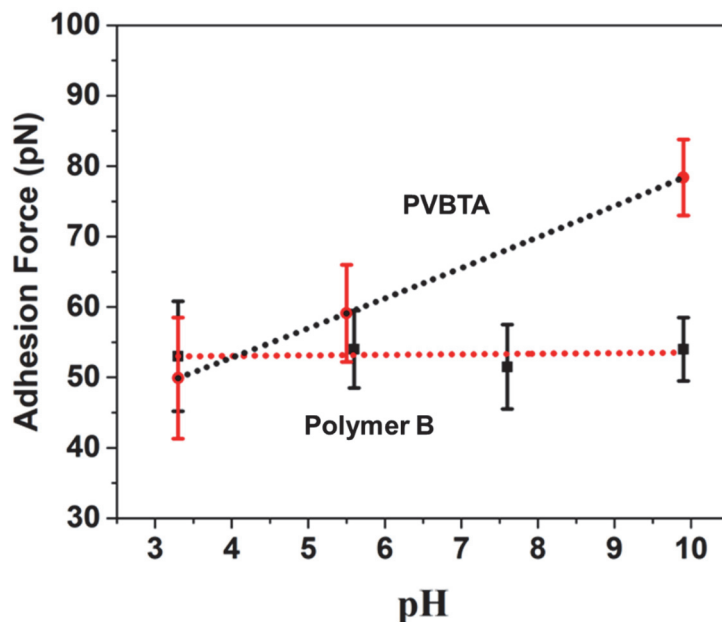


Figure B-2 Single-molecule adhesion force of studied polymer on basal surface of MoS₂ as a function of pH in presence of 1 mM NaCl solution.

The surface potential of MoS₂ basal surface is pH dependent. In detail, it changed from -28 mV (pH=3) to -44 mV when the pH is increased to 11¹⁴⁰. For cationic polymer PVBTA, a clear dependence of the single-molecule adhesion force on solution pH was observed. This demonstrated that the electric double layer interaction between the single polymer chain and MoS₂ substrate outshines itself by highly pH dependent single-molecule adhesion force. As no pH dependence on the solution pH on the single-molecule adhesion force was observed, it is reasonable to assume that electric double layer interaction does not play a role in our work between the neutral polymer and negatively charged MoS₂ basal surface.

2 NMR characterization of the synthesized polymer

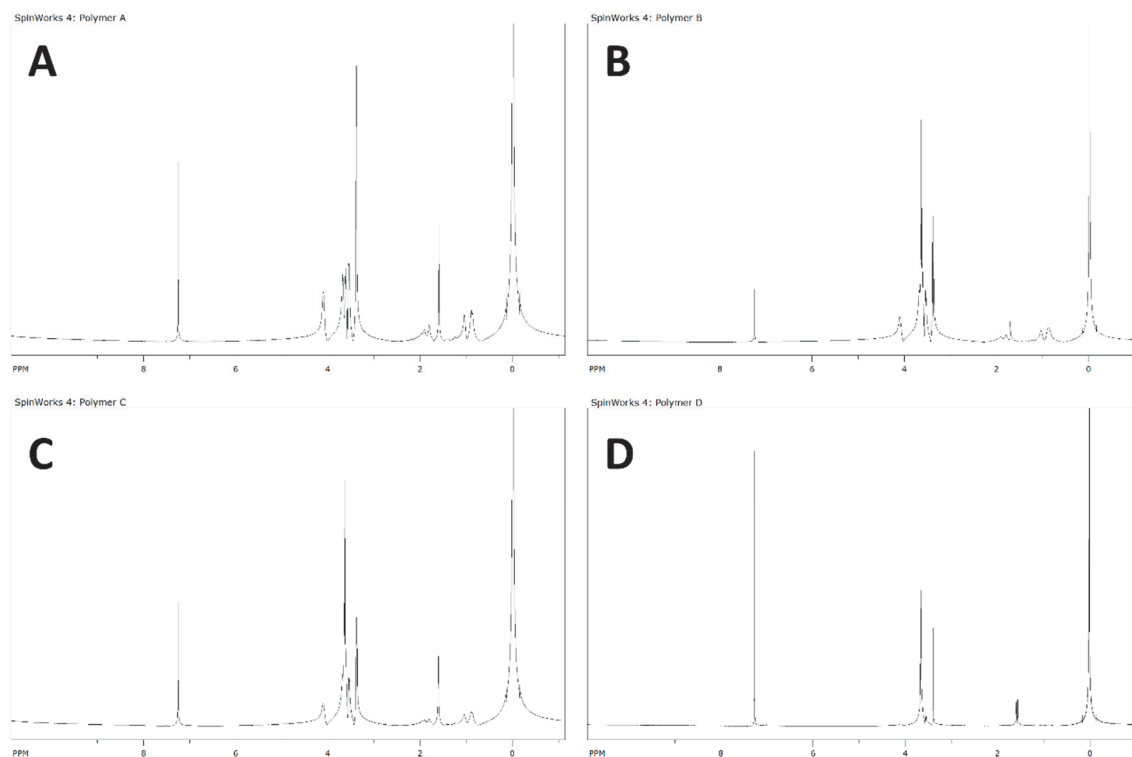


Figure B-3 NMR characterization of the studied oligo ethylene glycol copolymer. (A) Polymer A; (B) Polymer B; (C) Polymer C and (D) Polymer D.

3 Microtome cutting and AFM imaging

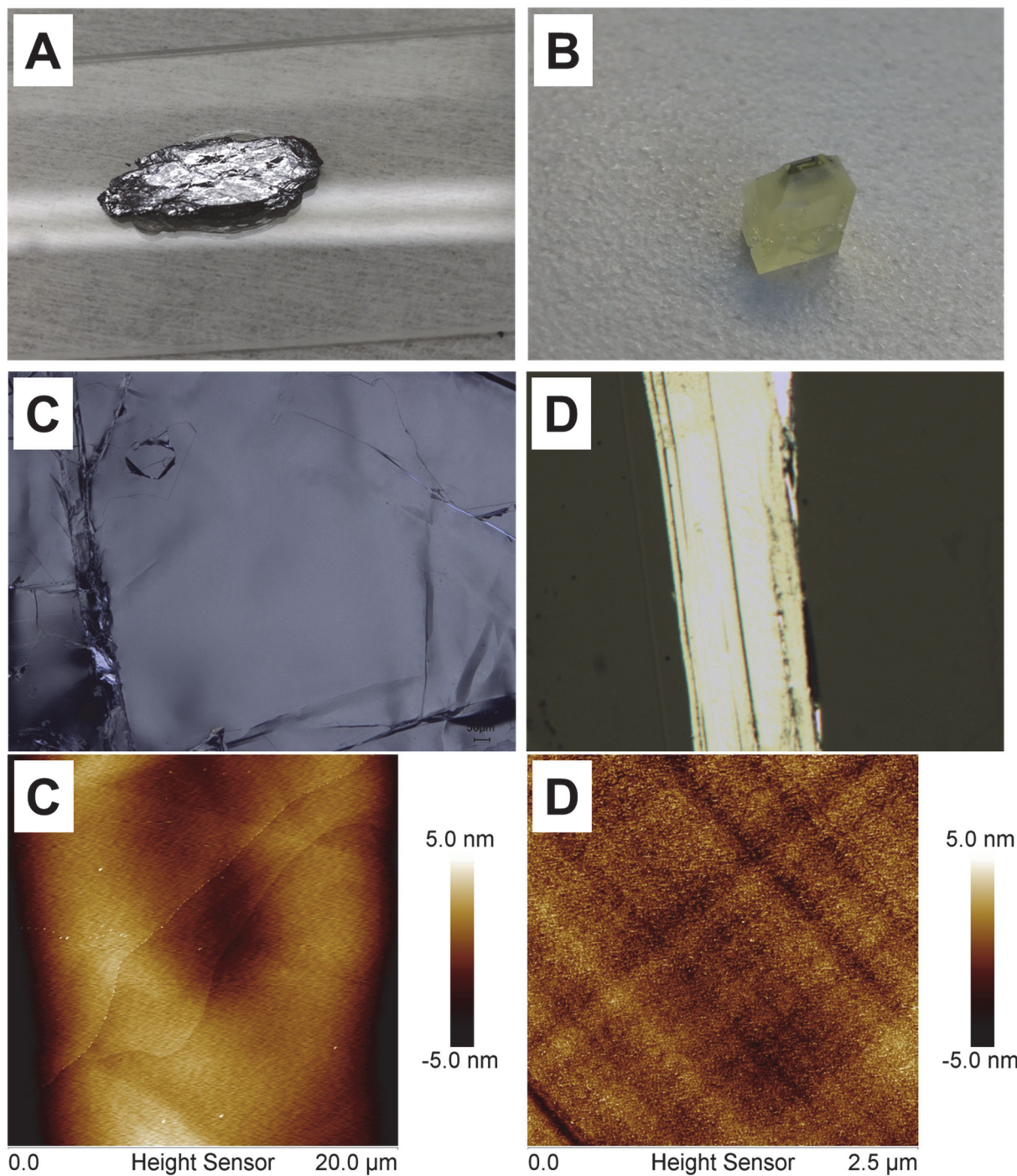


Figure B-4 Optical and AFM images of fresh peeled MoS₂ basal surface (A,C,E) and exposed smooth edge surface (B,D,F). The root-mean-square roughness of basal and edge surfaces were 0.3 nm and 2.1 nm, respectively.

Appendix C

Additional Figures for Chapter 5

1 The underwater single-molecule adhesion of copolymer on HOPG and MoS₂ surface.

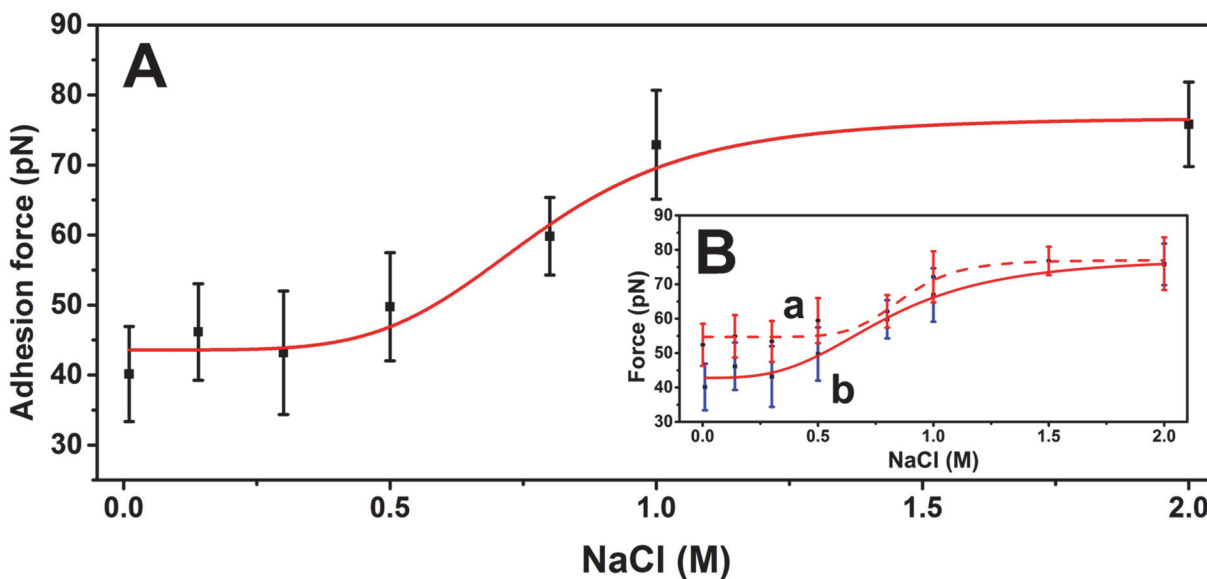


Figure C-1 The force required to peel a single oligo (ethylene glycol) copolymer chain from HOPG surface (A) in NaCl solution. The comparison of the single-molecule adhesion force quantified on different surfaces (B): copolymer-MoS₂ (a) and copolymer-HOPG (b) (the lines are drawn to guide the eyes). The data of single-molecule force on MoS₂ were taken from previous work¹⁶⁷.

2 Derivation of the analytical model

2.1 Hydration free energy

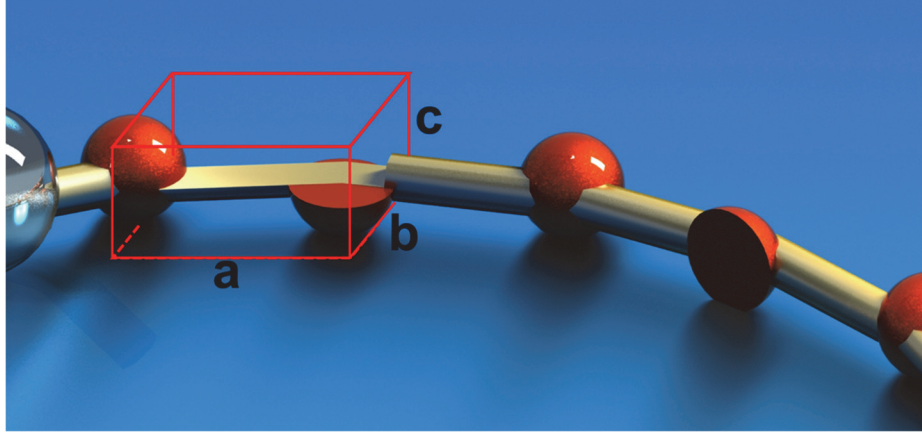


Figure C-2 Geometric parameters of the monomer.

Surface area of various interfaces:

$$A_{Polymer-solution} = A_{ps} = A_{Polymer} - A_{Substrate-polymer} \quad (1)$$

$$= a * (2b + 2c) * n - a * b * (n - n_i) = a * (b + 2c) * n + a * b * n_i$$

In the derivation, we assume the total surface area of the substrate exposed to solution before attachment of polymer is C. Thus, we can have the following mathematical description:

$$A_{Substrate-solution} = A_{ss} = C - a * b * (n - n_i) \quad (2)$$

$$A_{Substrate-polymer} = A_{sp} = a * b * (n - n_i) \quad (3)$$

$$G_{surface} = [a * (b + 2c) * n + a * b * n_i] * \gamma_{ps} + [C - a * b * (n - n_i)] * \gamma_{ss} + a * b * (n - n_i) * \gamma_{sub,p} \quad (4)$$

$$-\varepsilon * dn_i = dG_{surface} = ab(-\gamma_{sub,p} + \gamma_{ps} + \gamma_{ss})dn_i \quad (5)$$

$$\varepsilon = -ab(-\gamma_{sub,p} + \gamma_{ps} + \gamma_{ss}) \quad (6)$$

2.2 Entropic free energy

During the peeling process, the entropic elastic force of the desorbed chain balances the attractive interaction between the polymer and the surface. Since there is line tension along the polymer chain, the energy is also stored as entropic free energy in the desorbed portion of the polymer⁹⁵.

The entropic force along the polymer chain can be described as WLC model^{95, 147-148}:

$$F_{WLC} = \frac{K_B T}{L_p} \left[\frac{1}{4} \left(1 - \frac{x}{L} \right)^{-2} - \frac{1}{4} + \frac{x}{L} \right] \quad (7)$$

Thus, the energy stored in the desorbed chain as entropic free energy can be expressed as:

$$\begin{aligned} G_{entropic} &= \int_0^x F_{WLC} dx = \int_0^x \frac{K_B T}{L_p} \left[\frac{1}{4} \left(1 - \frac{x}{L} \right)^{-2} - \frac{1}{4} + \frac{x}{L} \right] dx \\ &= L \int_0^{\frac{x}{L}} \frac{K_B T}{L_p} \left[\frac{1}{4} \left(1 - \frac{x}{L} \right)^{-2} - \frac{1}{4} + \frac{x}{L} \right] d \frac{x}{L} \end{aligned} \quad (8)$$

Since force curves with plateaus feature were obtained in the measurement, the entropic elastic force should keep constant during the peeling process. As a result, the term $\frac{x}{L}$ is a constant. Thus:

$$G_{entropic} = \frac{K_B T}{L_p} * f(\varphi) * L \quad (9)$$

Where $f(\varphi) = \int_0^{\frac{x}{L}} \frac{K_B T}{L_p} \left[\frac{1}{4} \left(1 - \frac{x}{L} \right)^{-2} - \frac{1}{4} + \frac{x}{L} \right] d \frac{x}{L}$. $f(\varphi)$ is constant for each condition since $\varphi = \frac{x}{L}$ is constant for each NaCl concentration.

2.3 Mathematical relationship between adhesion force and hydrophobic hydration of the system

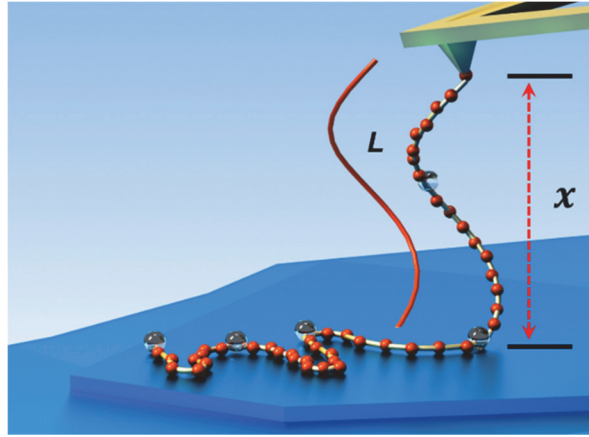


Figure C-3 Illustration of the force balance when the polymer chain is peeling from substrate.

When the AFM tip is retracted from the substrate, the work done by the cantilever should be equal to the change of surface free energy and entropic free energy of the system.

$$F_{WLC}dx = dG_{surface} + dG_{entropic} = ab(-\gamma_{sub,p} + \gamma_{ps} + \gamma_{ss})dn_i + \frac{K_B T}{L_p} * f(\varphi) * dL \quad (10)$$

Since $L = n_i * a$, we have:

$$dn_i = \frac{1}{a} dL \quad (11)$$

Thus we have the following relationship:

$$F_{WLC}dx = b(-\gamma_{sub,p} + \gamma_{ps} + \gamma_{ss})dL + \frac{K_B T}{L_p} * f(\varphi) * dL \quad (12)$$

As mentioned previously, the term $\frac{x}{L}$ is a constant for each NaCl concentration, then we have:

$$d\left(\frac{x}{L}\right) = \frac{1}{L}dx - \frac{x}{L^2}dL = 0 \quad (13)$$

$$dx = \frac{x}{L}dL \quad (14)$$

When eqn. 14 is applied, then we have:

$$F_{WLC}dx = F_{WLC} \frac{x}{L}dL \quad (15)$$

Finally, we have the mathematical relationship between adhesion force and hydrophobic hydration of the system:

$$F_{WLC} \frac{x}{L} = b(-\gamma_{sub,p} + \gamma_{ps} + \gamma_{ss}) + \frac{K_B T}{L_p} * f(\varphi) \quad (16)$$

$$\frac{1}{\varphi} = \frac{K_B T}{L_p * [b * (-\gamma_{sub,p} + \gamma_{ps} + \gamma_{ss}) + f(\varphi)]} \left[\frac{1}{4} (1 - \varphi)^{-2} - \frac{1}{4} + \varphi \right] \quad (17)$$

3 Contact angle of NaCl solution on HOPG surface

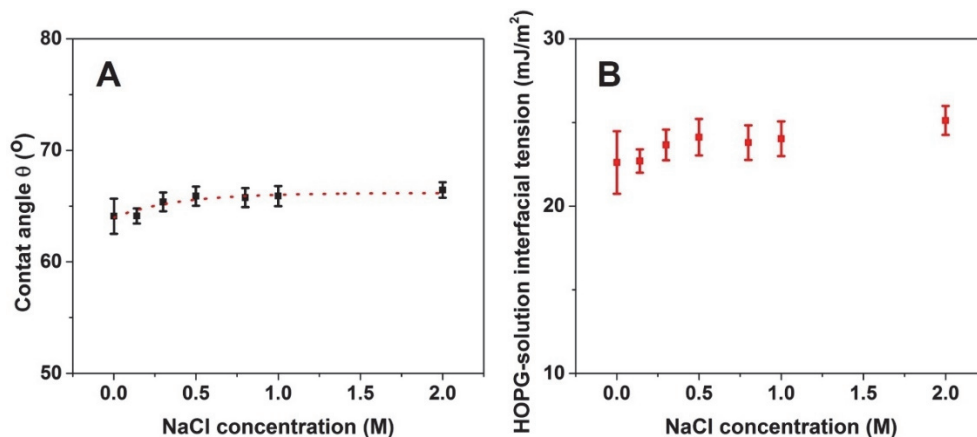


Figure C-4 Contact angle of NaCl solution on the HOPG surface (A) and the calculated HOPG-solution interfacial tension.

The interfacial tension of HOPG-solution was calculated using the solution contact angle on HOPG surface and surface energy of HOPG (54.5 mJ/m²)²¹³. The HOPG-solution interfacial tension stays almost constant in the studied salt range. The data of interfacial tension of oligo (ethylene glycol) copolymer were taken from ref.1.

Table C-1 The measured HOPG-solution and polymer-solution interfacial tension

Solvent	γ_{hopg-s} (mJ/m ²)	γ_{ps} (mJ/m ²)
1 mM	22.6	25.0
0.14 M NaCl	22.7	26.6
0.3 M NaCl	23.7	29.8
0.5 M NaCl	24.1	32.8
1.0 M NaCl	23.8	39.6
1.5 M NaCl	24.0	42.7
2.0 M NaCl	25.1	46.8

4 The fitting the single-molecule adhesion force with the derived model.

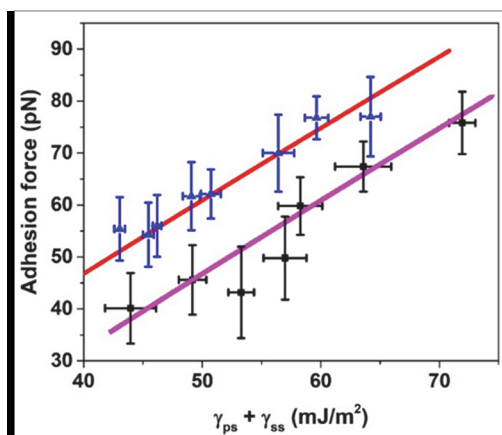


Figure C-5 Single-molecule adhesion force plotted against the total interfacial energy of polymer-solution and substrate-solution. The dots are experimental results and the curves are the adhesion force calculated with the model. The squares and triangles represent the single-molecule adhesion forces of HOPG-polymer and MoS₂-polymer respectively. The data on HOPG-polymer was obtained in this study and the data of MoS₂-polymer interaction were taken from ref.1. The interfacial tension of polymer-HOPG and polymer-MoS₂ in this study is fitting parameter.

4 1H-NMR characterization of the studied copolymer

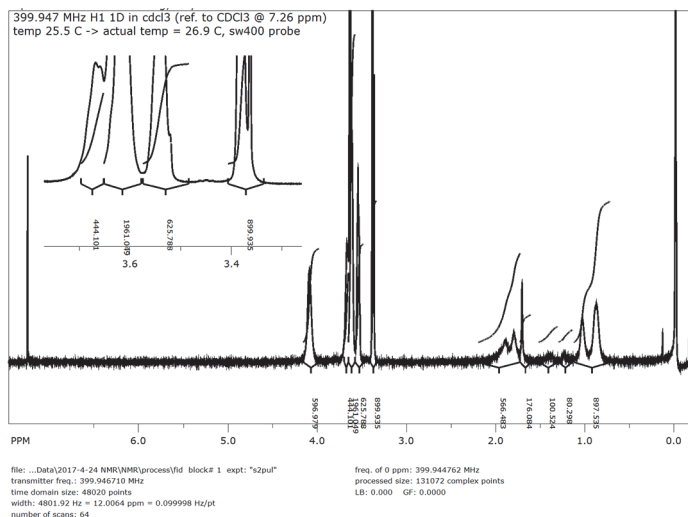


Figure C-6 1H-NMR (10 mg/L, CDCl₃, 400 MHz) characterization of synthesized oligo ethylene copolymer.

Appendix D

Additional Figures for Chapter 6

1 NMR characterization of the synthesized polymers

The NMR results of polymer N2 can be found in our previous published paper¹⁶⁷. The NMR data of polymer poly (vinylbenzyl trimethyl ammonium chloride) (polymer C1) and PMEO₂MA (polymer N1) is shown in Figure S1.

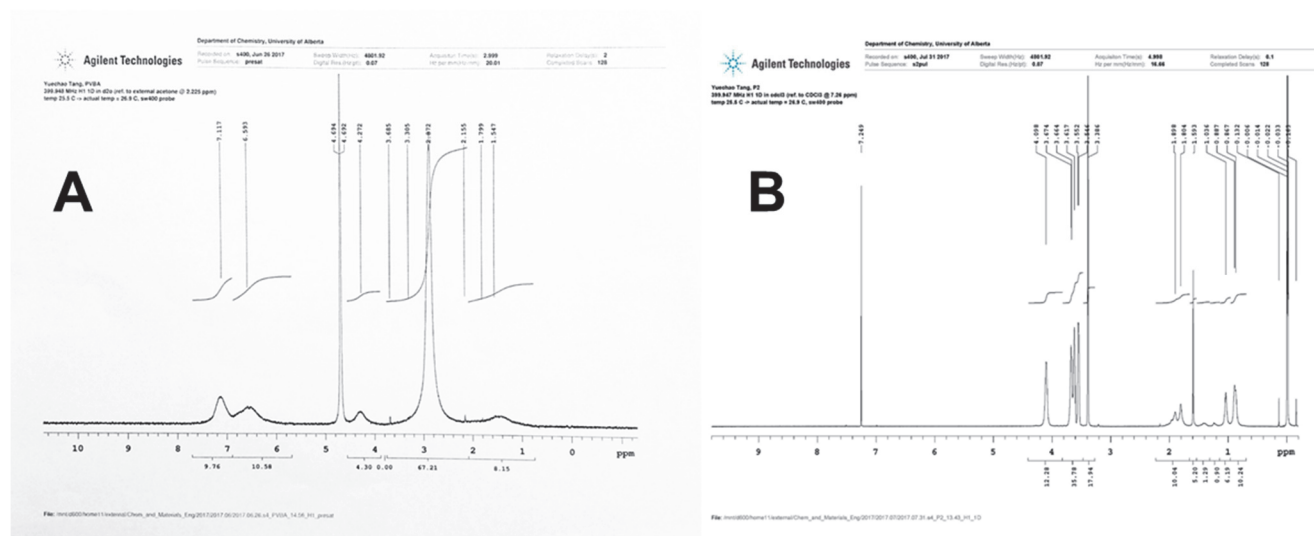


Figure D-1 ¹H-NMR analysis of the studied polymers: (A) polymer C1 and (B) polymer N1.

2 The dependence of single-molecule adhesion force on the retracting velocity

The data demonstrated that there was no obvious influence of tip velocity on the probed single-molecule force considering the uncertainty of AFM force measurement which is around 10%. In the experiment, the data with 500 nm/s retracting velocity were collected and analyzed to obtain the equilibrium single-molecule force for the studied polymers.

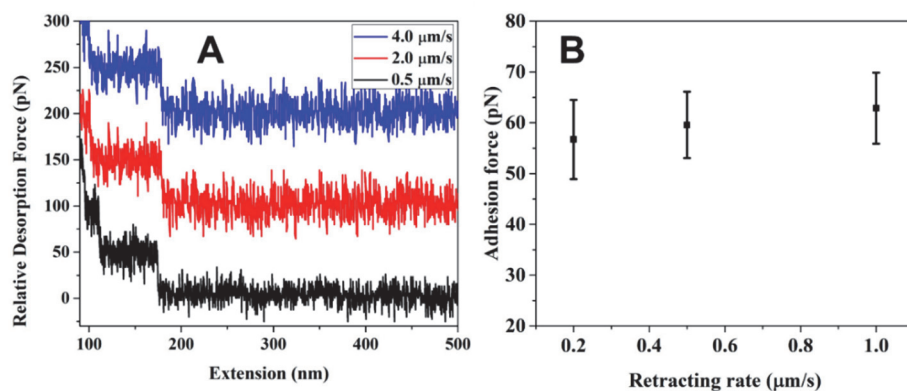


Figure D-2 Dependence of the single-molecule adhesion force on the retracting velocity of AFM cantilever for polymer N2 (A) and polymer C1 (B).

3 Preparation of smooth edge surface of MoS₂ using ultramicrotome.

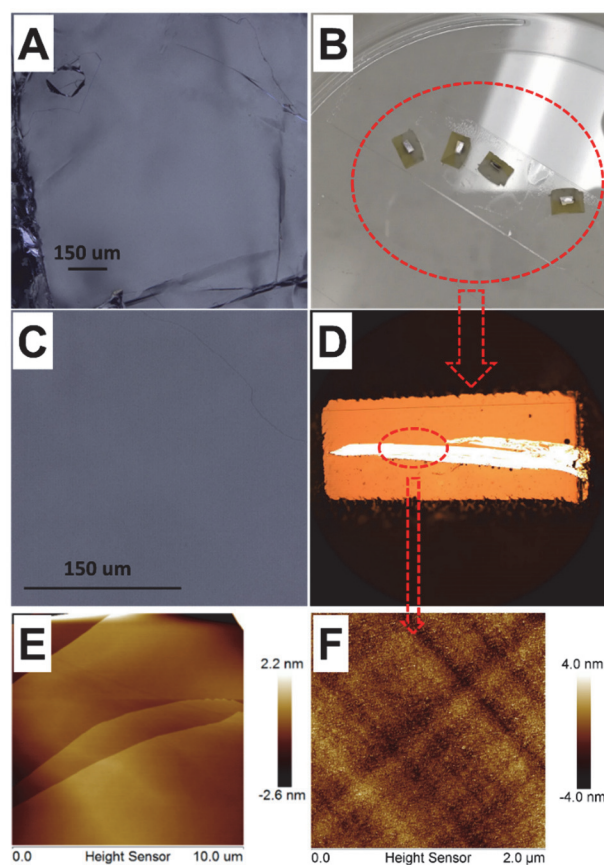


Figure D-3 Optical and AFM images of fresh peeled MoS₂ basal surface (A,C,E) and exposed smooth edge surface (B,D,F). The root-mean-square roughness of basal and edge surfaces were 0.1 nm and 2.1 nm, respectively.

4 The performance of the synthesized copolymer on exfoliation of MoS₂ powers

The SMFS results showed that the polymer C1 is an ideal candidate in functionalizing and exfoliating MoS₂ bulk powders since it could interact with both basal and edge surfaces. The binding of this polymer on these two surfaces resulted in a much higher energy barrier for the polymer-adsorbed MoS₂ nanosheets to re-aggregate. For comparison, the same dosage of the polymers and identical exfoliation procedures were used. The exfoliation was performed in a rotary grinding machine for 120 min. The solutions shown in Figure S4 were prepared by diluting the supernatants obtained by centrifuging the resultant dispersions at 8000 rpm for 4 times. DI water was used as a reference (Figure S3 A). As is shown in the optical graphed in Figure S4, the cationic polymer C1 is superior to the neutral polymer N1 since much more exfoliated MoS₂ nanosheets were produced.

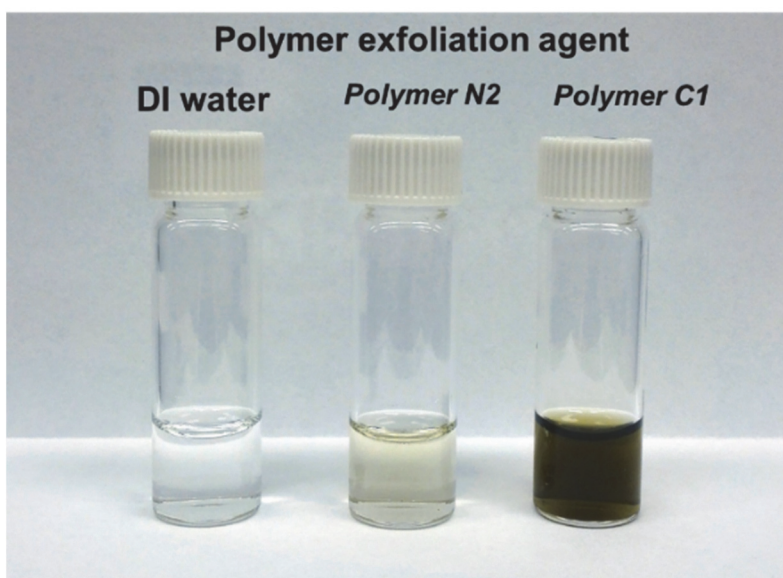


Figure D-4 Comparison of the exfoliation performance of the synthesized polymers.

5 TEM characterization of exfoliated MoS₂ sheets after grinding for 2 h and additional 2 h tip sonication

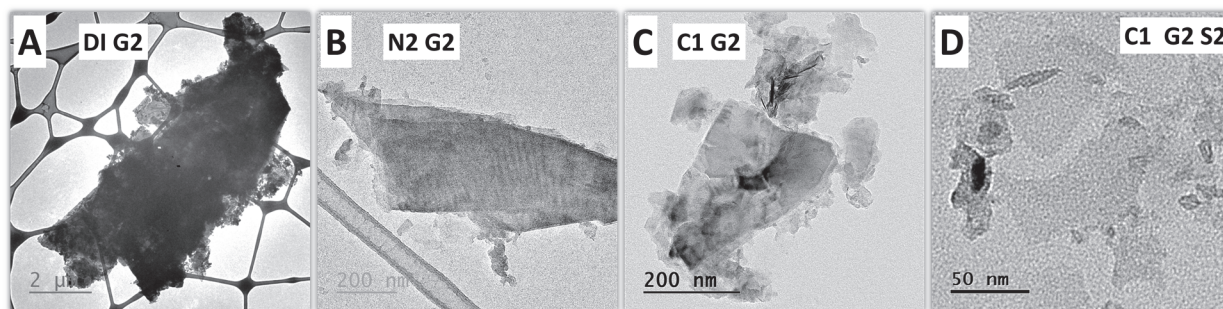


Figure D-5 TEM characterization of exfoliated MoS₂ (G: grinding; S: tip sonication). (A) Exfoliated MoS₂ sheets without addition of polymer exfoliation agent. As no exfoliated MoS₂ sheets were found in the supernatant after 8000 rpm centrifugation for 30 min, the precipitants were characterized. Exfoliated MoS₂ sheets obtained using polymer N2 (B) and polymer C1 (C) as exfoliation agent (centrifuge@8000 rpm for 30 min). (D) MoS₂ nanosheets produced after 2 h grinding and 2 h tip sonication (centrifuge @11500 for 30 min).

Without the addition of polymer exfoliation agent, no water dispersible MoS₂ sheets were obtained. Meanwhile, the size of the MoS₂ crystal in the sediments after centrifuge (8000 rpm for 30 min) was large in size (~6 μm). When polymer N2 was added, stable MoS₂ dispersion (after 8000 rpm centrifugation) was obtained. The size of the exfoliated MoS₂ was less than 1 μm. When polymer C1 was utilized, the size was reduced and the thickness of the obtained MoS₂ sheets was much less than that obtained by using polymer N2. Meanwhile, the concentration of the dispersed exfoliated MoS₂ were much higher.

As polymer C1 is much more effective in functionalization and exfoliation, experimental procedures were optimized to obtain single-layered MoS₂ nanosheets. Thus, after 2 h of grinding, 2 h additional tip sonication treatment was applied. Single-layer MoS₂ nanosheets with size around 50 nm were obtained (Figure D-5 D).

6 XRD characterization of the obtained exfoliated MoS₂ nanosheets

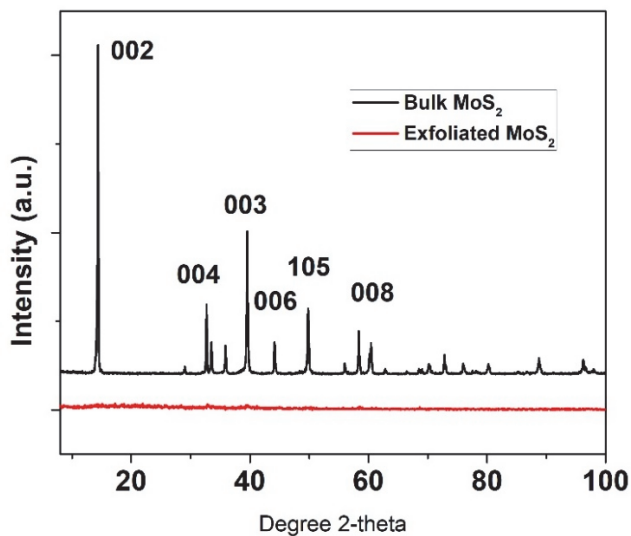


Figure D-6 The XRD pattern of the original bulk MoS₂ and the exfoliated MoS₂ nanosheets.

The XRD pattern of the exfoliated MoS₂ nanosheets did not show any reflection peaks that is typical for bulk MoS₂, indicating that there was no stacking of MoS₂ layers along c direction due to effective exfoliation and formation of single-layer nanosheets¹²⁸.

7 Raman characterization of obtained exfoliated nanosheets

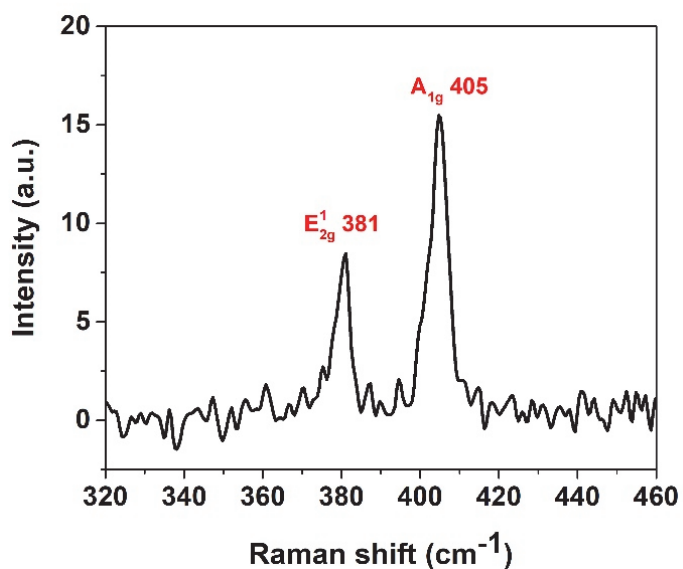


Figure D-7 Raman spectrum of single-layer MoS₂ nanosheets exfoliated by combined grinding and tip sonicating MoS₂ powder using polymer C1 as exfoliation agent.

The single-layer MoS₂ nanosheets exhibit bands at 381 and 405 cm⁻¹, which can be attributed to the in-plane vibration (E_{2g}¹) and out-of-plane vibration (A_{1g}) modes, respectively. Due to the surface adsorption by polymer C1, similar to the case where protein was used as exfoliation agent¹²⁸, the Raman data was not used to determine the layer number of exfoliated nanosheets.

8 Thermal gravimetric analysis (TGA) characterization of the bulk material and exfoliated MoS₂

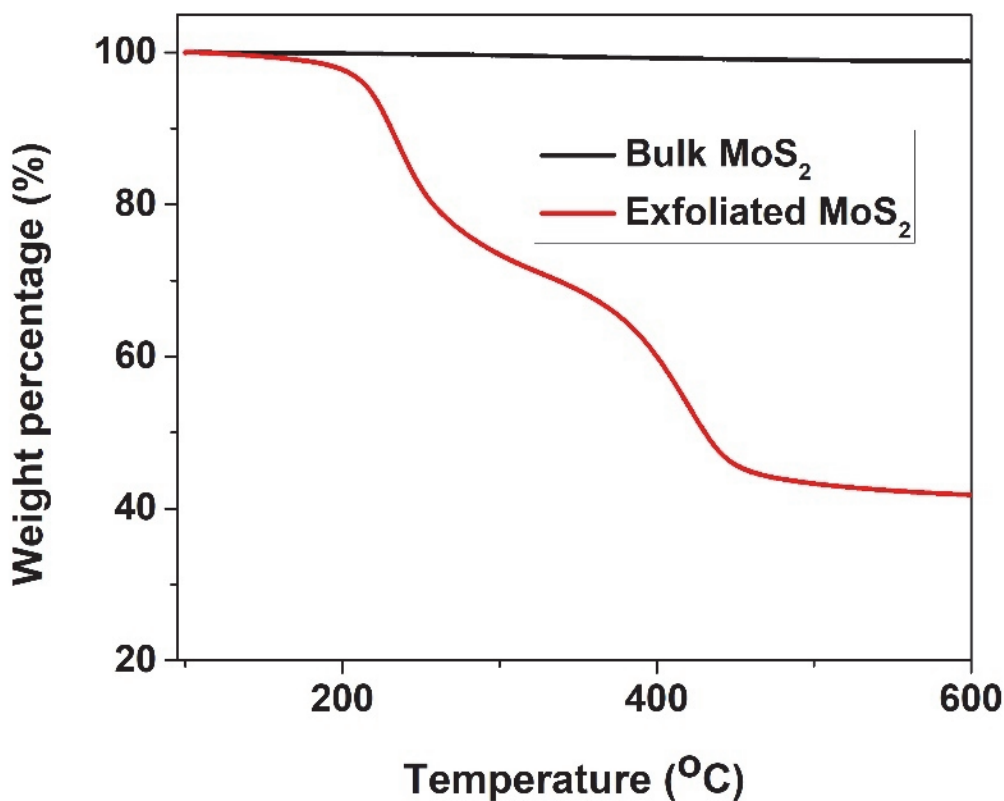


Figure D-8 Thermal gravimetric analysis (TGA) of the original bulk MoS₂ and exfoliated sample prepared using polymer C1 as exfoliation agent.

The weight loss of the bulk samples was around 1% while that of exfoliated MoS₂ sample was 60%. The results illustrated that the cationic polymer account for 60% of the obtained exfoliated MoS₂ sample.

9 GPC characterization of synthesized polymer C1

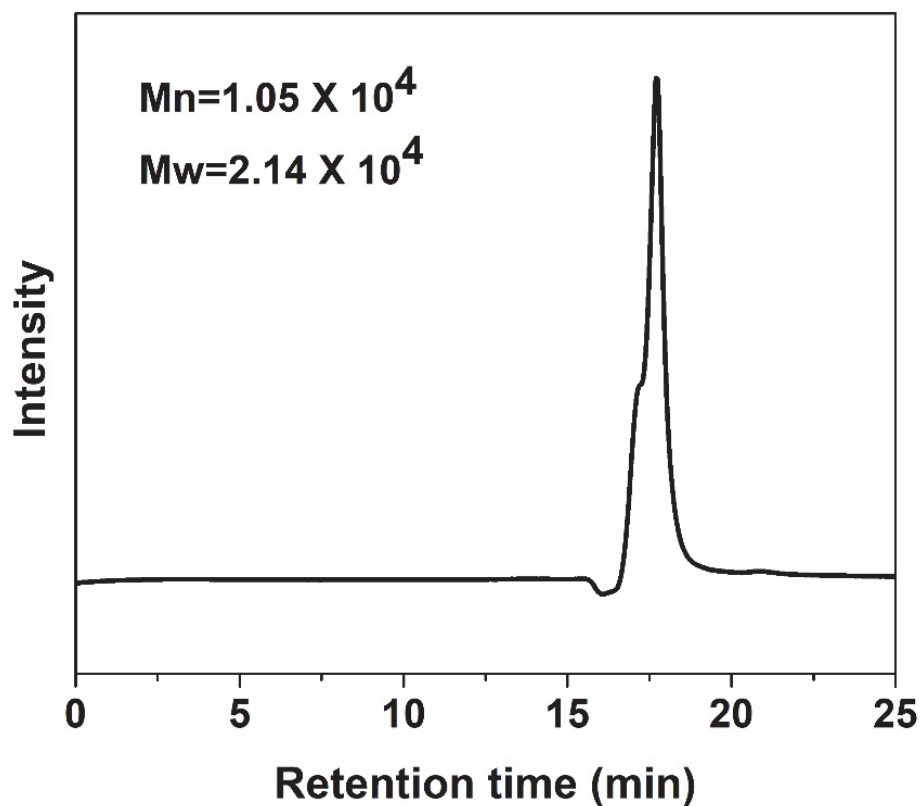
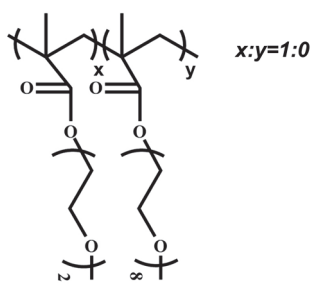
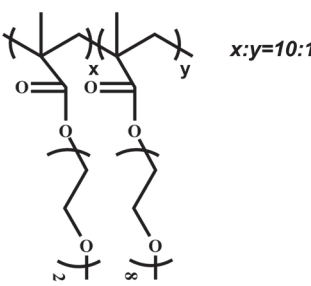
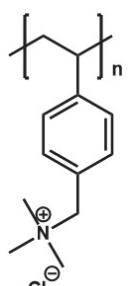


Figure D-9 GPC characterization of synthesized polymers. The polymers were synthesized using RAFT polymerization technique. The obtained molecular weight (M_n) for poly (vinylbenzyl trimethyl ammonium chloride) is 10.5 kDa with PDI close to 2. The molecular weight (M_n) for PMEO₂MA is 118 kDa with PDI close to 1.9. The M_n of oligo ethylene glycol copolymer is 200 kDa (PDI = 1.7).

Table D-1 The chemical structures and molecular weights of studied polymers

Polymer	Structure	Mn (kDa)	PDI
N1	 $x:y=1:0$	118	1.9
N2	 $x:y=10:1$	200	1.7
C1		10.5	2

10 Zeta potential characterization

Table D-2 The Zeta potential measurement of the obtained exfoliated MoS₂ sheets after 2 h combined treatment of grinding and 2 h tip sonication

Sample	Zeta potential (mV)	Standard deviation (mV)
Polymer N2 exfoliated MoS ₂	-5.5	6.2
Polymer C1 exfoliated MoS ₂	37.9	5.0